THE UNIVERSITY *of* EDINBURGH

Multiscale Remote Sensing of Plant Physiology and Carbon Uptake

Jon Atherton

THE UNIVERSITY
of EDINBURGH

Thesis submitted in fulfilment of
the requirements for the degree of
Doctor of Philosophy
to the
University of Edinburgh — 2012

Declaration

I declare that this thesis has been composed solely by myself and that it has not been submitted, either in whole or in part, in any previous application for a degree. Except where otherwise acknowledged, the work presented is entirely my own.

Jon Atherton

January 2012

Abstract

This study investigated the use of optical remote sensing for estimating leaf and canopy scale light use efficiency (LUE) and carbon exchange. In addition, a new leaf level model capable of predicting dynamic changes in apparent reflectance due to chlorophyll fluorescence was developed.

A leaf level study was conducted to assess the applicability of passive remote sensing as a tool to measure the reduction, and the subsequent recovery, of photosynthetic efficiency during the weeks following transplantation. Spectral data were collected on newly planted saplings for a period of 8 weeks, as well as gas exchange measurements of LUE and PAM fluorescence measurements. A set of spectral indices, including the Photochemical Reflectance Index (PRI), were calculated from the reflectance measurements. A marked depression in photosynthetic rate occurred in the weeks after outplanting followed by a gradual increase, with recovery occurring in the later stages of the experimental period. As with photosynthetic rate, there was a marked trend in PRI values over the study period but no trend was observed in chlorophyll based indices. The study demonstrated that hyperspectral remote sensing has the potential to be a useful tool in the detection and monitoring of the dynamic effects of transplant shock.

Relationships between hyperspectral reflectance indices, airborne carbon exchange measurements and satellite observations of ground cover were then explored across a heterogeneous Arctic landscape. Measurements were collected during August 2008, using the University of Edinburgh's research aircraft, from an Arctic forest tundra zone in northern Finland as part of the Arctic Biosphere Atmosphere Coupling at Multiple Scales (ABACUS) study. Surface fluxes of CO_2 were calculated using the eddy covariance method from airborne data that were collected from the same platform as hyperspectral reflectance measurements. Airborne CO_2 fluxes were compared to MODIS vegetation indices. In addition, LUE was estimated from airborne flux data and compared to airborne measurements of PRI. There were no significant relationships between MODIS vegetation indices and airborne flux observations. There were weak to moderate ($R^2 = 0.4$ in both cases) correlations between PRI and LUE and between PRI and incident radiation.

A new coupled physiological radiative transfer model that predicts changes in the apparent reflectance of a leaf, due to chlorophyll fluorescence, was developed. The model relates a physically observable quantity, chlorophyll fluorescence, to the sub leaf level processes that cause the emission. An understanding of the dynamics of the processes that control fluorescence emission on multiple timescales should aid in the interpretation of this complex signal. A Markov Chain Monte Carlo (MCMC) algorithm was used to optimise biochemical model parameters by fitting model simulations of transient chlorophyll fluorescence to measured reflectance spectra. The model was then validated against an independent data set. The model was developed as a precursor to a full canopy scheme. To scale to the canopy and to use the model on trans-seasonal time scales, the effects of temperature and photoinhibition on the model biochemistry needs to be taken into account, and a full canopy radiative transfer scheme, such as FluorMOD, must be developed.

Acknowledgements

Firstly, I need to thank Caroline not only for her top notch academic guidance but also for her friendship. I value both of these things dearly. Thanks go to Maurizio for his sage advice during the course of the project and for the positive encouragement that started during the first few months and continued throughout. I acknowledge Juan Suárez at Forest Research and the two organisations that funded the project; The University of Edinburgh through the Torrance bequest scheme and Forest Research, UK.

Thanks to Katie Simpson for the collaboration, Tom for being an ace flyer, Tim Hill for interesting discussions and always making the time, Rob Clement for his open door. Thanks to Albert Porcar-Castell for his help with the modelling project and for taking the time to send long and interesting replies to my scientific questions. Thanks to Christiaan van der Tol for providing the SCOPE code and also taking the time to reply to my myriad questions. I acknowledge Ana Prieto Blanco for producing the detailed land cover map that was used in chapter 4.

The Attic crowd made the Crew building a pretty special place to work, especially Steve, James, Oli, Nancy, Silvia, Antony, Lorna, Mack (and anyone else who I've forgotten!). Thank you to everyone at NASA who facilitated my stay, especially Forrest, Lahouari, Besty and Fred. Thanks to Chris and Alistair at FSF for the lone of instruments.

Thanks to my parents, who are always there when support is needed. Thanks to Will, Mat and Gui for the fun times, long may they continue. Thanks to everyone at Upper Gilmore place for letting me stay in your wonderful flat and not asking for a penny in return. And finally, to Hannah, for everything, x.

Marion You're not the man I knew ten years ago

Indy It's not the years, honey, it's the mileage

Contents

Declaration iii

Abstract iv

Acknowledgements vi

Contents ix

List of Tables xii

List of Figures xiii

List of Abbreviations and Symbols xvi

1 Introduction 1
- 1.1 Global biospheric research and remote sensing 2
  - 1.1.1 The light use efficiency model of productivity 4
  - 1.1.2 General aim of the thesis 6
- 1.2 Thesis objectives and chapter structure 6

2 Measurement and modelling of physiological reflectance 9
- 2.1 Measurement of physiological reflectance signals 10
  - 2.1.1 Reflectance spectroscopy 10
  - 2.1.2 The Photochemical Reflectance Index 11
  - 2.1.3 Passive remote sensing of chlorophyll fluorescence 16
- 2.2 Modelling of physiological reflectance signals 25
  - 2.2.1 Leaf and canopy radiative transfer models 27
  - 2.2.2 *PROSPECT* 27
  - 2.2.3 Radiative transfer simulations of chlorophyll fluorescence . 28
  - 2.2.4 PRI simulations 29

3 Remote sensing of transplant shock **31**
3.1 Introduction . . . 33
3.2 Methods . . . 36
3.2.1 Bedding and experimental design . . . 36
3.2.2 Spectral measurements . . . 37
3.2.3 Leaf gas exchange and PAM fluorescence . . . 38
3.2.4 Reflectance processing and statistics . . . 38
3.3 Results . . . 39
3.3.1 Meteorological conditions . . . 39
3.3.2 Time course of photosynthetic parameters . . . 40
3.3.3 Remote sensing of photosynthetic efficiency . . . 41
3.4 Discussion . . . 43
3.5 Acknowledgements . . . 48

4 Landscape scale remote sensing of light use efficiency **50**
4.1 Introduction . . . 52
4.2 Methods . . . 55
4.2.1 Study design . . . 55
4.2.2 Study site . . . 56
4.2.3 Airborne measurements . . . 57
4.2.4 Using MODIS SVIs to infer carbon exchange across the landscape . . . 59
4.2.5 Predicting LUE across the landscape . . . 65
4.3 Results . . . 70
4.3.1 CO_2 fluxes across the landscape . . . 70
4.3.2 Relationships between MODIS SVIs and CO_2 fluxes . . . 71
4.3.3 Estimating LUE across the landscape . . . 71
4.4 Discussion . . . 73
4.4.1 Future work . . . 78
4.4.2 Conclusions . . . 79

5 Modelling leaf level chlorophyll fluorescence **80**
5.1 Introduction . . . 82
5.2 Methods . . . 85
5.2.1 Coupled biochemical radiative transfer model description . . . 85
5.2.2 Experimental procedure and leaf measurements . . . 90
5.2.3 Calibration using the MCMC method . . . 91
5.3 Results . . . 94
5.3.1 Coupled biochemical radiative transfer model evaluation . . . 95
5.3.2 Parameter estimation and validation . . . 96
5.4 Discussion . . . 99
5.4.1 Future work . . . 102
5.4.2 Conclusions . . . 105

6 General conclusions **107**

Appendices **112**
.1 Publications 112
.2 Model code 134
..1 Biochemical leaf model code 134
..2 Radiative transfer leaf model code 142

Bibliography **150**

List of Tables

3.1 Reflectance index reference table. Where ρ_x is apparent reflectance at x nm and $D\rho_x$ is the first derivative spectra with respect to wavelength at x nm. 49

4.1 Data and instrumentation used in the study. The following key is used in the 'scale' column: {G = ground, A = airborne, S = satellite, T = flux tower }. 56
4.2 Transect statistics. Mean and standard deviations (in brackets) values are shown for length, altitude, plane speed relative to the gound and PPFD 59
4.3 Footprint model parameters 62

5.1 Prior and posterior parameter values for the biochemical sub-model. k_f and k_D were not optimised. 106

List of Figures

2.1 Example leaf reflectance and chlorophyll absorbance spectra (modelled using *PROSPECT*). 10
2.2 Chlorophyll fluorescence emission spectra for forward and backward directional emission 17
2.3 Fraunhofer infilling technique. Equations from Meroni *et al.* (2009). 23

3.1 Reflectance spectrum with the first derivative of the reflectance spectrum shown in the insert. 36
3.2 Meteorological conditions at the study site during the study period. Top (a) solar flux and bottom (b) air temperature. 39
3.3 Daily distributions of parameters of photosynthetic efficiency and reflectance indices ie during post-transplant acclimatisation. The median, 25th and 75th percentiles are shown by the middle lines, lower limits and upper limits of the boxes. The whiskers represent the maximum and minimum value within 1.5 times the interquartile range, values outside this range are shown as outliers. 40
3.4 Coefficients of determination between a set of spectral reflectance indices and (a) LUE, (b) $\Delta F/F'_m$, (c) PPFD and (d) leaf temperature 42
3.5 Linear regression models for (a) PRI Vs LUE, (b) PRI Vs $\Delta F/F'_m$, (c) PRI Vs PPFD and (d) PRI Vs leaf temperature 43
3.6 Linear regression models for (a) ND705 Vs LUE, (b) ND705 Vs $\Delta F/F'_m$, (c) ND705 Vs PPFD and (d) ND705 Vs leaf temperature 44

4.1 Flight transects for the 7th August 2008 overlaid onto digital photography of the study area collected using the airborne digital photography. 58
4.2 Ogive integrals for the cospectrum of CO_2 concentration and vertical wind speed calculated using airborne measurements. Each subplot represent the integrated contributions for a single transect for the full range of spatial scales. Thick black vertical lines are at 2.5 km. 61
4.3 Example of a flux footprint calculated using the Kljun *et al.* (2004) Parametrisation using the parameters shown in the figure. 63

4.4 MODIS EVI image with flux footprints for a single transect with a 2 km averaging window shown as magenta polygons. Each subplot represents a single flux measurement and associated footprint area. Inset histograms show EVI distributions within the footprint box, where N is the number of pixels per footprint. 65
4.5 Land-cover classification derived from IKONOS hyperspectral satellite imagery and ground survey data. 66
4.6 Diagram of ASD spectrometer and flux footprints (not to scale). Although there is some overlap between the two footprints, the ASD spectrometer and the eddy covariance systems are essentially measuring different areas. 68
4.7 Birch and wetland tower and airborne CO_2 fluxes for 07/08/2008 where airborne CO_2 fluxes were calculated using a 2500 m averaging window. 70
4.8 Average MODIS SVIs per flux footprint versus airborne CO_2 fluxes calculated using a 2500 m averaging window. Left: $NDVI_{MODIS}$ versus CO_2 flux, right: EVI_{MODIS} versus CO_2 flux. Standard error bars shown on MODIS SVIs. 72
4.9 PPFD, with standard error bars, versus airborne CO_2 flux measurements calculated using a 2500 m averaging window. 73
4.10 Land cover classification and hyperspectral measurements along a particular transect (marker number 47). From top to bottom: fractional land cover in ASD field of view, $NDVI_{ASD}$ and MODIS NDVI, incident PPFD and bottom, PRI_{ASD}. 74
4.11 Relationships and linear models between airborne hyperspectral SVIs and LUE and between airborne hyperspectral SVIs and PPFD. Top left: PRI_{ASD} versus LUE, top right: PRI_{ASD} versus PPFD, bottom left: $NDVI_{ASD}$ versus LUE, bottom right: $NDVI_{ASD}$ versus PPFD. 75

5.1 Flowchart for the combined predictive modelling and parameter estimation process. 85
5.2 Diagram of the biochemical modelling scheme. Absorption of light energy causes excitation of chlorophyll molecules, the excited energy is then used in one of the four pathways (ϕ_p, ϕ_N, ϕ_F, ϕ_D). The photochemical, ϕ_p, and NPQ pathways, ϕ_N, are modulated by two dynamic processes, plastoquinone reduction and the xanthophyll cycle, that are represented in the biochemical model as differential equations. 87
5.3 Modelled reflectance spectrum with and without fluorescence contribution. The spectral vegetation index, $R680/R630$, is shown in the insert. 92

5.4 Spectra utilised in the radiative transfer model; the vertical grey lines show the wavelengths of the reflectance index used in the MCMC optimisation. Top: chlorophyll fluorescence emission spectra for adaxial and abaxial sides of a leaf. These spectra are scaled using the fluorescence yield parameter, ϕ_f, to predict leaf-level chlorophyll fluorescence. Bottom: PROSPECT specific absorbtion spectra. PROSPECT uses combinations of these spectra to predict leaf reflectance, apparent reflectance is then predicted by combining prediction of leaf level fluorescence with PROSPECT predictions of leaf level reflectance. 93
5.5 Top: Modelled and measured reflectance indices. Squares represent measured reflectance index values after a dark adapted leaf has been exposed to strong sunlight. The shaded regions represent two different predictions of error, the dark line is the *best guess* modelled prediction calculated using the posterior parameter distributions. Bottom: simulated biochemical yields for the optimised parameters. 94
5.6 Prior (dotted lines) and posterior (solid lines) biochemical parameter distributions. 96
5.7 Posterior parameter correlations. Notice a relatively strong correlation between two NPQ parameters, k_N and k^b_{npq}. 97
5.8 Time-series of biochemical model yields for the validation data set. Where black squares are measured data points and thick lines are the optimised modelled predictions. 98
5.9 Time-series of the simulated and measured two peak reflectance index, $R690/R735$. This relfectance index is used to quantify the change of shape in the chlorophyll emission spectrum, the model is significantly different to the measured data during the first few seconds. 99

List of Abbreviations and Symbols

α_s	Canopy shadow fraction
ϕ_D	Yield of constitutive heat dissipation
ϕ_F	Yield of fluorescence
ϕ_N	Yield of NPQ
ϕ_P	Yield of photochemistry
σ_w	Instantaneous perturbations in vertical wind speed
ABACUS	Arctic Biosphere Atmosphere Coupling at Multiple Scales study
APAR	Absorbed Photosynthetically Active Radiation
ASD	Analytical Spectral Devices
BAT probe	Best Air Turbulence probe
BOREAS	The Boreal Ecosystem - Atmosphere Study
BRDF	Bidirectional reflectance distribution function
CHRIS/PROBA	The Compact High Resolution Imaging Spectrometer/Project for On-Board Autonomy
DEPS	Xanthophyll de-epoxidation state
DGVM	Dynamic Global Vegetation Model
E	NPQ quenching coefficient
ESA	European Space Agency

ETR	Electron transfer rate
EVI	Enhanced Vegetation Index
F_c	CO_2 flux measurement
F_t	Steady-state chlorophyll fluorescence
F_*	Flux footprint distribution
fAPAR	Fraction of absorbed photosynthetically active radiation
FLD	Fraunhofer Line Depth technique
FLEX	FLourescence EXplorer space mission proposal
FLIGHT	Monte Carlo canopy radiative transfer model
FluorMOD	Canopy scale fluorescence radiative transfer model
FLUXNET	Global network of flux towers
GOSAT	Global Greenhouse Observation by Satellite
GPP	Gross Primary Productivity
IRGA	Infrared Gas Analyser
k_D	Rate constant of constitutive heat dissipation
k_F	Rate constant of fluorescence
k_N	Rate constant of NPQ
k_P	Rate constant of photochemistry
k_{npq}^{build}	Rate constant for v_x to z_x conversion
k_{npq}^{relax}	Rate constant for z_x to v_x conversion
k_{pq}^{relax}	Rate constant for plastoquinone re-oxidation
L	Monin-Obukhov length
LAI	Leaf Area Index
LUE	Light Use Efficiency
MCMC	Markov Chain Monte Carlo
mND705	Chlorophyll based reflectance index

MOD17	MODIS daily photosynthesis and annual net primary productivity algorithm
MODIS	Moderate Resolution Imaging Spectroradiometer
MSS	MultiSpectral Scanner
NASA	National Aeronautics and Space Administration
ND705	Chlorophyll based reflectance index
NDVI	Normalised Difference Vegetation Index
NPQ	Non photochemical quenching
PAM	Pulse Amplitude Modulated Fluorometer
PAR	Photosynthetically Active Radiation
PPFD	Measurement unit of PAR, Photosynthetic photon flux density typically in μmol m^{-2} s^{-1}
PRI	Photochemical Reflectance Index
PROSPECT	Leaf scale optical model
PSII/PSI	Photosystem II/Photosystem I
Q	Photochemical quenching coefficient
R_e	Ecosystem Respiration
SAC	Specific Absorption Coefficient
SAIL	Scattering by Arbitrary Inclined Leaves model
SCOPE	Soil Canopy Observation, Photochemistry and Energy fluxes model
SR705	Chlorophyll based reflectance index
SVI	Spectral Vegetation Index
TOA	Top of Atmosphere
u_*	Friction velocity
v_x	Violaxanthin
z_0	Roughness length

z_m	Aircraft height above ground
z_x	Zeaxanthin
zt1 - zt6	Chlorophyll fluorescence based reflectance indices
ztd1, ztd2	Chlorophyll fluorescence based derivative reflectance indices

Chapter 1

Introduction

1.1 Global biospheric research and remote sensing

Climate change is one of the defining global and political issues of the 21^{st} century. There is now very strong evidence that greenhouse gas emissions are driving increases in global temperatures (IPCC, 2007a). In the latest series of reports the IPCC (2007a) predicted global mean temperature increases of between 1.1 - 6.4 °C over the next 90 years. In addition, there is increasing evidence that the polar regions are particularly sensitive to the changing climate system (IPCC, 2007a). There is an increased drive to understand the connections between the biosphere and atmosphere in these regions (and globally) because changes in these ecosystems could result in feed-backs that exacerbate or mitigate future warming trends (Frank *et al.*, 2010).

The terrestrial biosphere is one of two natural sinks for anthropogenic CO_2 emissions, the other is the Earth's oceans. Photosynthesis is estimated to account for the uptake of approximately 60 Gt of carbon per year. Ecosystem respiration is estimated to balance this flux by being a net source of approximately the same magnitude (IGBP Terrestrial Carbon Working Group, 1998). The feed-backs that link temperature, precipitation, photosynthesis and respiration are not yet fully understood at the global scale. It follows that a key objective of present-day ecological science is to accurately quantify photosynthesis across spatial scales of varying magnitude (from the canopy to the landscape to the global scale).

Flux tower systems use the eddy covariance technique to measure canopy scale fluxes of carbon and energy exchange. Flux towers are fitted with micro-meteorological suites of instrumentation capable of collecting the high frequency measurements of wind and gas concentrations that are required to calculate near surface fluxes of energy and carbon. The source region of a flux tower is referred to

as the *footprint*. Flux tower footprints are typically on the order of a few hundred meters. Each flux footprint contributes to a single measurement, usually at a frequency of a single measurement every 30 minutes. Therefore, taken in isolation, flux towers do not facilitate spatially-explicit estimates of photosynthesis.

Over the last 30 years the emergence of large-scale multi-disciplinary experiments, such as the Boreal Ecosystem Atmosphere Study (BOREAS), resulted in significant new understanding of energy and carbon exchange in Northern latitude forested regions (Hall, 1999). These studies were interdisciplinary in nature and combined measurements from flux towers, airborne campaigns, remote sensing and process-based models in an aim to assess the drivers of carbon and energy exchange and set a precedent for this type of research. BOREAS has left a lasting legacy by way of an international network of flux towers (FLUXNET, `http://daac.ornl.gov/FLUXNET/fluxnet.shtml`) which have proved invaluable in validating and calibrating process-based models.

Flux towers and large scale experiments can provide canopy scale and regional assessments of carbon exchange, however neither of these techniques directly provide spatially continuous, global estimates of photosynthesis. There are two main methods used to estimate global scale rates of photosynthesis: i. Dynamic Global Vegetation Models (DGVMs) and ii. space-borne remote sensing. In reality the two methods are not independent but intricately connected. DGVMs often use remote sensing derived data-sets as driving variables and parameter sets (Sellers *et al.*, 1996; Cramer *et al.*, 1999) and the MOD17 (Running *et al.*, 1999) algorithm, used by the MODerate resolution Imaging Spectroradiometer (MODIS) to calculate global rates of photosynthesis from space, is derived from a simple production efficiency type model (Haxeltine and Prentice, 1996).

The MODIS MOD17 algorithm builds on a significant body of work that dates back to the early 1970s, when canopy *greenness* was first observed from space

by the Landsat series of satellites. Landsat-1[1] was launched by NASA in 1972 to obtain information relating to a variety of Earth surface processes (including those relating to the geosphere, biosphere and cryosphere) and heralded the birth of a new type of multidisciplinary science, Earth Observation. As one of the two instruments (the other being a type of video camera) onboard Landsat-1, the MultiSpectral Scanner (MSS) was a broadband sensor capable of retrieving top of atmosphere (TOA) radiance in four bands, two visible and two infra-red. Rouse *et al.* (1973) proposed an algebraic combination of the red visible band and the infrared band to calculate a Spectral Vegetation Index (SVI) which came to be known as the Normalised Difference Vegetation Index (NDVI). Because green vegetation strongly absorbs electromagnetic radiation in the visible wavelengths and reflects and transmits radiation at longer wavelengths a large differential between the two bands signifies vegetative biomass (Tucker, 1979). NDVI became firmly established as an indicator of canopy productivity, and was used to estimate canopy structural parameters such as the fraction of photosynthetically active radiation absorbed by the canopy (fAPAR) (Myneni and Williams, 1994) and the Leaf Area Index (LAI).

1.1.1 The light use efficiency model of productivity

The amount of radiation absorbed by a canopy, or Absorbed Photosynthetically Active Radiation (APAR), is calculated as the product of fAPAR and the incident photosynthetically active radiation (PAR). The Monteith (1972, 1977) light use efficiency model is a simple way of calculating the rate of Gross Primary Productivity (GPP) (or biomass accumulation), where APAR is multiplied by a constant referred to as light use efficiency (LUE):

[1] On launch Landsat-1 was originally called the Earth Resources Technology Satellite (ERTS-1).

$$GPP = LUE \times APAR \tag{1.1}$$

This model forms the basis of several remote sensing based approaches to calculating photosynthesis (Running and Hunt Jr., 1993; Veroustraete *et al.*, 2002) including the MODIS photosynthesis algorithm, MOD17 (Running *et al.*, 1999). Although the model facilitates a simple method for estimating photosynthesis from space (provided fAPAR and PAR can be measured) there is one significant drawback; rather than being a constant as assumed in the simple linear model, LUE is inherently variable. LUE is representative of all the physical, biological and chemical processes that act to reduce the conversion efficiency of light energy to chemical energy such as reductions in carboxlation capacity caused by drought and temperature induced stress. Most algorithms to date, including MOD17, adjust an optimum biome-specific value of LUE by meteorological scalars that represent sub-optimal environmental conditions. However, because the scalars can prove difficult to estimate correctly, values of LUE can lead to the overestimation of GPP by 20-30% (Heinsch *et al.*, 2006).

Recent research (see Grace *et al.* (2007) and Coops *et al.* (2010)) has focused on developing new approaches for directly inferring LUE from remote sensing. There are two methods of inferring LUE from spectral radiance and reflectance measurements that have become established in recent years. The first method relates to a photo-protective process known as the xanthophyll cycle that occurs as a result of stress and causes subtle spectral changes in the visible wavelengths. These changes are quantifiable using an SVI known as the Photochemical Reflectance Index (PRI) (Gamon *et al.*, 1992). The second method relates to the passive detection of terrestrial chlorophyll fluorescence, a signal that has been used for over 80 years by plant physiologists (Kautsky and Hirsch, 1931) but has only recently been retrieved from space (Guanter *et al.*, 2007). Recent work has

also focused on accurately retrieving PRI from space (Drolet *et al.*, 2005, 2008; Hilker *et al.*, 2009, 2011). Neither chlorophyll fluorescence or PRI are presently used to infer LUE in an operational capacity (such as the MOD17 algorithm). This is because there are still several unanswered scientific questions that relate to the interpretation of these complex signals. Such questions include:

1. Are these signals limited to detecting reductions in LUE caused by specific types of stress? Can they be used in variable illumination conditions?
2. The majority of work has been conducted in dense coniferous canopies (Coops *et al.*, 2010), can these signals be used to detect changes in LUE across heterogeneous Arctic regions?
3. Can process-based models, such as the Farquhar *et al.* (1980) carboxylation model, be linked to radiative transfer models to predict dynamic changes in these signals at the leaf scale or at the canopy scale?

1.1.2 General aim of the thesis

The general aim of the thesis was to contribute to knowledge gaps in the interpretation and modelling of physiological remote sensing signals, working towards the goal of accurately inferring LUE from space.

1.2 Thesis objectives and chapter structure

The thesis is structured around three specific objectives designed to complete the general aim of the thesis:

1. Assess the usefulness of physiological remote sensing signals in detecting reductions in LUE at the leaf scale caused by transplant shock.

2. Relate physiological remote sensing signals to airborne measurements of carbon fluxes across the Arctic landscape.

3. Develop a leaf level model capable of predicting changes to apparent reflectance caused by leaf biochemical dynamics.

In order to complete the stated thesis objectives, a comprehensive literature review and three main studies were conducted. The first was a leaf level experiment (chapter 3), the second was a regional scale study that used airborne data (chapter 4) and the final study involved developing a new model that linked a process-based approach of photosystem dynamics to a leaf radiative transfer model (chapter 5). The chapter structure is as follows:

Chapter 1: Introduction

Chapter 2: Literature review A review of the measurement and modelling techniques used in regards to the optical remote sensing of plant physiology and light use efficiency.

Chapter 3: Leaf-level experiment. A leaf level study explored the effects of reductions in photosynthetic efficiency due to an imposed stressor on apparent reflectance.

Chapter 4: Regional scale photosynthesis efficiency Simple models were developed between airborne hyperspectral reflectance indices, satellite observations of land cover and airborne eddy covariance measurements to estimate photosynthetic efficiency across in a sub-Arctic region.

Chapter 5: Modelling chlorophyll fluorescence. A leaf level mechanistic model of the dynamic energy flow through photosystem II was coupled to a radiative transfer model to predict dynamic changes in fluorescence as a function of time. The model was inverted using an Markov Chain Monte Carlo (MCMC) algorithm and is a precursor to a full canopy scheme.

Chapter 6: General conclusions

Chapter 2

Measurement and modelling of physiological reflectance and radiance signals

2.1 Measurement of physiological reflectance and radiance signals

2.1.1 Reflectance spectroscopy

A reflectance spectrum, as measured by spectroradiometry, is obtained by taking the ratio of reflected radiance to incident irradiance in many narrow wavebands (typically in the visible to near-infrared regions of the electromagnetic spectrum). Leaf reflectance spectra have an instantly recognisable shape (see figure 2.1) which is due to strong absorption by plant pigments in the visible regions. Measurements of leaf reflectance spectra are referred to as *apparent* reflectance spectra. This is because the measured signals contain additional radiant flux from sources such as chlorophyll fluorescence and/or atmospheric scattering.

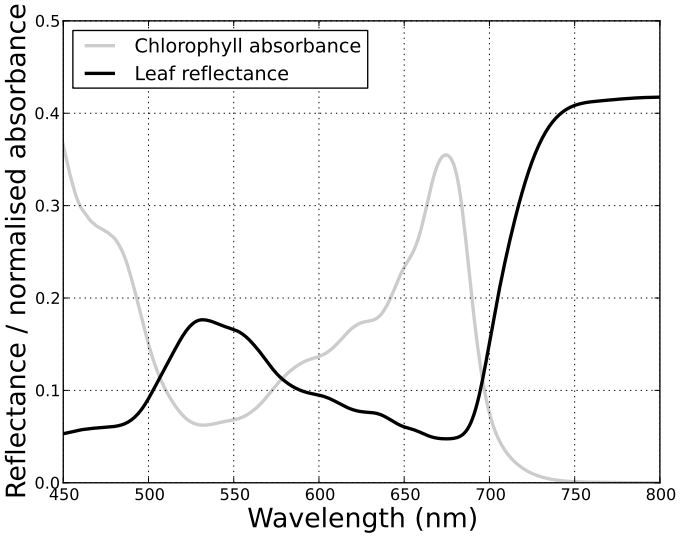

Figure 2.1: Example leaf reflectance and chlorophyll absorbance spectra (modelled using $PROSPECT$).

2.1.2 The Photochemical Reflectance Index

The xanthophyll cycle

Under conditions of strong sunlight, exacerbated by stress, a plant typically absorbs more energy than can be used in the photosynthetic reactions. Excess absorbed light energy can damage the photosynthetic apparatus through the formation of highly reactive oxygen states (Triantaphylidès *et al.*, 2008). Early chlorophyll fluorescence experiments revealed a photoprotective energy dissipation mechanism, however it was only until relatively recently that the actual mechanism of dissipation, the xanthophyll cycle, was discovered (Demmig-Adams *et al.*, 1987). Because the mechanism had the effect of reducing (or quenching) the yield of chlorophyll fluorescence, it was originally referred to as 'Non-photochemical quenching of chlorophyll fluorescence' (NPQ), a term used in chlorophyll fluorescence induction studies.

The xanthophyll cycle refers to the enzyme driven conversion of the carotenoid pigment violaxanthin (v_x) to zeaxanthin (z_x) via the intermediary pigment antheraxanthin (a_x). Changes in the xanthophyll cycle are driven by a lowering of pH within the lumen and ultimately result in the dissipation of excess energy as heat (Demmig-Adams and Adams III, 1996). The exact mechanisms by which the xanthophyll cycle dissipates the energy are not well understood but there are two main hypotheses. Firstly z_x (and/or a_x) acts like a lightning rod causing energy to be transferred from excited chlorophyll molecules to the carotenoids themselves and dissipated. Alternatively either z_x (and/or a_x) cause structural changes in the excited chlorophyll molecules that induce protonation based heat loss (Demmig-Adams and Adams III, 1996). In reality it is likely that both mechanisms contribute to energy dissipation.

Environmental stress such as drought or low temperatures causes a lowering in the

tolerance of vegetation to excess light levels and an increase in xanthophyll cycle activity (Adams III *et al.*, 1995). Furthermore increased amounts of z_x have been found in plants that undergo prolonged periods of stress, such as low temperature conditions during winter (Adams III *et al.*, 1995). Because v_x and z_x have differing absorption spectra, changes in the xanthophyll cycle can be detected using optical remote sensing. The Photochemical Reflectance Index (PRI)(Gamon *et al.*, 1992) was developed for this purpose.

History and formulation of the Photochemical Reflectance Index

In a pioneering study, Gamon *et al.* (1990) first measured changes in apparent leaf reflectance caused by xanthophyll cycle activity by exposing sunflower leaves to large increases in incident photosynthetically active radiation (PAR). Leaves were first covered with black cloth overnight and then the covers were removed at midday and measurements of spectral reflectance and the relative concentrations of the xanthophyll pigments in the seconds and minutes after the removal were taken. Gamon *et al.* (1990) reported a correlation of close to unity ($R^2 = 0.99$) between xanthophyll cycle activity, quantified as the relative size of xanthophyll pigments (or the de-epoxidation state, DEPS) and reflectance changes at 531 nm. Interestingly, in the same study Gamon *et al.* (1990) also reported changes in apparent reflectance at 685 nm and 738 nm due to the quenching of chlorophyll fluorescence. Following this Gamon *et al.* (1992) formulated the PRI as:

$$PRI = \frac{\rho_{Ref.} - \rho_{531}}{\rho_{Ref.} + \rho_{531}} \tag{2.1}$$

Where $\rho_{Ref.}$ denotes reflectance at a reference waveband and ρ_{531} denotes reflectance at 531 nm.

Normalised difference indices, such as the PRI, are designed to increase the signal-to-noise ratio of spectral observations. By definition, a difference index is calculated as the difference between a *reference* band and a *detection* band. The detection band is chosen to be most sensitive to the process, in the case of xanthophyll cycle activity a wavelength of 531 nm, ρ_{531} is used. The reference band, $\rho_{Ref.}$, is chosen to be insensitive to the process in question (the signal) but sensitive to other processes that may influence the detection band (the noise). By taking the difference between the reference band and the detection band, changes in reflectance in the detection band that are not related to the process in question, such as directional sunlight effects, are largely cancelled out.

As the xanthophyll cycle acts as a photo-protective mechanism to dissipate excess absorbed light energy, and because a key response to environmental stress is a reduction in the efficiency of the photosynthetic reactions leading to an excess of absorbed light energy, the PRI is able to track changes in photosynthetic efficiency due to stress. In the study in which PRI was first formulated Gamon *et al.* (1992) developed empirical models between PRI measurements and measurements of leaf-level light used efficiency (LUE). Peñuelas *et al.* (1995) investigated the link between PRI, gas exchanges measurements and $\Delta F/F'_m$ across a range of species in laboratory and field studies and found strong functional relationships between the different parameters of photosynthetic efficiency. Therefore the key finding of the early leaf level studies (Gamon *et al.*, 1990, 1992, 1993; Peñuelas *et al.*, 1995) was that there was now a spectral reflectance method for detecting changes in photosynthetic functionality on short timescales, that was simply not possible by using chlorophyll-based indices such as the Normalised Difference Vegetation Index (NDVI).

The xanthophyll cycle is not the only biological process that influences the PRI signal. On diurnal timescales, PRI is primarily a function of the xanthophyll cycle, however over longer periods (weeks to months) PRI is a function of the

xanthophyll cycle and changes in pool sizes of carotenoid and chlorophyll (Filella *et al.*, 2009). Guo and Trotter (2004) found strong relationships between the PRI signal and the ratio of carotenoids to chlorophyll, a recent modelling study confirmed this result (Garrity *et al.*, 2011).

Scaling PRI to the canopy

Gamon *et al.* (1992) recognised the potential of PRI for use as a canopy scale indicator of photosynthetic efficiency. Gamon *et al.* (1997) followed up the early leaf level work by conducting plot scale measurements of PRI using a tram system. The first airborne canopy study was conducted by Nichol *et al.* (2000), who identified a strong linear relationship between observations of canopy PRI made using a helicopter mounted spectrometer and eddy covariance tower based measurements of LUE for coniferous and deciduous species in the Canadian Boreal forest. Nichol *et al.* (2002) found a weaker relationship in a similar study conducted using helicopter measurements of PRI and flux tower estimates of LUE over Siberia and identified several factors that may act to weaken the PRI-LUE relationship at the canopy scale including: i. stand structural features such as low Leaf Area Index (LAI) values; ii. strong understory reflectance signals; iii. seasonal changes in pigment composition; iv. atmospheric effects.

Space-based observations of PRI

Several studies have attempted to relate Moderate Resolution Imaging Spectroradiometer (MODIS) based PRI observations to flux tower derived estimates of LUE (Rahman *et al.*, 2004; Drolet *et al.*, 2005, 2008; Garbulsky *et al.*, 2008; Goerner *et al.*, 2009) with varying degrees of success. The MODIS sensor has a

spectral band centred at 531 nm which was designed for use in ocean applications and therefore has a coarse spatial resolution of 1 km^2. However, perhaps the most important limitation identified in the MODIS studies was the extreme sensitivity of the PRI - LUE relationships to the sensor and solar geometry. As two consecutive MODIS observations can be at completely different view angles this proved to be a major issue.

The sensitivity of reflectance measurements to view and sensor geometries is a generic problem in Earth observation research, and is mathematically formalised as the bidirectional reflectance distribution function (BRDF). If the BRDF can be estimated, then observations from different angles can be compared by adjusting measurements to a standardised geometry. In most cases the BRDF is defined by the physical directional properties, referred to as the anisotropy, of the surface. However PRI is different to other indices (such as the NDVI) in that the biological processes that PRI quantifies are sensitive to changes in incident light levels. In effect, the BRDF of PRI is a function of canopy physics *and* short term changes in canopy biology.

In part, Drolet *et al.* (2008) circumvented the view angle issue by partitioning data into forward-scatter (dark regions of the canopy) and back-scatter (the so called canopy hot spot) groupings, and found improved relationships with LUE for back-scatter only observations. However if the use of PRI was to become operational a more robust method was needed.

Multi-angular measurements of PRI

To infer LUE from space using PRI it is neccessary to disentangle the biological from the physical view angle effects. One way to separate the biological directional effects from the physical directional effects is to consider the influence of canopy

shadow fraction, α_s, on reflectance measurements. Hall *et al.* (2008) used radiative transfer theory to establish a relationship between shadow fraction and PRI. In effect, Hall *et al.* (2008) showed that only a normalised difference index that was sensitive to physiology driven changes in a particular band would vary as a function of shadow fraction.

Building upon the previous work of Hall *et al.* (2008) and empirical canopy measurements that validated this theory (Hilker *et al.*, 2008), Hall *et al.* (2011) proposed that the rate of change of PRI with respect to shadow fraction, $\partial PRI/\partial\alpha_s$, should be used to quantify LUE from space rather than PRI alone. This is because the relationship between $\partial PRI/\partial\alpha_s$ and LUE is independent of sun-observer geometries and other non-physiological effects (in contrast to the relationship between the PRI signal and LUE). Hall *et al.* (2011) also reiterated the need for accurate atmospheric correction when deriving estimates of LUE from space-borne PRI and/or $\partial PRI/\partial\alpha_s$ observations. Hilker *et al.* (2011) used multi-angular satellite data from the CHRIS/PROBA sensor to demonstrate that $\partial PRI/\partial\alpha_s$ could be used to empirically model LUE from space with a coefficient of determination of $R^2 = 0.68$.

2.1.3 Passive remote sensing of chlorophyll fluorescence

A similar and complementary avenue of research to PRI is the passive remote sensing of chlorophyll fluorescence. Chlorophyll fluorescence is often referred to as the *probe* of photosynthesis (Bolhar-Nordenkampf *et al.*, 1989; Baker, 2008), and is measurable using optical remote sensing techniques as well as a suite of active instruments known as fluorometers.

Chlorophyll fluorescence is the re-emission of absorbed radiation at longer wavelengths. Chlorophyll fluorescence occurs when an electron in an electronically

excited chlorophyll molecule falls to a lower energy state thereby emitting a photon. Chlorophyll fluorescence competes with photochemistry (the photosynthetic reactions), constitutive heat dissipation, and regulatory heat dissipation (NPQ) as an alternate pathway for absorbed light energy. Because the pathways are in direct competition, there is an intrinsic, biochemical link between chlorophyll fluorescence and photosynthetic efficiency. Each energy dissipation pathway can be thought of as a yield, with the sum of all the yields equal to unity. Yields are properly defined as the ratio of the rate constant of the process of interest (chlorophyll fluorescence, heat dissipation, photochemistry) to the sum of all the rate constants. The rate constants are derived from a system of differential equations, thereby firmly routing chlorophyll fluorescence theory in quantitative modelling (Blankenship, 2002). More intuitively, yields can thought of as the probability that absorbed light will follow a particular pathway.

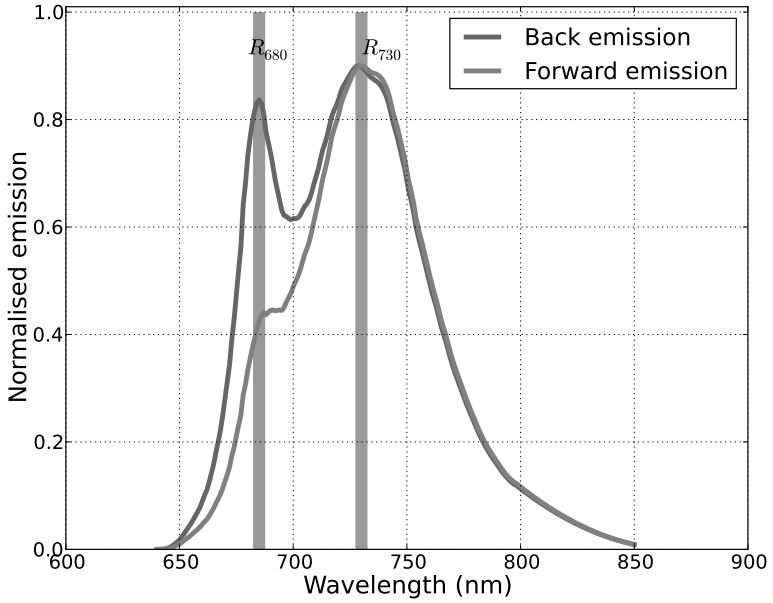

Figure 2.2: Chlorophyll fluorescence emission spectra for forward and backward directional emission

Figure 2.2 highlights that the chlorophyll emission spectrum of a leaf is characterised by two relatively broad (> 10 nm) peaks, which are centred at approximately 690 nm and 730 nm and referred to as red and far-red fluorescence respectively (see figure 2.2). In leaf tissue, the magnitude of the red peak is reduced by chlorophyll re-absorption (Krause and Weis, 1991) and the ratio between the two peaks is therefore a function of chlorophyll concentration (Rosema *et al.*, 1991). Chlorophyll from photosystem II (PSII) contributes exclusively to the shorter wavelength fluorescence peak, whereas the far-red fluorescence is a mixture of mostly PSII fluorescence with some PSI fluorescence. The fraction of far-red fluorescence arsing from PSI is known to increase when temperatures are sufficiently low (Krause and Weis, 1991).

The efficiency or yield of fluorescence is dependent on a number of factors including incident light level and stress conditions, such as low temperatures, but is typically around 3-5% of absorbed radiation. Rapid changes in the kinetics of chlorophyll fluorescence emission can be stimulated by transferring leaves from the dark to the light. The curve that results from the kinetics is known as the Kautsky curve (after Kautsky and Hirsch (1931)) and has been the subject of considerable study by plant ecophysiologists (see Maxwell and Johnson (2000) for introduction to techniques). Several parameters that relate to LUE can be derived from Kautsky kinetics, including the effective quantum yield (also known as the Genty *et al.* (1989) parameter), $\Delta F/F'_m$, using specialist instruments such as Pulse Amplitude Fluorometers (PAMs).

The influence of chlorophyll fluorescence on the apparent reflectance spectrum

At the leaf level chlorophyll fluorescence accounts for approximately 10 - 20% of the apparent reflectance spectrum, depending on the relative levels of photochemical and non-photochemical quenching and wavelength (Campbell *et al.*, 2008). Measurements of reflectance spectra alone cannot be used to derive radiometric estimates of chlorophyll fluorescence. However, reflectance spectra can be used to measure relative changes in chlorophyll fluorescence by identifying the bands where the fluorescence signal is expressed and deriving/calculating fluorescence based SVIs.

Early work by Buschmann and Lichtenhaler (1987) and Lichtenthaler (1989) established the contribution of chlorophyll fluorescence to apparent leaf reflectance at far-red and near-infrared wavelengths. In the same study that pioneered the use of reflectance spectroscopy to measure changes in the xanthophyll cycle, Gamon *et al.* (1990) reported changes in leaf reflectance at red (685 nm) and infrared wavelengths (738 nm) after dark-adapted sunflower leaves were exposed to high levels of solar irradiation. Gamon *et al.* (1990) compared these changes to PAM measurements and found a near identical Kautsky curve trace proving that spectral reflectance measurements could be used to monitor chlorophyll fluorescence kinetics. By taking the time difference between a reflectance spectrum measured at low levels of incident radiation ($\sim$ 10 μmol m^{-2} s^{-1}) and a spectrum measured at high levels of incident radiation ($\sim$ 1900 μmol m^{-2} s^{-1}), Gamon *et al.* (1990) was able to elucidate the double peak, Gaussian-like shape of the chlorophyll fluorescence emission spectrum.

The chlorophyll emission wavelengths overlap with longer wavelength chlorophyll absorption, leading to the re-absorption of emitted red fluorescence. This complicates the interpretation of chlorophyll fluorescence and has important

implications for seasonal and tran-seasonal studies as well as radiative transfer modelling. Lichtenthaler (1989) identified the effects of changing chlorophyll pool size on the fluorescence flux and devised a correction factor by taking the ratio between the two peak values of the chlorophyll emission spectra. Because the shorter wavelength peak is strongly affected by re-absorption, this ratio correlates with the total pool size. Gitelson *et al.* (1999) used this ratio to predict leaf chlorophyll content with very high levels of accuracy ($R^2 > 0.95$), although these retrievals were conducted with chlorophyll emission spectra obtained from an active instrument.

Zarco-Tejada *et al.* (2000a) measured and modelled (using radiative transfer) changes in apparent reflectance due to chlorophyll fluorescence at the leaf scale. This work formulated a number of fluorescence-based reflectance indices and also utilised a long-pass filter to isolate the fluorescence signal from the reflectance signal. A companion study then used airborne data to scale apparent reflectance observations to the canopy scale, by developing relationships between ground-based measurements of F_v/F_m and airborne measurements of fluorescence-based spectral reflectance measurements (Zarco-Tejada *et al.*, 2000b).

In addition to fluorescence based indices calculated using reflectance spectra, first derivative reflectance indices have also been used to calculate vegetation indices to detect the chlorophyll fluorescence signal (Zarco-Tejada *et al.*, 2003). Reflectance spectra can also be used to measure changes in the shape of the fluorescence emission spectrum though the calculation of 'difference spectra'. Difference spectra are calculated as the difference between individual spectral measurements and the resultant residuals (as a function of wavelength) are representative of the fluorescence contribution to the apparent reflectance. Difference spectra can either be calculated by measuring apparent reflectance as a function of time (Gamon *et al.*, 1990) or by using a filter-based system (Zarco-Tejada *et al.*, 2000a; Campbell *et al.*, 2008). Chlorophyll fluorescence absorption mainly occurs in

the visible wavelengths (< 700 nm), by filtering an artificial source for these wavelengths and then remeasuring the same target with an unfiltered source a difference spectrum is obtained.

In a series of experiments that subjected grapevines to heat and water stress Dobrowski *et al.* (2005) analysed the relationships between various fluorescence based spectral reflectance indices and parameters of photosynthetic efficiency. This study concluded that although spectral indices could track stress induced changes in photochemistry there was no single, consistent relationship between the rate of photosynthesis and fluorescence. Dobrowski *et al.* (2005) further found a negative relationship between steady state fluorescence , F_t, and photosynthetic rate under low light conditions, early in the diurnal cycle. Under warmer and higher light conditions this relationship reversed and F_t was found to be positively correlated with photosynthetic rate. The authors hypothesised that as temperature and light levels increased a shift occurred from photochemical to non-photochemical quenching accounting for the reversal of the relationship. Flexas *et al.* (2000) studied the effects of water stress on F_t using a custom built fluorimeter and found a marked reduction in F_t under highly irradiated, water stressed conditions, also signalling an induction of non-photochemical quenching.

In a relatively recent study Campbell *et al.* (2008) analysed the percentage contribution of fluorescence to apparent reflectance spectra for maple, corn and soybean. Campbell *et al.* (2008) found significant differences between the species, with the maple leaves emitting significantly more fluorescence than the other two species.

The infilling technique

The Fruanhofer infilling technique facilitates the measurement of solar induced fluorescence in radiometric units, provided that coincident (in time) measurements of solar irradiance and target (plant matter) radiance can be made. Work conducted in the mid 1970s by Plascyk and Gabriel (1975); Plascyk (1975) first developed a helicopter mounted passive instrument capable of retrieving radiometric solar induced fluorescence by exploiting Fraunhofer lines. Fraunhofer lines are dark, narrow regions of the solar spectrum caused by the absorption properties of gases in the Sun and Earth's atmosphere. Several of these lines, in particular the solar Hα line centred at 656 nm, and the telluric (Earth based) lines due to O_2 absorption close to 687 nm and 761 nm, occur in the same spectral region as chlorophyll fluorescence, which in comparison to the Fraunhofer lines is relatively broad. In effect, the chlorophyll fluorescence emission illuminates the dark regions and can therefore be retrieved by comparing a measurement of the dark region without the emission to an infilled measurement. Figure 2.3 presents a graphical representation of the retrieval technique, as well as the equations that are used to solve for the infilled radiometric fluorescence flux.

The standard version of the Fraunhofer Line Depth/Discriminator (FLD) algorithm as shown in figure 2.3 assumes constant reflectance, r, and fluorescence, F, at the two measured wavelengths. In reality this is often not the case, hence the development of a number of improved FLD methods. These include the 3FLD method (Maier *et al.*, 2003) and the $iFLD$ method, which uses linear correction coefficients to correct for the assumptions in the original algorithm. A comprehensive review of the many variants of the FLD algorithm can be found in Meroni *et al.* (2009).

There have been several successful applications of the FLD method towards detecting short term changes in F_S driven by physiology at the canopy scale. Moya

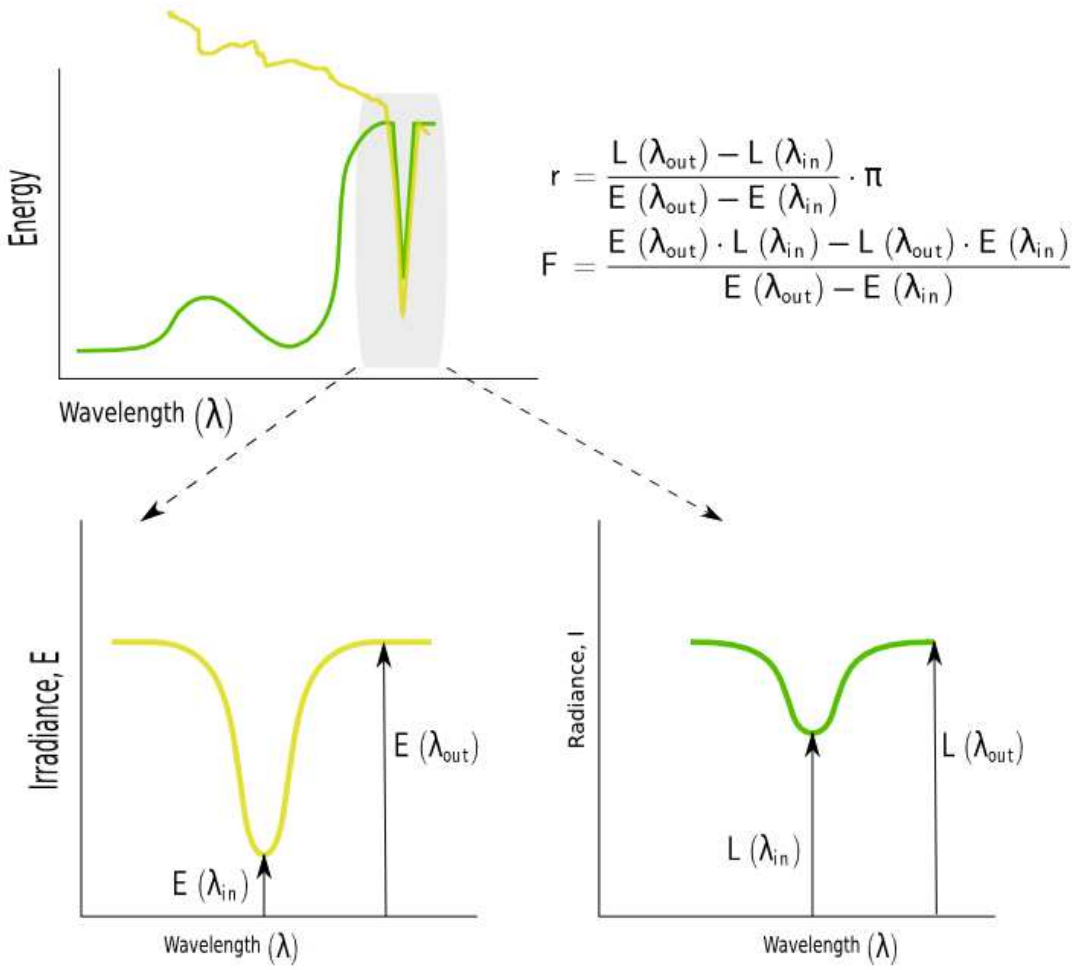

Figure 2.3: Fraunhofer infilling technique. Equations from Meroni *et al.* (2009).

(2004) used a custom built instrument to detect increases in F_S in a herbicide treated maze canopy, that were concomitant with reductions in photosynthetic rate and conductance. Perez-Priego *et al.* (2005) successfully used the infilling method to detect reductions in F_t of water stressed trees using an above-canopy mounted spectrometer. In a series of experiments, Damm *et al.* (2010) measured F_t and PRI over various crop types as well as measuring carbon exchange using the eddy covariance technique. Damm *et al.* (2010) found a strong correlation between F_t and flux-tower estimates of LUE, after a time-shift correction had

been applied to account for footprint mismatches between the two system. In effect the canopy spectrometer was *looking* at a different footprint to the one used by the flux system and the time shift correction was used to account for this discrepancy. The Damm *et al.* (2010) study highlighted the potential for the use of F_t in LUE based models. In a novel recent study, Zarco-Tejada *et al.* (2012) applied several variants of the infilling algorithm to retrieve chlorophyll fluorescence using a micro-hyperspectral camera on-board an Unmanned Aerial Vehicle (UAV).

Fluorescence from space

The FLourescence EXplorer (FLEX) project (Rascher *et al.*, 2008) is a current proposal for a new space mission submitted to ESA in 2006, which as of November 2010 was moved to Phase-A status. Phase-A/B1 status means that FLEX is one of two possible missions that will be selected for launch. FLEX has generated a significant body of work that has significantly advanced the understanding and interpretation of the F_t signal, including the FluorMOD modelling project and SEN2FLEX field campaigns.

The first space retrieval of F_t using the FLD method was conducted by Guanter *et al.* (2007). Guanter *et al.* (2007) used data from the MEdium Resolution Imaging Spectrometer (MERIS), which has a band at 760.6 nm and another at 753.8 nm, to calculate F_t for an area of experimental green vegetation constructed as part of the SEN2FLEX project. Guanter *et al.* (2007) measured F_t signals that were of similar magnitude to ground-based observations, which suggested that the technique had potential. Joiner *et al.* (2011) applied the FLD method to data collected by the Fourier-Transform Spectrometer aboard the GOSAT platform, and produced both global and seasonal estimates of F_t from space.

Space estimates of F_t are complicated by atmospheric scattering effects that can bias the resulting retrievals which are not present in near-surface measurements. Therefore careful characterisation and correction of the atmospheric state is needed. Frankenberg *et al.* (2011a) developed an improved version of the FLD method using a least-squares method, to separate atmospheric scattering from fluorescence. Frankenberg *et al.* (2011b) compared retrievals of F_t from the improved space-borne retrieval using data from GOSAT to modelled GPP estimates and found strong, positive relationships.

2.2 Modelling of physiological reflectance and radiance signals using radiative transfer and biochemical models

Radiative transfer models complement empirical studies by grounding measurable quantities in physical theory. In addition, radiative transfer models can be used to retrieve biophysical parameters such as leaf chlorophyll content through model *inversion*. Radiative transfer models simulate remote sensing signals through the mathematical abstraction of the physical processes that produce such signals. The processes and mathematical formula that are used to simulate remote sensing signals depend on the scale of the system. In general most models either simulate leaf scale signals or canopy scale signals.

Pigments such as chlorophyll absorb electromagnetic radiation in the visible wavelengths. Therefore pigment pool sizes are typically represented in leaf models as model parameters. In full canopy simulations structural parameters such as LAI influence the observable signal and are used as parameters. The process of

model inversion involves fitting model predictions to measurements in order to retrieve accurate estimates of model parameters, such as chlorophyll content.

Model calibration, validation and inversion

Model **calibration** refers to the process of tuning model parameters to match observed states that are predicted by the model. Model **validation** refers to the process of testing (tuned) models with independent data. Both calibration and validation are important aspects of developing land surface and radiative transfer models. In classical statistics, parameters of models are considered as fixed point estimates. This is in contrast to Bayesian statistics, where parameters are assigned probability distributions. Parameters are often ill-defined and/or unobservable in complicated models, and as such the Bayesian framework is particularly suited to ecological modelling (Reichert and Omlin, 1997). This distinction, combined with computing advances (both in Bayesian algorithms and hardware resources), means that Bayesian techniques of estimating model uncertainty are increasingly popular with the ecological modelling community (Quaife *et al.*, 2008; Hill *et al.*, 2011b; Williams *et al.*, 2005; Malve *et al.*, 2007; Laine, 2008).

Model inversion typically involves using numerical algorithms to find an optimum set of parameters that best predict measured data. In effect, the aim of model inversion is to find the optimum calibration. Bayesian methods such as Markov Chain Monte Carlo, MCMC[1], offer arguably more flexibility than traditional least squares algorithms when dealing with complex models and large parameter spaces.

Data assimilation is the process of using statistical algorithms to fuse data and model predictions with the aim of improving the predictions (by reducing error). Although data assimilation is cosmetically similar to inversion, data

[1]MCMC methods are based on the pioneering work of Metropolis *et al.* (1953), see Laine (2008) for some recent ecological applications of MCMC

assimilation is generally concerned with estimating model states (predicted quantities that change with time), whereas inversion focuses on retrieving model parameters. Recent work has used data assimilation methods to combine remote sensing measurements with process-based models in order to better constrain model estimates of carbon fluxes (Quaife *et al.*, 2008). Such models utilise radiative transfer models as the interface between measurements and the biological processes (states) that give rise to the changes in such signals.

2.2.1 Leaf and canopy radiative transfer models

Leaf radiative transfer models, such as PROSPECT (Jacquemoud and Baret, 1990), are used to simulate the spectral properties of leaves and can be coupled to canopy radiative transfer models, such as the Scattering by Arbitrary Inclined Leaves (SAIL) model (Verhoef, 1984) to simulate canopy level reflectance.

2.2.2 *PROSPECT*

PROSPECT (Jacquemoud and Baret, 1990) was originally designed to model broad-leaf spectral properties but has also been applied to needleleaf species in its standard form (Zarco-Tejada *et al.*, 2004) and in a modified form (Moorthy *et al.*, 2008). PROSPECT is based on the plate theory of radiative transfer (Allen *et al.*, 1969, 1970) where the leaf is considered as consisting of a number of horizontal stacked layers. Each layer is then assumed to contain several absorbing species (chlorophyll, water, other pigments and substances) that absorb light, and the (non-smooth) plate boundaries are assumed to cause isotropic scattering. Because the absorbance properties of the individual substances are known apriori, a number of equations can be derived to solve for the path of light through the plates in terms of absorbance, transmittance and reflectance.

2.2.3 Radiative transfer simulations of chlorophyll fluorescence

The literature on the radiative transfer modelling of chlorophyll fluorescence is relatively sparse, however there are at least two models currently in use: i. the Rosema *et al.* (1991) model and ii. the flourMOD model (Miller *et al.*, 2005). Rosema *et al.* (1991) developed a leaf and canopy level chlorophyll fluorescence model to simulate laser-induced fluorescence. The model was based on the Kubelka-Monk system of differential equations which models fluorescence as upward and downward propagating fluxes. The leaf-level chlorophyll fluorescence model, fluspect, which is implemented in the SCOPE land-surface scheme (van der Tol *et al.*, 2009b) is an updated version of the Rosema *et al.* (1991) model.

The development of the FluorMOD model (Miller *et al.*, 2005) was undertaken by the European Space Agency (ESA) as a precursor to the FLEX mission. This work resulted in a leaf model, FluorMODleaf (Pedrós *et al.*, 2010), and a full canopy model, FluorMOD. FluorMODleaf was largely based on the PROSPECT (Jacquemoud *et al.*, 2009) model. The key challenge for a fluorescence radiative transfer model was accurately modelling the effects of re-absorption on the emitted flux. Like PROSPECT, FluorMODleaf considers the leaf as a stack of plates, each plate acts like a network both transmitting and absorbing radiation to varying amounts dependant on the pigment pool concentrations in the plates. From these plate networks a series of equations can be derived that allows the upward and downward emitted fluxes of fluorescence to be solved for, as a function of the incident radiation and a source function representing the quantum yield of fluorescence (ϕ_f). Pedrós *et al.* (2010) compared FluorMODleaf to a Kubelka-Monk type model and found that FluorMODleaf more accurately simulated the effect of increasing chlorophyll concentration on the emission.

Middleton *et al.* (2008) compared FluorMOD simulations to observations of

chlorophyll fluorescence above a corn canopy. The default version of FluorMOD performed poorly in this study, however when a revised version of FluorMOD was used good agreement was found between measurements and simulations.

Canopy radiative transfer models contain parameters such as chlorophyll content and canopy structure that directly affect net rates of photosynthesis and the surface energy balance. The Soil Canopy, Photochemistry and Energy fluxes model ($SCOPE$) model (van der Tol *et al.*, 2009b,a) consists of a physiological leaf model coupled to a radiative transfer model and is designed to predict chlorophyll fluorescence as well as a range of other canopy states such as net photosynthesis.

2.2.4 Radiative transfer and biochemical simulations of PRI

To date, there have been relatively few studies that use radiative transfer modelling to simulate the PRI signal. This is, at least in part, due to the fact that the reflectance changes that are quantified by the PRI occur at longer wavelengths than the changes in the equivalent measurable xanthophyll absorption spectra. The issue of wavelength shifts between absorption spectra *in vitro* and spectra measured *in vivo* are not unique to xanthophyll pigments. Shifts in the order of 10 nm also occurs with chlorophyll and other carotenoids (Jacquemoud *et al.*, 1996). Jacquemoud *et al.* (1996) ascribed the differences as being due to a combination of solvent effects and the fact that *in vivo* pigments are usually found in complex multi-pigment/protein structures. PROSPECT accounts for this by using empirically obtained specific absorption coefficients (SACs) for mixtures of pigments and proteins. The newest version of PROSPECT (v5) (Feret *et al.*, 2008) includes the specific absorption coefficients (SACs) for bulk carotenoids (β-carotenes, xanthophylls and others), but as of yet, no SACs exists for the relative contributions of the pigments of the xanthophyll cycle.

Although there is no explicit radiative transfer model capable of simulating PRI, a limited number of sensitivity studies have been conducted using canopy radiative transfer models to assess the effects of extraneous factors on the PRI signal. Barton and North (2001) used a 1-dimensional ray tracing canopy radiative transfer model to characterise the effects of canopy architecture and solar geometry on the PRI signal and found that PRI was particularly sensitive to LAI. Suárez *et al.* (2009) coupled PROSPECT 4 with SAIL and a 3D version of FLIGHT to predict spectral signals over a corn canopy and orchards respectively and found that the signal was affected by structural parameters such as LAI and sun-sensor geometry. In a recent study Garrity *et al.* (2011) compared predictions made with the latest version of PROSPECT (v5) to measurements of chlorophyll and carotenoid concentrations and found very strong relationships ($R^2 > 0.95$) between the ratio carotenoid/chlorophyll pool and modelled PRI.

Over the past 20 or so years several dynamic biochemical models that predict changes in NPQ and xanthophyll pool sizes as a function of time have been developed (Sielewiesiuk and Gruszecki, 1991; Porcar-Castell *et al.*, 2006; Ebenhöh *et al.*, 2011). Although these models typically operate on the scale of the photosynthetic unit rather than the leaf and calculate dynamics on very short ($<$ 1 second) and short (seconds and minutes) time-scales, they have the potential to be adapted for the dynamic prediction of PRI providing a suitable radiative transfer scheme is realised.

Chapter 3

Remote sensing of transplant shock

Paper title: The utility of optical remote sensing for characterising changes in the photosynthetic efficiency of Norway maple (*Acer platanoides* L.) saplings following transplantation

Accepted for publication in: *International Journal of Remote Sensing*

Abstract

Following outplanting, trees undergo a period of stress known as transplant shock. Tree mortality rates are known to increase during this period; monitoring the effects of transplant shock is therefore key to improving the future survival rates of outplanted trees. Leaf reflectance spectra, measured by field spectrometry, can be used to derive reflectance indices that are related to a number of biophysical parameters including photosynthetic efficiency and leaf chlorophyll content. Field spectrometry has the advantage of being non-invasive and relatively cheap and is therefore a suitable candidate for the monitoring of the effects of transplant shock. The objective of this study was to assess the applicability of passive remote sensing as a tool to measure the reduction, and the subsequent recovery, of photosynthetic efficiency during the weeks following transplantation. Spectral reflectance, gas exchange and chlorophyll fluorescence measurements of Norway maple (*Acer platanoides* L.) saplings were collected over an 8 week period, following transplantation from a glasshouse to an outdoor environment. Very low photosynthetic rates were measured in the week after outplanting. This was followed by a gradual increase in measured photosynthetic rates, with recovery occurring several weeks after transplantation. Spectral data were collected on newly planted saplings in both clear and cloudy conditions, and the relationships between spectral reflectance indices, photosynthetic light use efficiency (LUE), and the quantum yield of photosystem II (estimated using the fluorescence parameter $\Delta F/F'_m$) were explored. The Photochemical Reflectance Index was weakly to moderately correlated with LUE ($R^2 = 0.22$, $p < 0.05$), $\Delta F/F'_m$ ($R^2 = 0.35$, $p < 0.05$) and $PPFD$ ($R^2 = 0.30$, $p < 0.05$). Several chlorophyll-based spectral indices were moderately correlated with LUE, including $ND705$ ($R^2 = 0.45$, $p < 0.05$). As with LUE, there was a marked trend in PRI values over the study period but no trend was observed in chlorophyll-based indices. The study demonstrates that hyperspectral remote sensing, and in particular the PRI, has

the potential to be a useful tool in the detection and monitoring of the dynamic effects of transplant shock.

3.1 Introduction

Transplant shock describes the effects of a number of physiological stresses that occur following "outplanting" (re-planting in a new environment). Transplant shock is characterised by reduced growth and increased mortality rates. The effects of transplant shock are most obvious in the days and months after planting, although reduced growth rates have been recorded several years after outplanting (Zaczek *et al.*, 1997). During the acclimatisation period stored carbohydrates are used for new root growth, but if the stored carbohydrates are exhausted then the tree is at risk of death (Rietveld, 1987). Any number of biotic and abiotic stress factors can contribute to the overall transplant shock effect, including: differences in the light environment or in the nutritional status between the nursery and field, drought stress, frost, mechanical damage or competition with surrounding vegetation (Close *et al.*, 2004).

Measurements of the effects of transplant shock on outplanted trees fall into two broad categories: i. morphological and ii. physiological. Morphological measurements, such as the Tree Planting Index (Zaczek *et al.*, 1997), Transplant Stress Index (South and Zwolinski, 1997) and the Tree Health Index (Anastasiou and Brooks, 2003), are based on repeated measures of tree height before, during and/or after the transplant shock period. Morphological measurements are simple and cheap, however it is only with physiological measurements that detailed information about the underlying biological state of the trees can be obtained. The drawback with physiological measurements is that they can

be time-consuming and difficult to successfully apply and interpret. Examples of physiological measurements include leaf gas exchange (Close and Beadle, 2003), chlorophyll fluorescence (Close and Beadle, 2003) and leaf nitrogen levels (Anastasiou and Brooks, 2003).

Optical remote sensing is a passive, non-destructive technique that has the potential to measure several aspects of the physiological effects of transplant shock. The physiological application of optical remote sensing is a rapidly advancing field and cheap, portable commercial systems are now available for operational use to end-users such as foresters. Leaf-level studies that employ optical remote sensing typically measure the leaf reflectance spectrum (in the visible to near-infrared wavelengths), which is the ratio of reflected radiance to incident irradiance (see figure 3.1). Changes in leaf-level physiology, such as pigment pool sizes, which may occur during the transplant shock period directly affect the measured reflectance spectrum. Spectral bands, defined by their respective wavelengths, that are sensitive to changes in physiology can then be selected to monitor changes in reflectance due to environmental stressors. The characteristic 'red-edge' feature of a leaf spectrum is visible as a sharp increase in reflectance between 675 - 750 nm. The red edge is caused by the contrast between strong chlorophyll absorption in the red region of the spectrum and a lack of absorption in the adjacent near-infrared region (Myneni *et al.*, 1995). Several reflectance indices, usually calculated as the ratio and/or differences between two or more spectral bands, that target the red-edge region of the spectrum have been developed to estimate leaf chlorophyll content across a range of species (Sims and Gamon, 2002).

In addition to leaf chlorophyll content, reflectance spectra can also be used to detect changes in light use efficiency (LUE). LUE is defined as the ratio of photosynthetic rate to absorbed Photosynthetic Photon Flux Density (PPFD), and is an indicator of plant health. The Photochemical Reflectance Index (PRI)

was developed by Gamon *et al.* (1992, 1993) as a way to measure reversible changes in carotenoid pigments, known as the xanthophyll cycle. The xanthophyll cycle is part of a complex system of reactions that acts to dissipate potentially harmful excess absorbed light energy as heat. *PRI* has been widely applied in a range of plant stress studies to gain insight into LUE (Thenot *et al.*, 2002; Meroni *et al.*, 2008; Sarlikioti *et al.*, 2010; Garrity *et al.*, 2011).

Reflectance spectra can also be used to detect changes in chlorophyll fluorescence, a process that is referred to as a 'direct probe' into the photosynthetic apparatus (Bolhar-Nordenkampf *et al.*, 1989; Baker, 2008). Chlorophyll fluorescence is the re-emission of absorbed radiation at longer wavelengths and competes with photosynthesis and heat dissipation as an alternate pathway for absorbed light energy. As well as several reflectance indices that have been specifically developed to measure chlorophyll fluorescence, chlorophyll fluorescence can be measured in absolute radiometric units using a technique known as Fraunhofer infilling (see Meroni *et al.* (2009) for a list of fluorescence indices and a comprehensive review of the literature). Pulse Amplitude Modulated Fluorometers (PAMs) are active instruments that detect rapid changes in the chlorophyll fluorescence signal and can be used to estimate a range of photosynthetic efficiency parameters which reflect the underlying physiological status of the tree. Close and Beadle (2003) used PAM data to investigate the effects of photoinhibition on a sample of transplanted saplings, and found a marked depression in photosynthetic efficiency in the weeks following planting.

The objective of this study was therefore to investigate the applicability of using passive remote sensing methods to detect changes in tree physiology during the transplant shock period. Results are presented from an experiment conducted under natural light conditions in which the photosynthetic recovery of transplanted Norway maple (*Acer platanoides* L.) saplings was investigated

using a combination of gas exchange, PAM fluorescence and spectroradiometer measurements.

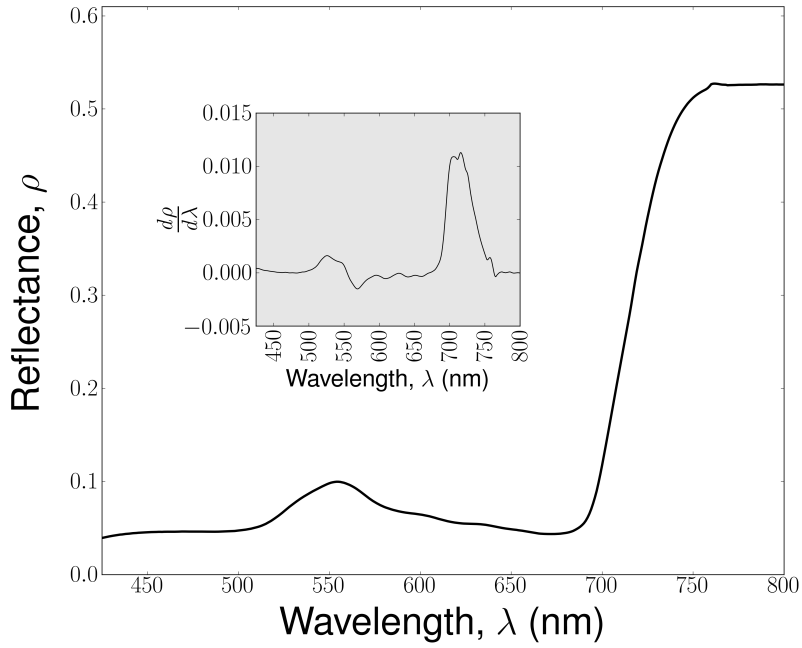

Figure 3.1: Reflectance spectrum with the first derivative of the reflectance spectrum shown in the insert.

3.2 Methods

3.2.1 Bedding and experimental design

A population of 100 Norway maple saplings were planted between the 5th and the 9th June 2008. The saplings were planted on a purpose built plot in a 5 x 20 tree grid formation, at Kings Buildings, University of Edinburgh, UK. The saplings were 2.5 years old and 1.25 to 1.5 m tall at the time of purchase and had previously been stored in a glasshouse for 6 weeks until the leaves

were fully developed. Measurements of leaf reflectance and gas exchange were collected on 7 days during an 8 week period, from planting until the 5th August 2008. PAM fluorescence measurements were not carried out on 23rd June and 16th July but were carried out on all other measurement days. On the 23rd June measurements were collected from 1400-1600 local time, on the 5th August measurements were collected during early morning (0900-0930), midday (1200-1230) and late afternoon (1530-1600). On all other days measurements were collected between the hours of 1000 and 1300.

3.2.2 Spectral measurements

Repeated observations were carried out on leaves from a subset of 20 trees. The 20 trees were located at the southern end of the site, and were chosen for the homogeneity of the light conditions and for ease of access. An Analytical Spectral Devices FieldSpec Pro (ASD Inc., Boulder, CO, U.S.A.) was used to collect spectra in a single sensor biconical configuration. The spectrometer was used in conjunction with an 8° field of view fore-optic. Reflectance spectra were calculated by normalising leaf spectra to measurements of a calibrated, near-lambertian reflective standard (Spectralon, Labsphere, North Sutton, NH, U.S.A). Spectra were collected during both clear sky and cloudy conditions, with each leaf measurement followed by a measurement of the standard. Each spectrum was an average of 25 measurements and three spectra were collected per leaf sampled. Spectra were sampled in the nadir position at a fixed distance from the adaxial side of the leaf, which resulted in a spot radius of 2.81 cm.

3.2.3 Leaf gas exchange and PAM fluorescence

An LCPro+ portable photosynthesis system (ADC Bioscientific Ltd., U.K.) was used to collect measurements of photosynthetic rate at a fixed incident photosynthetic photon flux density (PPFD) of 870 μmol m^{-2} s^{-1}. Photosynthetic light use efficiency (LUE) was calculated as photosynthetic rate / PPFD. The Quantum yield of Photosystem II, $\Delta F/F'_m$, was estimated using a Walz Diving PAM (Heinz Walz GmbH, Effeltrich, Germany) as well as indident PPFD and leaf temperature. Photosynthesis and PAM fluorescence measurements were collected from the same leaves as the spectra, as close in time (under 5 minutes) as possible. A weather station positioned within 500 m of the plot recorded atmospheric pressure, rainfall, air temperature, wind speed, relative humidity, and short-wave radiation at 1 minute intervals.

3.2.4 Reflectance processing and statistics

Statistical analysis and data processing were performed using the Python programming language. For the purposes of exploring the utility of spectral indices for monitoring photosynthetic efficiency during the transplant shock period, a number of spectral reflectance and first derivative indices were calculated (with the formulations and references listed in table 1). First derivative spectra were calculated using a Savitzky-Golay filter (Savitzky and Golay, 1964). A per sample leaf average and standard error was calculated from the repeat spectra. Linear models were developed between spectral indices and LUE, $\Delta F/F'_m$, $PPFD$ and leaf temperature and using the SciPy (Python) statistics library.

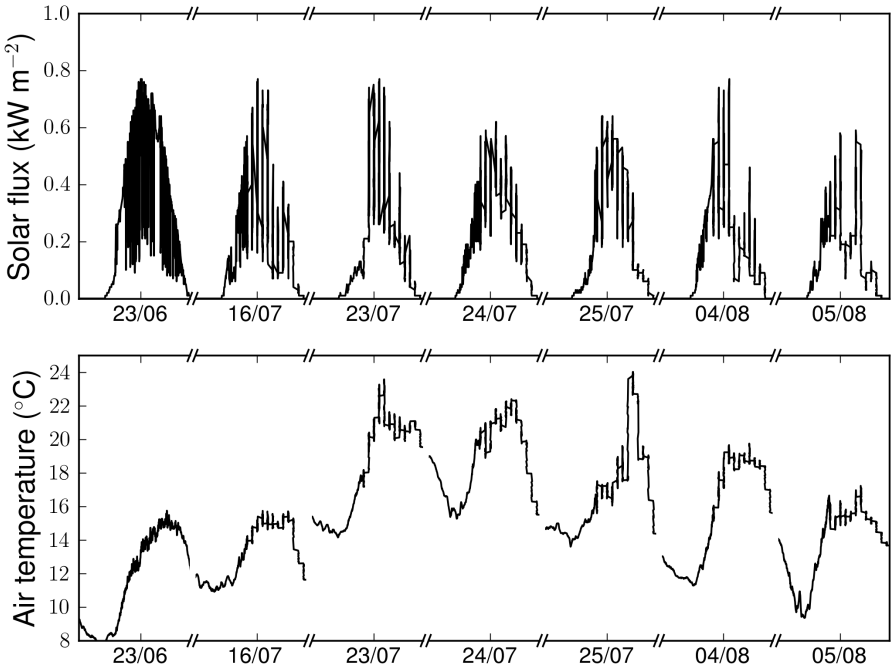

Figure 3.2: Meteorological conditions at the study site during the study period. Top (a) solar flux and bottom (b) air temperature.

3.3 Results

3.3.1 Meteorological conditions

Time series of half hourly average temperature and half hourly average solar flux during the experimental study period are shown in figure 3.2. The experimental period was predominately wet (data not shown) and cloudy. The maximum day time temperature during the study period was 24.7 °C and the minimum night time temperature was 6.34 °C.

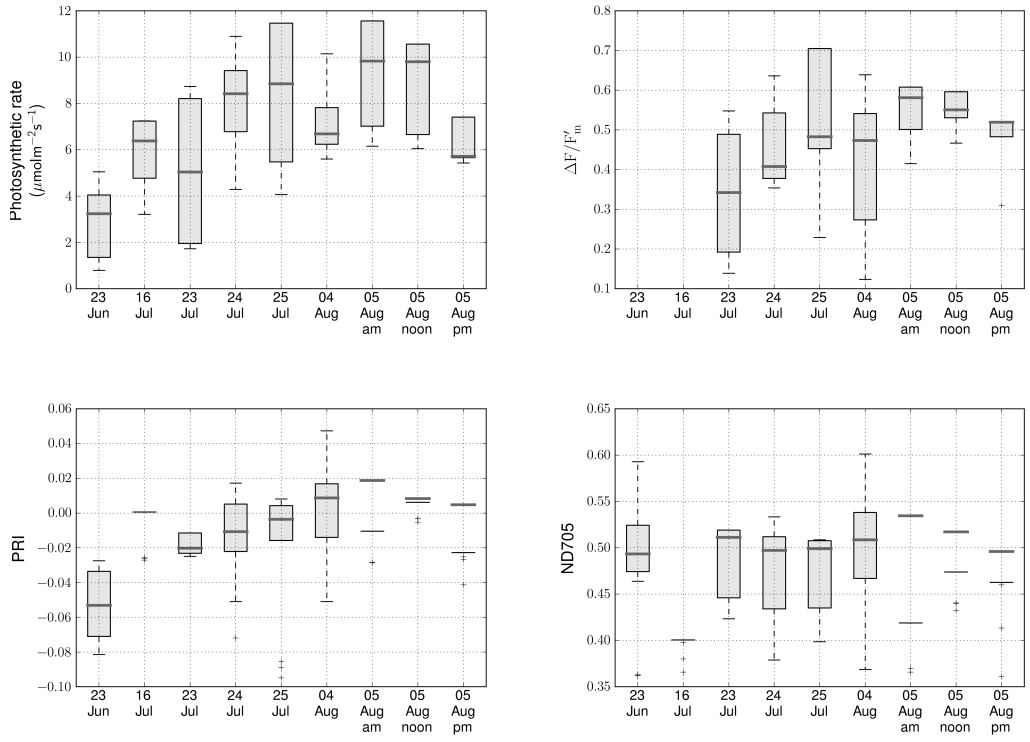

Figure 3.3: Daily distributions of parameters of photosynthetic efficiency and reflectance indices ie during post-transplant acclimatisation. The median, 25th and 75th percentiles are shown by the middle lines, lower limits and upper limits of the boxes. The whiskers represent the maximum and minimum value within 1.5 times the interquartile range, values outside this range are shown as outliers.

3.3.2 Time course of photosynthetic parameters

Daily photosynthetic rate measurements are shown in figure 3.3a. The lowest value of photosynthetic rate, 0.79 μmol m^{-2} s^{-1}, was measured at the start of the sampling period on the 23rd June at 15:26. The maximum value of photosynthetic rate, 11.56 μmol m^{-2} s^{-1}, was measured at the end of the sampling period on the 5th August at 15:26. On the 5th August similar photosynthetic rates were measured during the early morning and noon periods with median values of 9.80 and 9.82 μmol m^{-2} s^{-1} respectively. Reduced photosynthetic rates were

recorded during the late afternoon period (median value 5.71 μmol m^{-2} s^{-1}). All measurements of photosynthetic rate collected during the late afternoon period on the 5th August were greater in value than the maximum photosynthetic rate (5.43 μmol m^{-2} s^{-1}) measured on the 23rd June

The time course of measurements of $\Delta F/F'_m$ are shown in Figure 3.3b. The lowest value of $\Delta F/F'_m$, 0.30, was measured on the 23rd July, the lowest daily median value, 0.43, was measured on the 24th July. The maximum value, 0.70, was measured on the 25th July and the maximum median value, 0.52, occurred on the final day of sampling, 5th August during the early morning period. A slight decrease in $\Delta F/F'_m$ was measured in the noon sampling period on the 5th August, with a median value of 0.55 in comparison with the early morning median of 0.55. A subsequent fall in $\Delta F/F'_m$ values was measured in the late afternoon with a median of 0.52.

3.3.3 Remote sensing of photosynthetic efficiency

Relationships were explored between leaf gas exchange, PAM fluorescence, reflectance indices and meteorological conditions to test the applicability of optical remote sensing for detecting the physiological effects of transplant shock. A suite of spectral indices sensitive to physiological status were analysed by testing the linear dependence of said indices with other parameters of photosynthetic efficiency. These results are summarised in Figure 3.4. A moderate relationship ($R^2 > 0.4$, $p < 0.05$) was found between several chlorophyll-based spectral indices, namely $SR705$, $ND705$, $mND705$, $ND705$, and LUE. A weak to moderate relationship was found between PRI and $\Delta F/F'_m$ ($R^2 = 0.35$, $p < 0.05$) and PRI and $PPFD$ ($R^2 = 0.3$, $p < 0.05$). No significant relationship (all $p >= 0.05$) was found between any of the spectral indices tested and leaf temperature (figure 3.4b).

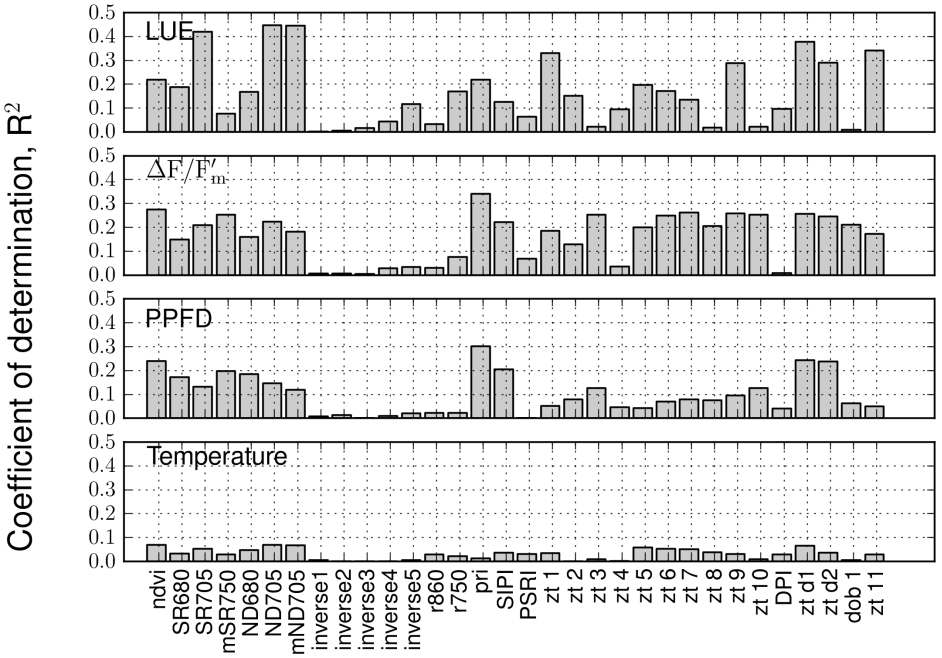

Figure 3.4: Coefficients of determination between a set of spectral reflectance indices and (a) LUE, (b) $\Delta F/F'_m$, (c) PPFD and (d) leaf temperature

Figure 3.3c and figure 3.3d shows time courses for PRI and the chlorophyll-based index, $ND705$, respectively. The lowest median value of PRI, -0.053, occured on the 23rd June with the maximum value, 0.047, recorded on the 4th August. PRI values on the 5th of August are higher in the early morning period when compared to the noon and late afternoon. There is little change in the median $ND705$ medians values over the full time-course of the experiment. However, on the 5th August the highest $ND705$ values are recorded during the early morning period with the lowest values occurring in the late afternoon.

Weak to moderate relationships ($0.25 > R^2 < 0.4$) were found between several

fluorescence-based indices and LUE (figure 3.4a). A moderate to weak relationship was found between a first derivative index, $ZTd2$, and $PPFD$ ($R^2 = 0.28$, $p < 0.05$).

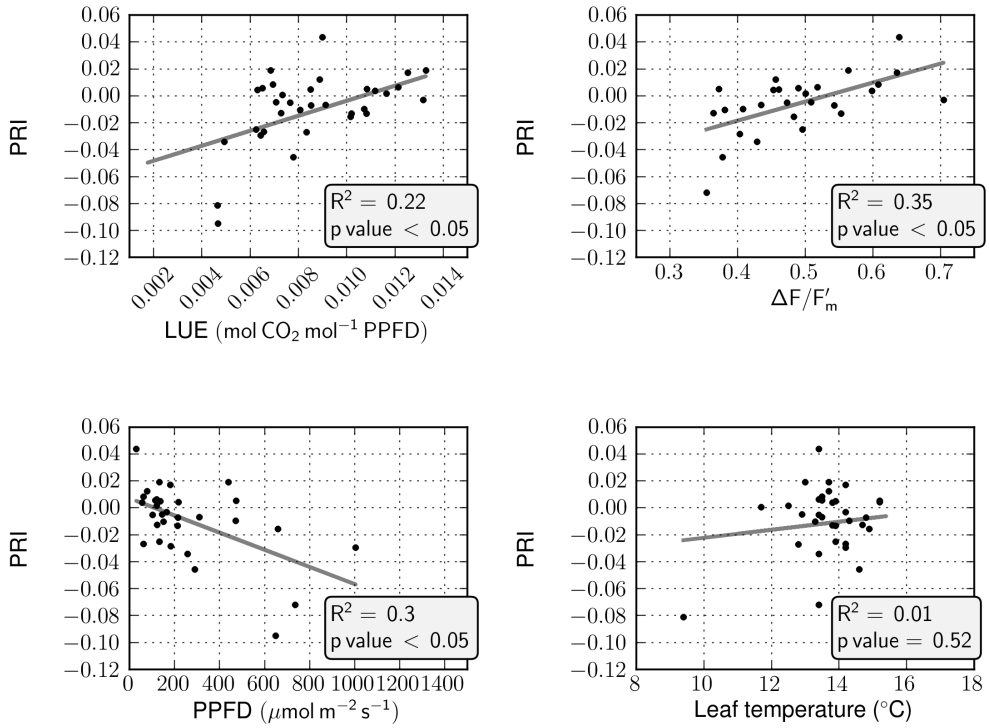

Figure 3.5: Linear regression models for (a) PRI Vs LUE, (b) PRI Vs $\Delta F/F'_m$, (c) PRI Vs PPFD and (d) PRI Vs leaf temperature

3.4 Discussion

This study investigated the applicability of spectral reflectance indices for detecting the physiological effects of transplant shock on Norway maple saplings. The recovery of photosynthetic efficiency of a sample of saplings following outplanting was tracked using gas exchange, chlorophyll fluorescence parameters and

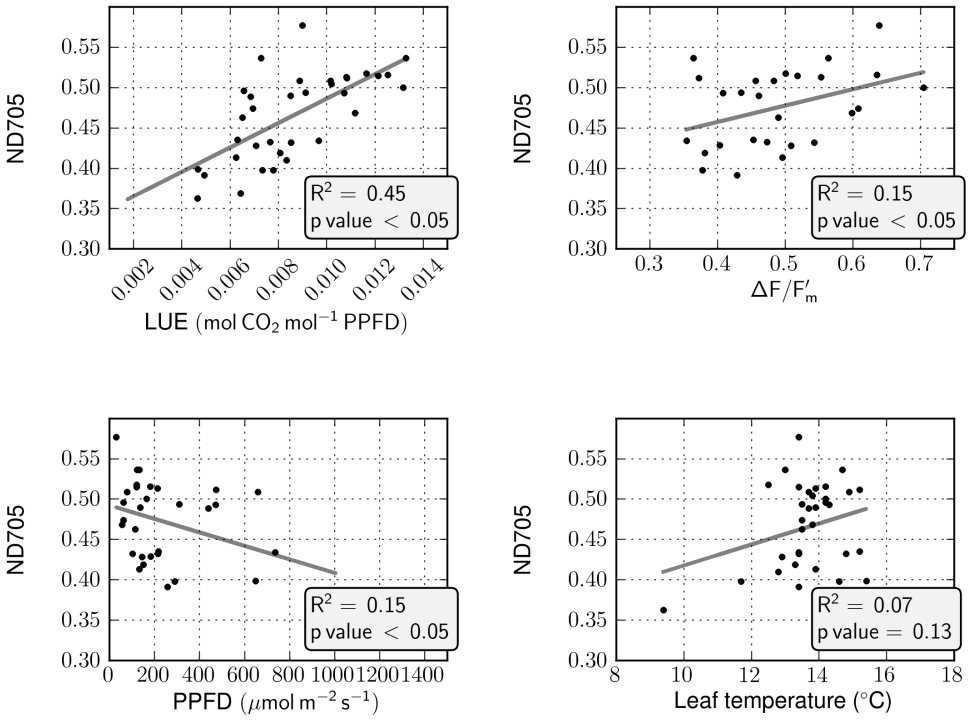

Figure 3.6: Linear regression models for (a) ND705 Vs LUE, (b) ND705 Vs $\Delta F/F'_m$, (c) ND705 Vs PPFD and (d) ND705 Vs leaf temperature

hyperspectral reflectance measurements. Linear models were developed between reflectance indices and parameters of photosynthetic efficiency.

Very low rates of photosynthesis were measured at the beginning of the study followed by a transient recovery during the following weeks. Reduced photosynthetic rates are a typical symptom of transplant shock (Close *et al.*, 2004), however reduced rates of photosynthesis can also be caused by sub-optimal environmental conditions. In particular it has been shown that Norway maple growth may be limited by extreme temperatures, low precipitation and high soil pH (Nowak and Rowntree, 1990). Temperatures during the study were within the normal

range for the time of year and rainfall was plentiful. This suggests that, assuming soil pH was constant during the study, temporal changes to meteorological conditions were not the limiting factor in relation to measured photosynthetic rates. Photosynthetic rate is also influenced by leaf growth, and as leaves mature both photosynthetic rate and leaf chlorophyll content undergo rapid changes (Dougherty *et al.*, 1979). Although the sapling leaves used in this study were fully expanded prior to planting, it is possible that some measurements may have been made on leaves that were close to the end of the developmental maturation process. It follows that the measured photosynthetic rates at the start of the study may have been reduced due to a combination of the effects of transplant shock and leaf growth.

As with LUE, there was a clear increase in PRI values over the study period (Figure 3.3c) and PRI was found to be weakly to moderately correlated with LUE and $\Delta F/F'_m$. This is in agreement with Nakaji *et al.* (2007) who found similar correlations ($R^2 = 0.38$) with PRI and LUE under cloudy conditions. The PRI signal is a function of the changing state of the xanthophyll cycle, which is a biochemical response to excess light levels brought about by physiological stress. As transplant shock occurs, in part, due to the acclimatisation of plants to higher light environments (Close *et al.*, 2004) the correlation found between PRI and $PPFD$ is to be expected (Figure 3.5c). Moderate correlations were found with spectral indices designed to measure leaf chlorophyll content, such as $ND705$, and LUE. However, unlike LUE and PRI there was no clear trend in $ND705$ over the study period. Furthermore there were very weak or no significant relationships found between $ND705$ and $\Delta F/F'_m$ and $PPFD$. It is thereby proposed that although chlorophyll-based indices can provide a general indication of photosynthetic efficiency, one must use indices that are sensitive to more rapid changes in plant biochemistry to capture the dynamic nature of the effects of transplant shock.

There was a slight positive trend in $\Delta F/F'_m$ over the study period, however data were missing in the early part of the study therefore no firm conclusions can be drawn. Close and Beadle (2003) found a similar trend in pre-dawn $\Delta F/F'_m$ for a sample of *Eucalyptus nitens* with the main difference being a longer recovery period (20 to 30 weeks), although the Close and Beadle (2003) study was conducted under low temperature conditions. In general, similar correlations were found between chlorophyll fluorescence indices ($ztd1$, $ztd2$) and chlorophyll content indices ($ND705$, $mND705$) and parameters of photosynthetic activity (Figure 3.4). It is well known that fluorescence indices are sensitive to changes in total chlorophyll content and this could account for the similar relationships (Meroni *et al.*, 2009). In any case, the relationship between absolute chlorophyll fluorescence and photosynthetic rate is not simple: under low light conditions fluorescence may be negatively correlated with photosynthetic rate and under high light conditions this relationship may reverse (Rosema *et al.*, 1998), hence care must be taken when interpreting fluorescence-based indices as indicators of photosynthetic efficiency.

Due to the prevailing meteorological conditions during the study period (figure 3.2a), there were few opportunities to collect spectra in clear sky conditions, therefore spectra were collected under both clear and cloudy skies. Measurement error may be present in the spectra collected under cloudy conditions, which may have acted to reduce the correlations between spectral indices and LUE. Firstly, the limitation of the single-beam spectrometer method is that accurate measurements of reflectance rely on the assumption of identical illumination conditions between measurements of the leaf and reference panel (Milton *et al.*, 2009). In practice, this error can be reduced by sampling in optimal low-cloud conditions and minimising the time lag between target and reference measurements. In this study, leaf and reference measurements were taken alternately to reduce the time difference to the order of seconds. A second possible

source of error occurs due to bidirectional reflectance distribution function (BRDF) effects. The BRDF describes, mathematically, how observed reflectance is dependant on the angle of the observer and the direction of the incoming radiation. Under diffuse light conditions, the BRDF of vegetation is different to the BRDF of vegetation under clear sky conditions. In particular, measured reflectance in the visible region of the spectrum increases linearly as the proportion of diffuse radiation increases (Gilabert and Meliá, 1993). As PRI, and several other spectral indices, make use of visible bands, the signal may be influenced by confounding effects under cloudy sky conditions unrelated to xanthophyll cycle activity.

Relatively few studies have been carried out that explore the use of passive (or active) remote sensing techniques for detecting the effects of transplant shock and as such there are several suggestions for further work. Firstly, by their nature, spectral measurements are indirect. Direct sampling of plant pigments during the recovery period would be useful in testing the hypothesis that PRI may be more useful than chlorophyll-based indices in dectecting dynamic changes in photosynthetic efficiency during the transplant shock period. Secondly, a study under clear sky conditions or with a dual-beam spectrometer may increase the measured correlation coefficients. Thirdly, this study concentrated on measuring the early onset effects of transplant shock. Transplant shock can also cause long term (seasonal and trans-seasonal) reductions in photosynthetic efficiency due to water stress (Barton and Walsh, 2000), which may be measurable using physiological remote sensing. In addition, measurements of rates of photosynthesis prior to outplanting would also be useful as these would demonstrate the initial decline and recovery more clearly. Nonetheless, the study demonstrated that hyperspectral remote sensing has the potential to be a useful tool in the detection and monitoring of the dynamic effects of transplant shock.

3.5 Acknowledgements

This project was conducted in collaboration with K. Simpson who collected the bulk of the photosynthesis measurements and designed the experimental plot for a separate Aphid-based experiment. The work of J. Atherton was supported by a PhD studentship awarded as a Torrance bequest scholarship by The University of Edinburgh (UK) and Forest Research. The NERC Field Spectroscopy Facility is acknowledged for the loan of a PAM fluorometer. K. Anderson and P. J. Zarco-Tejada are thanked for their illuminating correspondence.

Table 3.1: Reflectance index reference table. Where ρ_x is apparent reflectance at x nm and $D\rho_x$ is the first derivative spectra with respect to wavelength at x nm.

Shortened name	Formula	Pigment/process	Citation
broadband NDVI	$\frac{\rho_{NIR}-\rho_{Vis.}}{\rho_{NIR}+\rho_{Vis.}}$	chlorophyll	Vogelmann *et al.* (1993)
SR 680	$\frac{\rho_{800}}{\rho_{680}}$	chlorophyll	Sims and Gamon (2002)
SR 705	$\frac{\rho_{750}}{\rho_{705}}$	chlorophyll	Sims and Gamon (2002)
mSR 750	$\frac{\rho_{750}-\rho_{445}}{\rho_{750}+\rho_{445}}$	chlorophyll	Sims and Gamon (2002)
ND 680	$\frac{\rho_{800}-\rho_{680}}{\rho_{800}+\rho_{680}}$	chlorophyll	Sims and Gamon (2002)
ND 705	$\frac{\rho_{750}-\rho_{705}}{\rho_{750}+\rho_{705}}$	chlorophyll	Sims and Gamon (2002)
mND 705	$\frac{\rho_{750}-\rho_{705}}{\rho_{750}+\rho_{705}-2\times\rho_{445}}$	chlorophyll	Sims and Gamon (2002)
inverse 1 to 5	$\frac{1}{\rho_{500,670,530,550,700}}$	chlorophyll	Gitelson *et al.* (2003)
r 750	$\frac{\rho_{750}-\rho_{800}}{((\rho_{750}-\rho_{695})-1)}$	chlorophyll	Gitelson *et al.* (2003)
PRI	$\frac{\rho_{531}-\rho_{570}}{\rho_{531}+\rho_{570}}$	carotenoids/chlorophyll	Gamon *et al.* (1992)
SIPI	$\frac{\rho_{800}-\rho_{445}}{\rho_{800}+\rho_{680}}$	carotenoids/chlorophyll	Peñuelas *et al.* (1995)
PSRI	$\frac{\rho_{678}-\rho_{500}}{\rho_{750}}$	carotenoids/chlorophyll	Merzlyak *et al.* (1999)
zt 1	$\frac{\rho^2_{683}}{\rho_{675}\times\rho_{690}}$	fluorescence	Zarco-Tejada *et al.* (2000a)
zt 2	$\frac{\rho_{750}}{\rho_{800}}$	fluorescence	Zarco-Tejada *et al.* (2000a)
zt 3	$\frac{\rho_{685}}{\rho_{655}}$	fluorescence	Zarco-Tejada *et al.* (2000a)
zt 4	$\frac{\rho_{690}}{\rho_{655}}$	fluorescence	Zarco-Tejada *et al.* (2000a)
zt 5	$\frac{\rho_{680}}{\rho_{630}}$	fluorescence	Zarco-Tejada *et al.* (2000b)
zt 6	$\frac{\rho_{685}}{\rho_{630}}$	fluorescence	Zarco-Tejada *et al.* (2000b)
zt 7	$\frac{\rho_{687}}{\rho_{800}}$	fluorescence	Zarco-Tejada *et al.* (2000b)
zt 8	$\frac{\rho_{690}}{\rho_{630}}$	fluorescence	Zarco-Tejada *et al.* (2000b)
zt 9	$\frac{\rho^2_{685}}{\rho_{675}\times\rho_{690}}$	fluorescence	Zarco-Tejada *et al.* (2000a)
zt 10	$\frac{\rho_{685}}{\rho_{655}}$	fluorescence	Zarco-Tejada *et al.* (2000b)
zt 11	$\frac{\rho^2_{683}}{\rho_{675}\times\rho_{691}}$	fluorescence	Zarco-Tejada *et al.* (2000a)
DPI	$\frac{\rho_{688}\times\rho_{710}}{\rho^2_{697}}$	fluorescence	Zarco-Tejada *et al.* (2003)
zt d1	$\frac{D\rho_{705}}{D\rho_{722}}$	fluorescence	Zarco-Tejada *et al.* (2000b)
zt d2	$\frac{D\rho_{730}}{D\rho_{706}}$	fluorescence	Zarco-Tejada *et al.* (2000b)
dob 1	$\frac{\rho_{690}}{\rho_{600}}$	fluorescence	Dobrowski *et al.* (2005)

Chapter 4

Linking CO_2 fluxes and optical remote sensing measurements across a heterogeneous Arctic landscape

Abstract

There is growing evidence that the Arctic is warming at a faster rate than the rest of the world. Arctic ecosystems are thought to be particularly sensitive to temperature changes. With regards to the carbon cycle higher temperatures are expected to lengthen the growing season, although this may be balanced in part by increased rates of heterotrophic respiration. Airborne measurements were combined with multi-sensor satellite observations to explore spatial relationships between carbon exchange and vegetation cover across an Arctic landscape. Airborne data were collected from the Kevo Natural Park region, Northern Finland, during August 2008; where a mix of sparse birch forests, mire, small lakes and pine contribute to a spatially complex and heterogeneous landscape. Surface fluxes of CO_2 were calculated using the eddy covariance method from airborne data. Airborne CO_2 fluxes were compared to MODIS vegetation indices. In addition, landscape light use efficiency (LUE) was estimated for the birch forests by combining airborne flux measurements with tower estimates of respiration and satellite-based estimates of the fraction of absorbed photosynthetically active radiation (fAPAR). Landscape LUE was compared to coincident airborne measurements of PRI and NDVI. There were no significant relationships between MODIS spectral indices and airborne flux observations. There were weak to moderate (R^2 = 0.4 in both cases) correlations found between PRI and LUE and between PRI and indicident photosynthetically active radiation. In conclusion, aircraft observations of CO_2 fluxes were found to be sensitive to changes in incident solar radiation across the heterogeneous Arctic landscape, and hyperspectral reflectance indices such as the PRI were found to have the potential to quantify this sensitivity.

4.1 Introduction

There is growing evidence that the Arctic is warming at a faster rate than the rest of the world (IPCC, 2007b; McBean *et al.*, 2005). The instrumental record indicates that Arctic regions (above 60° N latitude) have warmed at an average rate of 0.09 °C per decade during the 20th century, in comparison with a Northern Hemisphere rate of 0.06 °C per decade (McBean *et al.*, 2005). Rapid warming in the Arctic is caused by the sensitivity of snow and ice cover to small increases in temperature, causing changes in local and regional precipitation patterns (McBean *et al.*, 2005).

Arctic ecosystems are thought to be particularly sensitive to temperature changes. This is because Arctic species are often highly specialised and in lower latitude Arctic regions, subtle changes in ecosystem composition may lead to the loss of some species (Callaghan *et al.*, 1995; IPCC, 2007b). With regards to the carbon cycle, higher temperatures are expected to lengthen the growing season (Linderholm, 2006). Although this may be balanced by increased rates of heterotrophic respiration, as Arctic soils act as significant long-term stores of organic carbon (Hartley *et al.*, 2008).

Remotely sensed data has the potential to measure changes in Arctic ecosystems at a range of scales. The Normalised Difference Vegetation Index (NDVI) is a spectral vegetation index (SVI) that has found widespread application in Arctic applications (Stow, 2004). NDVI is typically used as an indicator of the amount of green vegetation and has been used to infer Leaf Area Index (Riedel *et al.*, 2005; Williams *et al.*, 2008) at smaller scales and changes in productivity at larger scales (Myneni *et al.*, 1997). Due to the remoteness of the observed regions, a key challenge in Arctic ecosystems is validating remotely sensed measurements. Huemmrich *et al.* (2010) found that significant changes in NDVI could occur

within species, signalling that care must taken when interpreting changes in NDVI as indicators of different species.

La Puma *et al.* (2007) explored the relationships between NDVI and gross primary productivity (GPP) and between NDVI and ecosystem respiration (R_e) for an Alaskan Arctic ecosystem. An initial analysis revealed strong relationships between carbon fluxes and NDVI. However after accounting for seasonal variations, NDVI was found to explain no more than 25% of the variance in flux measurements. This work suggests that NDVI alone is an inadequate measure of ecosystem productivity on short timescales.

The Monteith [1972, 1977] light use efficiency (LUE) model is widely used to predict photosynthesis from optical remote sensing, however Arctic applications have been limited in number. The model states that photosynthesis can be calculated as the product of absorbed radiation (APAR) and an efficiency term, LUE: $GPP = APAR \times LUE$. APAR is estimated as the product of the fraction of absorbed radiation (fAPAR) and incident photosynthetically active radiation (quantified as the photosynthetic photon flux density, PPFD). fAPAR has a near linear relationship with NDVI and so can be derived from remote sensing observations. LUE is representative of the biophysical processes that limit photosynthesis, such as drought or temperature induced stress, and can be estimated from meteorological conditions or flux tower measurements. LUE can also be inferred from physiological remote sensing observations such as the Photochemical Reflectance Index (PRI) (Coops *et al.*, 2010). Huemmrich *et al.* (2010) developed a LUE based model to predict photosynthesis as a function of absorbed radiation for Arctic tundra species. Huemmrich *et al.* (2010) found significant differences in LUE between species, however a warming treatment did not cause changes in LUE within species.

Airborne remote sensing observations are typically collected at much higher

spatial and spectral resolutions than satellite measurements. In addition to hyperspectral reflectance measurements, it is also possible to measure surface fluxes of carbon and energy exchange from airborne platforms using the eddy covariance technique. The key difference between airborne and tower based eddy covariance measurements is that airborne fluxes are measured across the landscape, whereas towers are fixed point systems (although the tower footprint changes as a function of the prevailing wind direction). In theory, this makes airborne flux measurements particularly useful for characterising fluxes across spatially heterogenous regions such as the lower latitude Arctic. In reality, airborne flux measurements are constrained by a minimum averaging length requirement analogous to the temporal averaging requirement of tower based data. Minimum averaging lengths are on the order of a few km, depending on the surface characteristics and the local meteorological conditions. In a recent study Zulueta *et al.* (2011) compared satellite observations of NDVI from the Moderate Resolution Imaging Spectroradiometer (MODIS) sensor to airborne CO_2 flux estimates across the Alaskan Barrow land peninusla, an area populated by wet sedge tundra species such as *Carex aquatilis*. Zulueta *et al.* (2011) found a correlation of moderate strength ($R^2 = 0.5$) between satellite derived NDVI observations and CO_2 measurements after the data had been filtered for water pixels.

The objective of this study was to explore spatial relationships between carbon exchange and optical remote sensing measurements across the Arctic landscape. The study aimed to test two hypotheses: 1. Relationships exist between MODIS SVIs and airborne flux observations across a heterogeneous Arctic landscape; 2. Hyperspectral reflectance indices can be used to infer LUE across the same landscape.

4.2 Methods

4.2.1 Study design

This study combined data from multiple instruments to assess carbon exchange across the Arctic landscape. A summary of the data-sets and instrumentation used is shown in table 4.1. There were two main parts to the study:

Objective 1: Explore the relationships between airborne CO_2 flux measurements and spatial measurements of NDVI and EVI observed by MODIS. To accomplish this task the flux footprint was first estimated and then the relationships between within footprint EVI/NDVI pixels and corresponding flux measurements were analysed.

Objective 2: Evaluate the relationships between landscape LUE and hyperspectral reflectance indices. LUE was calculated for birch dominated land-cover only by combining aircraft measurements of net carbon fluxes with tower based respiration estimates, and MODIS derived fAPAR. The relationships between hyperspectral reflectance indices calculated from airborne measurements and LUE were then analysed.

Table 4.1: Data and instrumentation used in the study. The following key is used in the 'scale' column: {G = ground, A = airborne, S = satellite, T = flux tower }.

Data-set	Scale	Platform (instrument)	Date collected
Land-cover map	S, G	IKONOS, ground survey	30-Sep-2007, 2007-2008
EVI, NDVI	S	MODIS MOD13	27-Jul-2008 to 11-Aug-2008
PRI_{ASD}, $NDVI_{ASD}$	A	Dimona motor glider (2 × ASD FieldSpec)	7-Aug-2008
PPFD	A	Dimona motor glider (ASD FieldSpec)	7-Aug-2008
CO_2 flux	A	Dimona motor glider (BAT probe/IRGA)	7-Aug-2008
R_e	T	Birch flux tower	every half hour

4.2.2 Study site

The study site is classed as a sub-Arctic forest tundra zone, although the site is within the bounds of the Arctic circle. The site is located in the northern most commune of Finland, Utosjoki, and is part of the Kevo Nature Reserve, which covers approximately 720 km^2 of protected land (Heikkinen *et al.*, 1998). The local vegetation consists of a patchy mix of sparse, low density polycormic (multi-stemmed) birch (*Betula pubescens*) trees, lichen and *Vaccinium* species such as bilberry bushes and a limited amount of Scots Pine (*Pinus sylvestris* L.). There are also several small lakes and mire areas which contribute to the complex, heterogeneous nature of the landscape. In the 1960s an outbreak of *Epirrita autumnata* L. (Autumnal Moth) larvae defoliated large areas of the nature reserve. Significant areas of forest are still damaged, as birch in these areas recover particularly slowly (Heikkinen *et al.*, 1998). The Kevo Sub-Arctic

Research Station is located within the study area at approximately 69.45°N, 27.01°E.

4.2.3 Airborne measurements

An airborne campaign was conducted during August 2008 using the University of Edinburgh's research aircraft, as part of the Arctic Biosphere Atmosphere Coupling at Multiple Scales (ABACUS) project. The ABACUS project was a large scale experiment that used a variety of techniques to quantify water, carbon and energy exchange at a range of scales in the Arctic region. The University of Edinburgh's research aircraft, a HK-36 TTC ECO Dimona single engine motor glider (Diamond Aircraft, Austria), was used to collect airborne data on the 7th August 2008. Eight low level transects (altitude < 70 m) were flown between 10:28 and 11:00 local time in a star-like formation, in an attempt to cover most of the study site landscape (see figure 4.1). Cloud conditions on the 7th August were variable, with periods of diffuse sunlight interspersed with high-level, direct sunlight.

The aircraft carries the bulk of its instrumental payload in two specially designed under-wing pods. The aircraft is equipped with a variety of instrumentation including an airborne eddy covariance system, dual-view hyperspectral spectroradiometers and a CO_2 and H_2O profiling system. To estimate surface fluxes using the eddy covariance method, high frequency (20 Hz) measurements of the scalar of interest, such as CO_2 concentration, are collected in conjunction with high frequency measurements of wind velocity with respect to the Earth. An Li-7500 (Li-Cor, Lincoln, Nebraska) open-path infra-red gas analyser (IRGA) was used to collect fast response measurements of CO_2 and H_2O concentrations (the scalars of interest). The aircraft uses a Best Air Turbulence (NOAA, USA) probe to measure wind speed relative to the aircraft, and an RT3003 differential GPS-INS

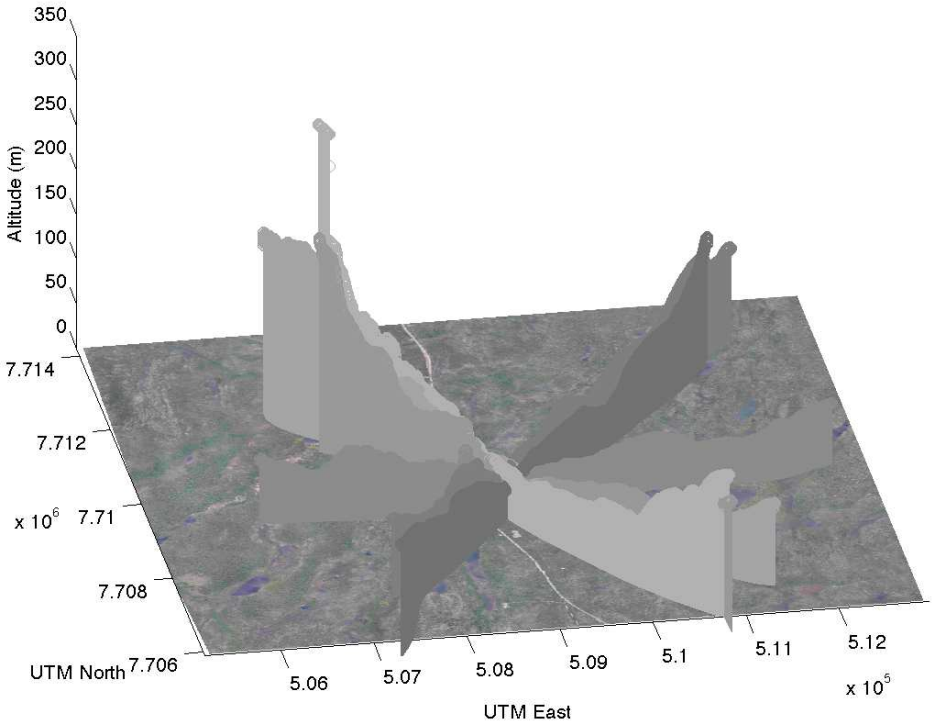

Figure 4.1: Flight transects for the 7th August 2008 overlaid onto digital photography of the study area collected using the airborne digital photography.

system (Oxford Technical Solutions, UK) is then used to estimate aircraft speed relative to Earth.

The aircraft also carries two Analytical Spectral Devices FieldSpec Pro spectrometers (ASD Inc., Boulder, CO, USA). These instruments detect electromagnetic radiation in the wavelength range 350 - 2500 nm with a maximum spectral resolution in the visible wavelengths (350 - 700 nm) of 3 nm. The instruments are arranged in dual-field of view mode. The field-of view for one instrument faces upwards/skywards and the other faces the ground. The upward-facing spectrometer is fitted with a cosine detector and measures solar irradiance.

Table 4.2: Transect statistics. Mean and standard deviations (in brackets) values are shown for length, altitude, plane speed relative to the gound and PPFD

marker	start time	end time	length (m)	altitude (m)	speed (m s^{-1})	PPFD (μmol m^{-2} s^{-1})
41	10:28:55	10:31:57	7980	63.82 (12.96)	43.85 (1.64)	578.75 (47.97)
42	10:33:32	10:36:52	8600	74.60 (26.05)	43.00 (1.90)	819.00 (211.38)
43	10:37:57	10:40:47	7688	64.51 (20.13)	45.22 (2.48)	985.00 (327.54)
44	10:45:02	10:47:37	6313	53.04 (10.74)	40.73 (2.03)	869.77 (332.83)
45	10:50:22	10:52:47	6779	86.29 (38.64)	46.75 (2.27)	641.33 (6.91)
46	10:54:17	10:57:32	7351	85.96 (57.42)	37.70 (1.83)	841.05 (222.64)
47	10:57:52	11:00:32	7259	99.67 (57.87)	45.37 (1.16)	862.56 (281.77)
48	11:01:07	11:03:47	6220	87.11 (35.73)	38.88 (1.39)	875.69 (307.00)

4.2.4 Using MODIS SVIs to infer carbon exchange across the landscape

Spatial measurements of SVIs made by the MODIS sensor were compared to airborne CO_2 flux measurements from across the landscape. Flux footprints were calculated using a simple parametrisation (Kljun *et al.*, 2004), and average MODIS vegetation index values from within the footprints were compared to the corresponding CO_2 flux measurements.

Airborne CO_2 flux measurements

Fluxes of CO_2 were estimated from the aircraft measurements of wind and scalar concentrations using the eddy covariance technique. Flux values, F_c, are estimated as the covariance of high frequency perturbations from the mean vertical wind velocity component, $w\prime$, and the mean scalar concentration, $c\prime$:

$$F_c = \langle w\prime c\prime \rangle \tag{4.1}$$

The main difference between aircraft and tower based eddy covariance systems is that a spatial averaging window is used to derive the mean values of velocity and scalars in aircraft systems rather than the temporal windows used in tower systems.

An ogive analysis was conducted to help to choose an optimum averaging length. The ogive technique refers to the calculation of the cumulative integral of the co-spectrum of the vertical velocity and scalar of interest and has been widely applied in airborne studies (Saucier *et al.*, 1991; Mauder *et al.*, 2007; Desjardins *et al.*, 1989). A co-spectrum is a representation of flux data in frequency (or wave-number) space, which is potentially very useful in determining the length scales that contribute to flux measurements. However co-spectra typically appear noisy thereby limiting applicability. By taking the cumulative integral of the co-spectrum from the highest frequency to the lowest frequency the noisy co-spectrum is used to produce a much clearer plot (figure 4.2) the so-called ogive integral. The ogive integral, O_g, is calculated as follows:

$$O_g(f_0) = \int_{\infty}^{f_0} Co(f)\, df \tag{4.2}$$

where f is frequency and Co is the co-spectrum.

Figure 4.2 shows the ogive integrals for the transects flown on the 7th August 2008. On figure 4.2 the x-axis is reversed so that larger wavenumbers, which represent smaller turbulent eddies, are closer to the origin. At large wavenumbers (close to 10^{-1}) the gradient of the ogive integral is close to zero. A region of maximum

gradient occurs at mid size wavenumbers, whereas at lower wavenumbers the gradient of the integral is also expected to be close to zero. To choose a suitable flux averaging length, a cut off point (vertical lines on figure 4.2) is selected that occurs as the gradient re-approaches zero at lower wavenumbers. This ensure that the flux method adequately samples larger turbulent eddies. On some of the ogive integrals (Figure 4.2, Marker number = 42) the gradient of the curve does not re-approach zero. This may be indicative of under-sampling of the turbulent spectrum leading to less reliable flux estimates (Foken *et al.*, 2006).

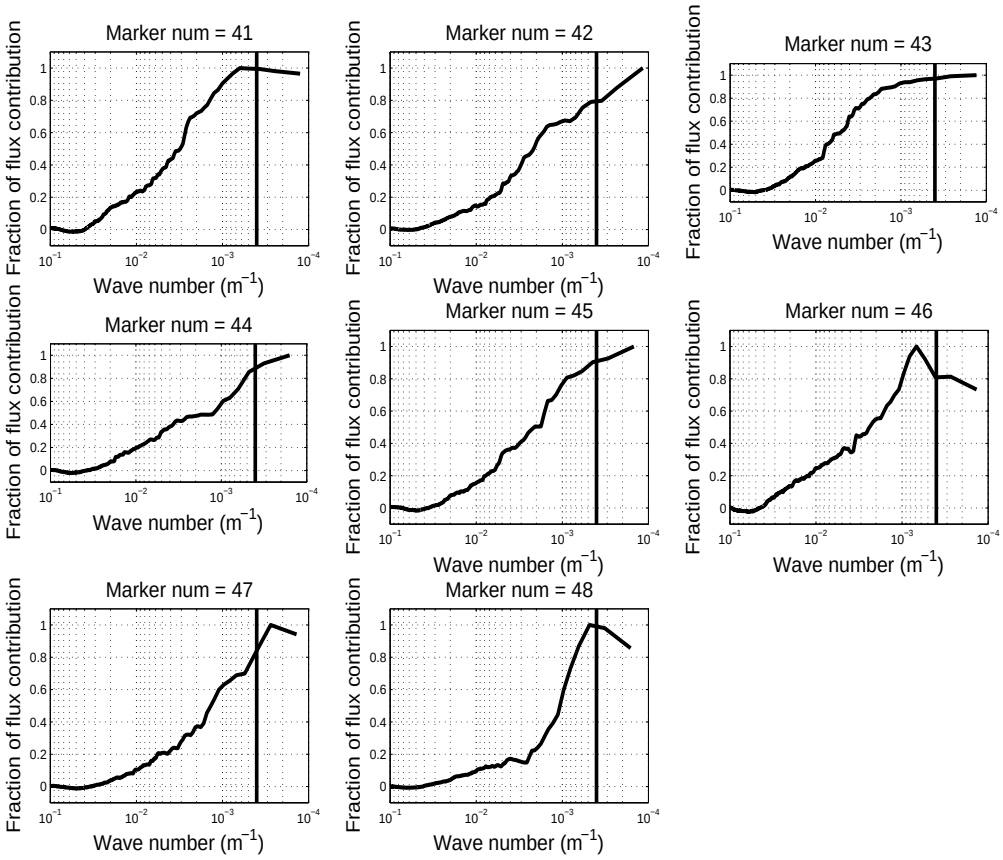

Figure 4.2: Ogive integrals for the cospectrum of CO_2 concentration and vertical wind speed calculated using airborne measurements. Each subplot represent the integrated contributions for a single transect for the full range of spatial scales. Thick black vertical lines are at 2.5 km.

To compare remote sensing observations to airborne flux measurements it was necessary to estimate the geographical source region of the flux. The footprint function, F_*, is formulated as an up-wind probability distribution as a function of distance from the instrument. Peak probability values typically appear a few hundred meters up-wind from the measurement system (dependant on the surface roughness and meteorological conditions). Lagrangian stochastic models can be used to simulate F_*, however these are computationally expensive. The Kljun *et al.* (2004) parametrisation was developed as a simplified functional approximation using output from a set of Lagrangian model simulations and has been previously applied in airborne eddy covariance studies (Kirby *et al.*, 2008; Zulueta *et al.*, 2011). Estimates of footprints derived from the Kljun *et al.* (2004) parametrisation are referred to as $\hat{F}_*$ (see 4.3 for an example $\hat{F}_*$ footprint distribution) and were used the estimate flux footprints in this study.

$\hat{F}_*$ is calculated as a function of the standard deviation of the vertical wind velocity, σ_w, friction velocity, u_*, aircraft height, z_m, the Monin-Obuhov length, L, and the roughness length, z_0. A single roughness length was used, z_0, based on the dominant land-cover type, birch, and the other parameters were estimated using meteorological observations.

Table 4.3: Footprint model parameters

parameter	symbol	unit	value
P.B.L. height	h	m	dependant on transect
friction velocity	u_*	m s^{-1}	dependant on transect
roughness length	z_0	m	0.1
standard deviation of vertical wind speed	w'	m s^{-1}	dependant on transect

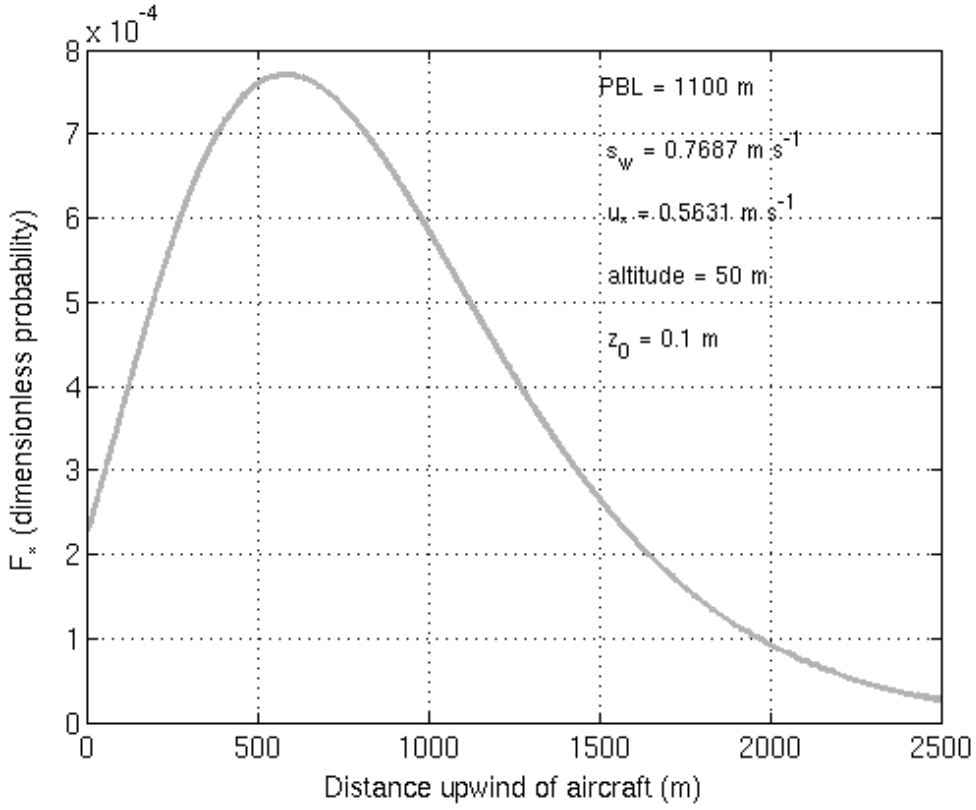

Figure 4.3: Example of a flux footprint calculated using the Kljun *et al.* (2004) Parametrisation using the parameters shown in the figure.

MODIS images

MODIS gridded and subsetted EVI and NDVI SVI data products (MOD 13, collection 5) were downloaded for a 20 km square area surrounding the study site from the ORNL DAAC website (Oak Ridge National Laboratory Distributed Active Archive Center (ORNL DAAC), 2010). In addition to the SVI products, SVI quality and pixel reliability data were also downloaded. Reflectance data from MODIS bands centred at blue (469 nm), red (645 nm) and near-infrared (858 nm) wavelengths are used to calculate SVIs, based on the following equations (Huete *et al.*, 1999):

$$NDVI = \frac{\rho_{nir} - \rho_{red}}{\rho_{nir} + \rho_{red}} \tag{4.3}$$

$$EVI = 2 \cdot \frac{\rho_{nir} - \rho_{red}}{L + \rho_{nir} + C_1\rho_{nir} + C_2\rho_{blue}} \tag{4.4}$$

Where ρ can be either top-of-atmosphere or ground reflectance, L is a vegetation canopy adjustment factor and C1 and C2 are aerosol correction weights. The SVIs are processed as 16 day products; the SVI products used in this analysis had the datenumber 209 (referring to the period starting on the 27th July, day 209, and ending on the 11th August 2008) The spatial resolution of the SVI products is 250 m and the projection is sinusoidal. Only pixels that were flagged as 'good quality' in the MOD 13 pixel reliability product were used for further analysis.

MODIS linear models

Linear models were developed between mean weighted footprint MODIS SVIs, SVI_{MODIS}, and airborne $CO2_2$ flux measurements. SVI_{MODIS} values were estimated for each separate airborne flux measurement. The weights were derived using the flux footprint function, $\hat{F}_*$. From $\hat{F}_*$, the up-wind distance from which 95% of the flux originates was estimated. Using the 95 % limit of each $\hat{F}_*$, a flux footprint box was then defined with the window extrema acting as the cross-wind limits. SVI pixels that fell within this box formed an SVI flux footprint distribution (Figure 4.4). $\hat{F}_*$ was also used to derive the individual upwind weighting for each SVI value, w_i, and the mean SVIs are calculated as:

$$SVI_{MODIS} = \frac{\sum_{i=1}^{n} w_i SVI_i}{\sum_{i=1}^{n} w_i} \tag{4.5}$$

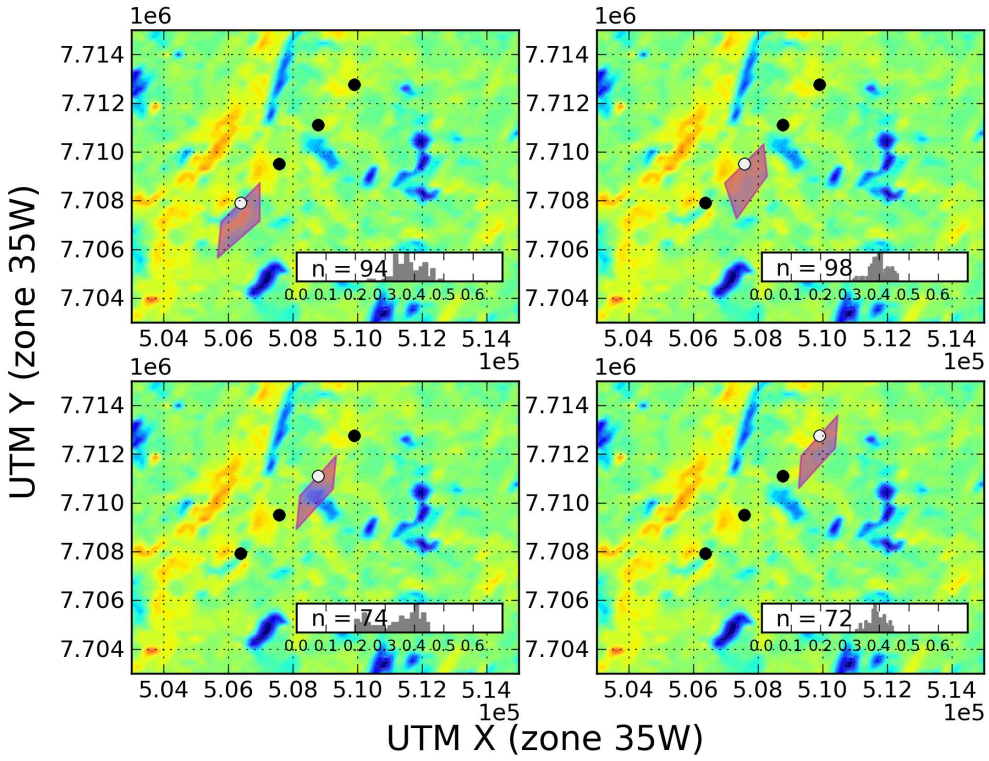

Figure 4.4: MODIS EVI image with flux footprints for a single transect with a 2 km averaging window shown as magenta polygons. Each subplot represents a single flux measurement and associated footprint area. Inset histograms show EVI distributions within the footprint box, where N is the number of pixels per footprint.

4.2.5 Predicting LUE across the landscape

LUE was calculated by combining aircraft and tower flux observations and MODIS satellite measurements for birch forest regions only. This was principally because birch was the dominant land cover type. The relationships between birch LUE

and airborne hyperspectral SVIs were then explored. The response of airborne CO_2 fluxes and hyperspectral SVIs to changes in PPFD levels were also analysed.

Land-cover classification

A very high resolution (4 m^2) landcover classification map (figure 4.5) was derived using IKONOS satellite imagery acquired on the 30th September 2007. The land-cover map classified the surface into 5 categories: i. mire ii. birch iii. coniferous forest iv. bare ground and v. water. The map was made using a maximum likelihood classification algorithm (ENVI v4.4) trained using ground vegetation surveys, with an estimated classification accuracy against the survey data of 96%.

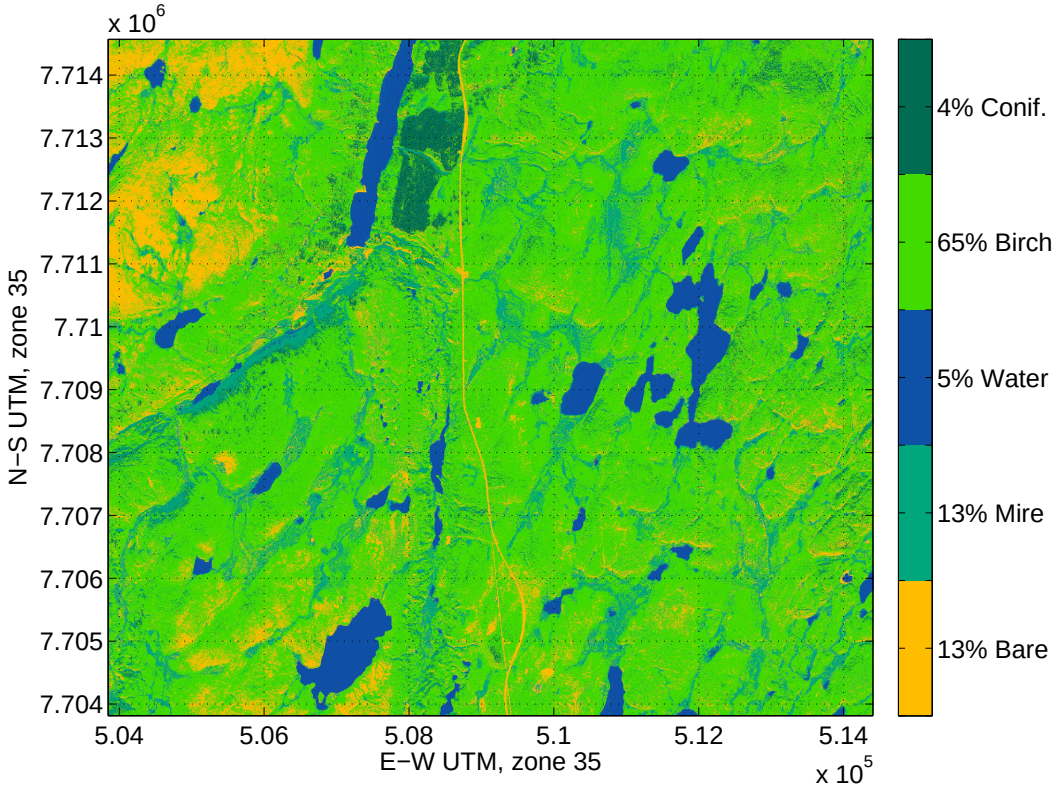

Figure 4.5: Land-cover classification derived from IKONOS hyperspectral satellite imagery and ground survey data.

Hyperspectral reflectance measurements

Along transect incident photosynthetic photon flux density (PPFD) was estimated by integrating the solar irradiance measured by the upwards facing spectrometer across the photosynthetically active wavelengths. Reflectance spectra were calculated by normalising measurements of radiance collected by the downward facing radiometer by measurements of solar irradiance collected by the upward facing radiometer. The hyperspectral reflectance spectrum were used to calculate along transect NDVI (referred to as NDVI_{ASD}) as well as along transect values of the Photochemical Reflectance Index (PRI, referred to as PRI_{ASD}), according to:

$$NDVI_{ASD} = \frac{\rho_{830} - \rho_{660}}{\rho_{830} + \rho_{660}} \tag{4.6}$$

$$PRI_{ASD} = \frac{\rho_{531} - \rho_{570}}{\rho_{531} + \rho_{570}} \tag{4.7}$$

where ρ_x is reflectance at $_x$ nm.

The spectral indices were also calculated for the downward pointing spectrometer only. This is because during some of the transects rapid changes in illumination conditions saturated the upward pointing spectrometer, resulting in spurious reflectance spectra. By design, a normalised difference index corrects for changes in illumination by incorporating a reference band, hence PRI_{ASD} and NDVI_{ASD} should theoretically be effective for radiance based data. The saturation at high irradiances also had the effect of rendering some of the high PPFD measurements inaccurate.

The downward pointing spectrometer footprint is typically located directly underneath the aircraft, in contrast to the up-wind footprints of the eddy covariance

system. When stationary the spectrometer footprint is circular. An altitude of 40 m with a field of view of 25° results in a footprint diameter of approximately 17 m (see figure 4.6 for a graphical comparison of spectrometer and flux footprints). Because the aircraft is not stationary the circular footprint becomes elongated into an ellipse. This was calculated from the aircraft speed and the spectrometer integration time. In addition, the true footprint location also depends on the aircraft pitch and roll.

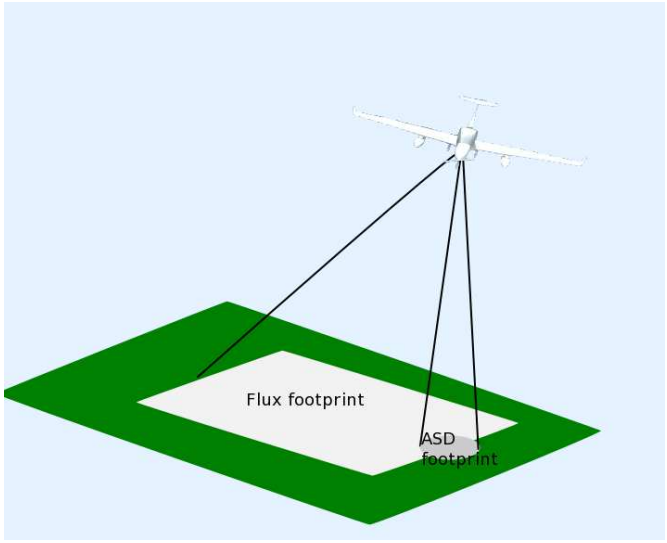

Figure 4.6: Diagram of ASD spectrometer and flux footprints (not to scale). Although there is some overlap between the two footprints, the ASD spectrometer and the eddy covariance systems are essentially measuring different areas.

Once the footprints were known, the land-cover types inside the footprints were used to assign land-cover classes to each spectrometer measurement based on the dominant footprint type. The relationships between incident PPFD and PRI_{ASD} and PPFD and NDVI_{ASD} were explored by calculating coefficients of determination and developing linear models.

Light Use Efficiency models

LUE was estimated for the birch land cover class by combining airborne flux estimates with hyperspectral radiometer measurements of PPFD, MODIS SVIs, and a simple temperature-based respiration model:

$$LUE = \frac{-1 \times (F_c - R_e)}{fAPAR \times PPFD} \tag{4.8}$$

The mean footprint EVI_{MODIS} was used as a surrogate for fAPAR ($fAPAR = EVI$). This is because the MODIS fAPAR product is at a coarser resolution (1 km) than the MODIS EVI product (250 m). Ecosystem respiration was estimated using data collected during August 2008 from a birch stand flux tower system (located at 69.491°N, 27.234°E). An empirical relationship described in van Gorsel *et al.* (2009) was used to estimate day time respiration from night time flux and temperature observations. The relationships between LUE and hyperspectral SVIs that were coincident in time and dominated by the birch landcover class were analysed by calculating coefficients of determination and developing linear models.

In addition to the birch site, there was also a flux tower measuring surface carbon and energy exchange at a wetland site during the study period (located at 69.494°N, 27.230°E).

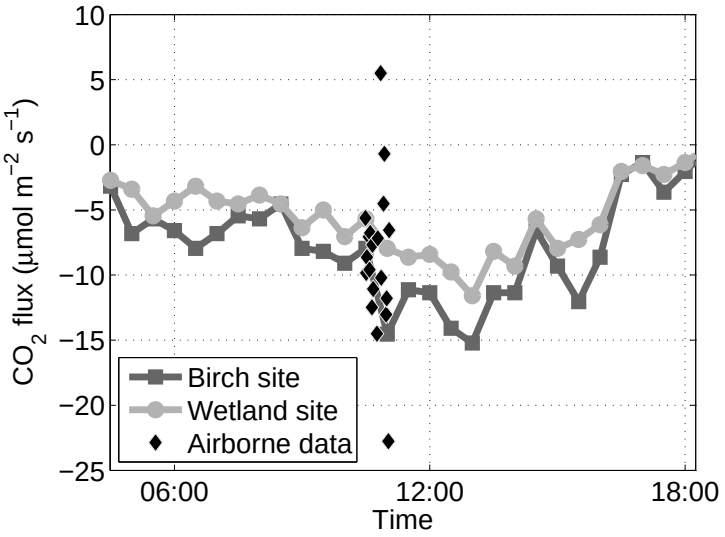

Figure 4.7: Birch and wetland tower and airborne CO_2 fluxes for 07/08/2008 where airborne CO_2 fluxes were calculated using a 2500 m averaging window.

4.3 Results

4.3.1 CO_2 fluxes across the landscape

From 11:00 am to 11:30 am CO_2 fluxes of -9.54 μmol m^{-2} s^{-1} and -4.09 μmol m^{-2} s^{-1} were measured at the birch and wetland tower sites respectively. Most of the fluxes measured by the aircraft were within a similar range, 0 - 15 μmol m^{-2} s^{-1}, to the fluxes observed by the stationary towers (figure 4.7). With regards to the airborne flux measurements, there were a limited number (depending on the step size) of extreme flux values ($<$ -20 μmol m^{-2} s^{-1} or $>$ 0 μmol m^{-2} s^{-1}).

4.3.2 Relationships between MODIS SVIs and CO_2 fluxes

The mean and variance were calculated for EVI and NDVI images after masking for pure water pixels (water-dominated pixels were defined as EVI < 0.003 and NDVI < 0.019). The mean and variance pixel values for the water masked EVI image were calculated as 0.36 and 0.01 respectively. The mean and variance pixel values for the water masked NDVI image were calculated as 0.68 and 0.01 respectively. Whilst the EVI distribution demonstrated mainly positive skew with a slight negative skew, the NDVI distribution was strongly negatively skewed (data not shown).

Linear models were developed between MODIS SVIs and airborne CO_2 flux measurements (figure 4.8). All CO_2 flux values were calculated using a 4 km averaging window with a 2.5 km step size. There was no significant relationship between EVI_{MODIS} and CO_2 flux values, there was also no significant relationship between $NDVI_{MODIS}$ and CO_2 flux values. Linear models were also developed between average PPFD values (calculated as mean values per 4 km flux window) measured by the upwards pointing radiometer and airborne flux measurements (figure 4.9). There was also no significant relationship between PPFD and CO_2 flux values.

4.3.3 Estimating LUE across the landscape

Airborne hyperspectral measurements

Hyperspectral data from a single transect is plotted in figure 4.10 to highlight features that are typical within the range of observations. Figure 4.10 shows along transect SVIs calculated from the downward pointing radiometer as well as PPFD calculated from the upward pointing radiometer for a single transect

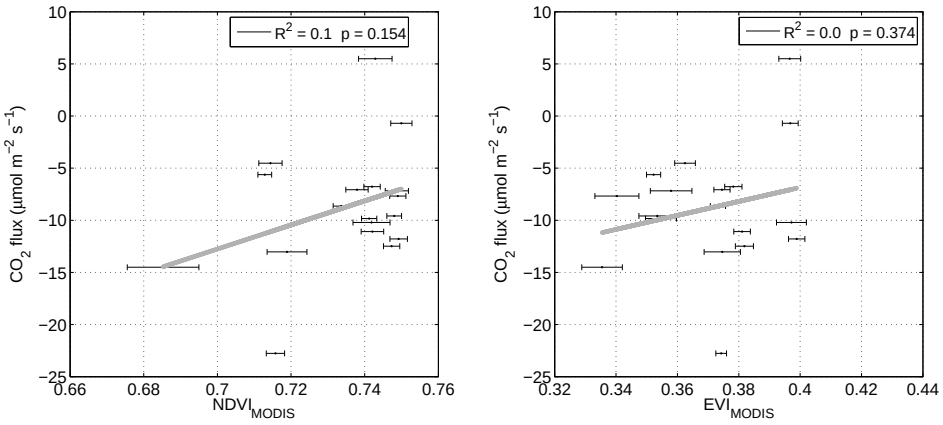

Figure 4.8: Average MODIS SVIs per flux footprint versus airborne CO_2 fluxes calculated using a 2500 m averaging window. Left: $NDVI_{MODIS}$ versus CO_2 flux, right: EVI_{MODIS} versus CO_2 flux. Standard error bars shown on MODIS SVIs.

(marker number 47). Figure 4.10 also shows the land-cover type within the spectrometer footprint and the closest (by distance) MODIS NDVI pixel value to the spectral measurements for the same transect. MODIS NDVI values are generally greater in value across transect number 47 in comparison to $NDVI_{ASD}$. For transect number 47, $NDVI_{ASD}$ values range from less than 0 to 0.77, whereas MODIS NDVI measurements have a much narrower range, from 0.68 to 0.81.

PPFD values were variable along the transect, high values were measured midway through the measurement period which corresponded to periods of direct sunlight. Low PRI_{ASD} values were coincident with high PPFD values, whereas the highest PRI_{ASD} values occurred coincidentally with low $NDVI_{ASD}$ values. Along transect $NDVI_{ASD}$ did not appear to change with PPFD. Although birch was the dominant along transect land-cover class, the other landcover classes were highly variable during the length of the transect.

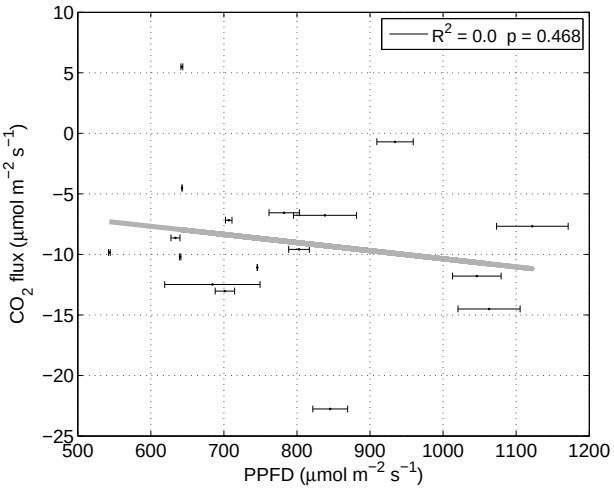

Figure 4.9: PPFD, with standard error bars, versus airborne CO_2 flux measurements calculated using a 2500 m averaging window.

Inferring LUE using hyperspectral SVIs

Figure 4.11 shows relationships between SVIs measured by the downward pointing spectrometer and LUE and between the same SVIs and PPFD. These measurements were filtered to exclude measurements that were not dominated by birch (measurements where birch cover was < 50 % were excluded from further analysis). There was a weak to moderate relationship between PRI_{ASD} and LUE ($R^2 = 0.4$, $p < 0.05$). A similar relationship was found between PRI_{ASD} and PPFD ($R^2 = 0.4$, $p < 0.05$). There was no significant relationship ($p > 0.05$) found between either $NDVI_{ASD}$ and LUE or between $NDVI_{ASD}$ and PPFD.

4.4 Discussion

Remote sensing derived SVIs are important indicators of ecosystem productivity. However, our results show that under variable illumination conditions broadband SVIs, such as the MODIS NDVI and EVI products, are inadequate predictors of

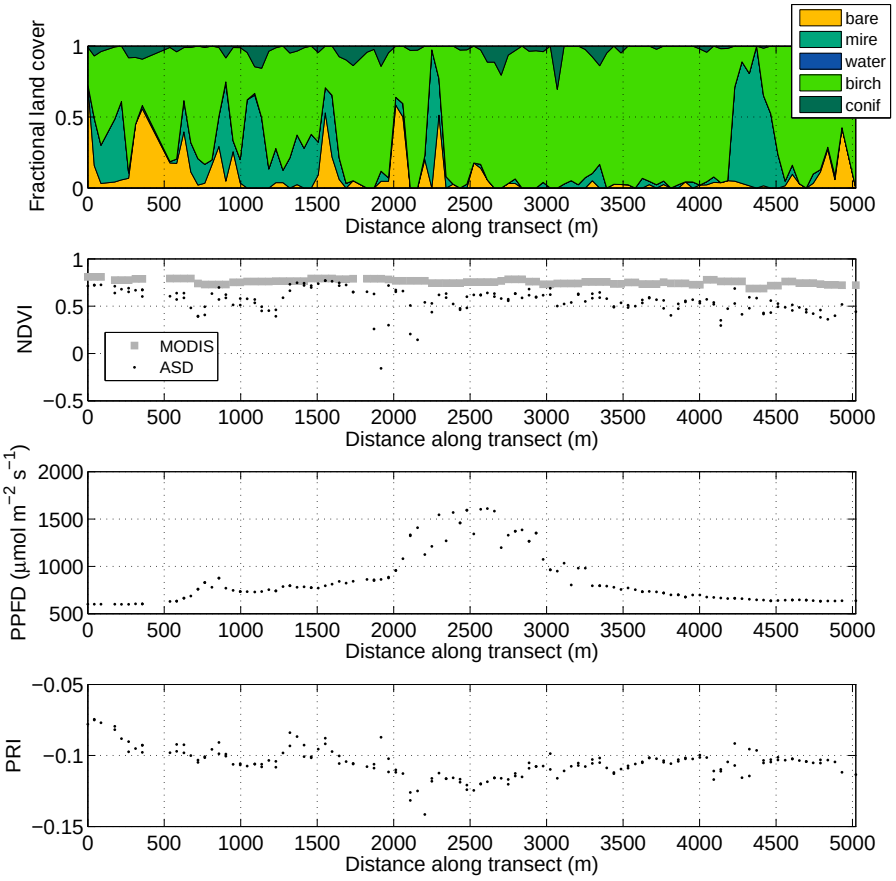

Figure 4.10: Land cover classification and hyperspectral measurements along a particular transect (marker number 47). From top to bottom: fractional land cover in ASD field of view, $NDVI_{ASD}$ and MODIS NDVI, incident PPFD and bottom, PRI_{ASD}.

CO_2 exchange across the Arctic landscape. In addition, airborne hyperspectral SVIs such as the PRI were found to have the potential to measure landscape scale changes in LUE.

Although no significant relationships were found between satellite SVIs and CO_2 flux observations, moderate relationships were found between airborne PRI measurements and landscape LUE; and between airborne PRI measurements and PPFD. This suggests two things. Firstly SVIs alone cannot be used to infer

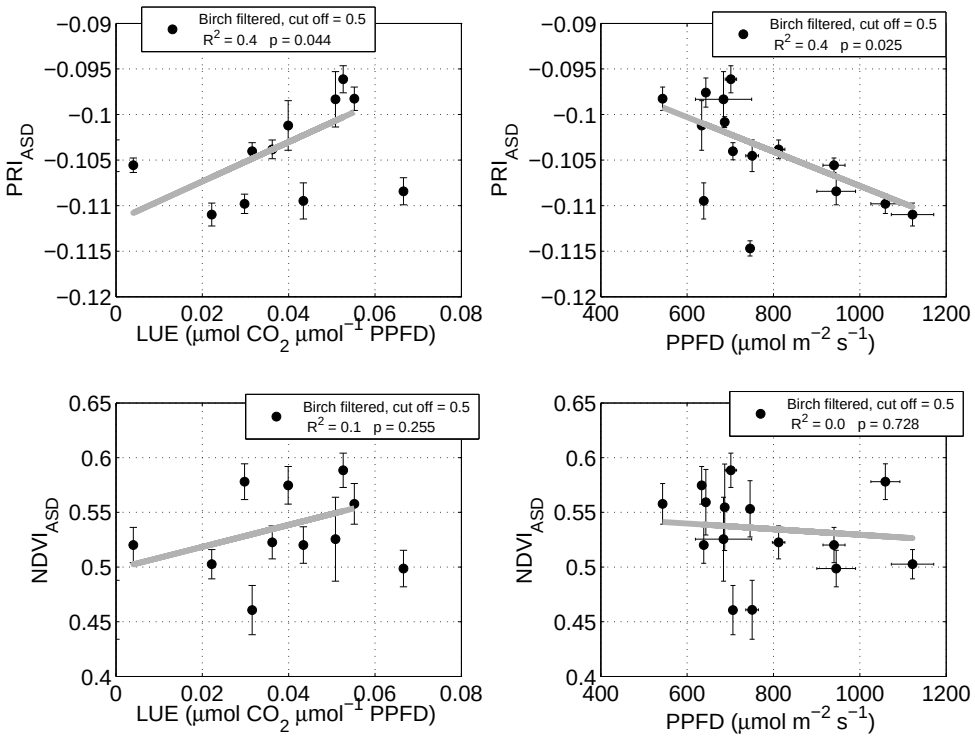

Figure 4.11: Relationships and linear models between airborne hyperspectral SVIs and LUE and between airborne hyperspectral SVIs and PPFD. Top left: PRI_{ASD} versus LUE, top right: PRI_{ASD} versus PPFD, bottom left: $NDVI_{ASD}$ versus LUE, bottom right: $NDVI_{ASD}$ versus PPFD.

carbon fluxes across the Arctic landscape in changing light conditions. Secondly, airborne flux measurements can be used to detect changes in net carbon fluxes across the landscape on short time scales due to rapidly changing illumination conditions. In agreement with this study, Desjardins *et al.* (2006) found that the relationship between airborne CO_2 flux measurements and NDVI degraded during changeable light conditions for measurements collected over an agricultural region. On the second point, Mauder *et al.* (2007) conducted an innovative experiment by measuring airborne fluxes during a solar eclipse event. Mauder *et al.* (2007) found a significant decrease in CO_2 flux observations during and immediately after the eclipse, consistent with a decrease in photosynthetic activity

driven by a fall in PPFD. Zulueta *et al.* (2011) recently used MODIS NDVI observations to upscale airborne flux measurements across the Alaskan Arctic landscape. Because no significant relationships were found between satellite SVIs and flux observations this approach was not feasible with the data presented in this study. It is therefore hypothesised that changing light conditions drive changes in photosynthetic activity across the landscape on short time scales. It follows that to use SVIs to predict net carbon fluxes in changing illumination conditions it is necessary to use an LUE based model.

In this study hyperspectral measurements from a relatively small footprint spectrometer (∼30 m) were compared to 2.5 km averaged flux values over a particularly heterogeneous landscape. In addition, relationships between a relatively coarse spatial resolution satellite sensor (MODIS) and airborne flux and hyperspectral measurements were explored, therefore understanding the issue of spatial scale is key to the study. MODIS observations present near unrivalled spatial and temporal coverage. However, coarse resolution satellite pixels miss many fine resolution features present in heterogeneous environments. Such an effect is clear when comparing airborne along-transect NDVI observations to satellite observations (see figure 4.10). One obvious solution is to use higher resolution imagery from a different satellite sensor, though for a variety of reasons (temporal or spatial coverage, cost and time constraints) this may not always be possible. With the increasing use of coarse resolution Earth observation data the question of scale and information loss is a key issue in landscape scale studies. Recent innovative work by Stoy *et al.* (2009) used information theory to quantify optimum remote sensing pixel sizes across Arctic regions, whereas Hill *et al.* (2011a) proposed a data assimilation approach for quantifying non-linear information loss.

The flux averaging window length is key to producing accurate flux measurements, and is also of paramount importance when comparing flux measurements to

remote sensing land surface observations. If the averaging length is too short then measurements are likely to underestimate flux contributions from mesoscale structures (Desjardins *et al.*, 2006). In contrast, large averaging lengths will result in large flux footprints and information is invariably lost in a heterogeneous landscape such as Kevo. In theory, it is possible to estimate the full range of wavelengths of turbulent structures that contribute to the flux measurements from the flux cospectrum (Desjardins *et al.*, 1989). This approach was used to help to determine an optimum size of 2.5 km. Although the majority of flux contributions were accounted for by the 2.5 km windows, it is clear from the Ogive plots (figure 4.2) that there are particular transects (such as marker numbers 42 and 45) with flux losses. For several European sites Gioli *et al.* (2004) found optimal windows of 3 - 4.5 km using this method. Other studies, particularly those which relate flux measurements to remote sensing observations (Hutjes *et al.*, 2010; Chen *et al.*, 1999), used lower averaging lengths ($\sim$ 2 km).

Although the requirement for a minimum averaging length restricts the spatial resolution of airborne flux observations, several studies have used innovative methods to estimate fluxes from specific land cover types based on airborne flux observations and (remote sensing derived) land cover maps (Chen *et al.*, 1999; Ogunjemiyo *et al.*, 2003; Kirby *et al.*, 2008; Hutjes *et al.*, 2010). These methods typically solve systems of linear equations based upon individual flux measurements and the types of ground cover present in estimated flux footprints. The solutions to the systems of equations are estimates of fluxes for each land-cover type. Because of the heterogenous illumination conditions, and the observed vegetation response, a simple linear unmixing approach was not possible for this particular data-set, however it may be possible to combine an LUE based approach with such an analysis. In a similar approach to the one proposed, Maselli *et al.* (2010) used a process-based ecosystem model to predict carbon fluxes across the

landscape and found that these predictions compared favourably with aircraft flux observations.

Systematic error was not quantified for the flux measurements due to the lack of a wind tunnel calibration. The wind perturbation, $w\prime$, is estimated relative to the Earth by removing the aircraft speed, calculated from the INS system, from wind measurements made relative to the aircraft using the BAT probe. The accurate calculation of winds relies on an ideal flow model over the BAT probe, in reality there are deviations from this model caused by the shape of the aircraft and the position of the probe (under the wing). Both the fuselage and the wing itself will cause deviations in the airflow around the probe. At present the error related to these factors is unknown, however a full wind tunnel calibration for the BAT probe is due to be conducted in 2012.

4.4.1 Future work

A new hyperspectral imaging system fitted to the University of Edinburgh's research aircraft will enable spatially explicit measurements of vegetation indices, from within flux footprints, to be collected during the 2012 season. Improved calibration of the eddy covariance flux measuring equipment will lead to more robust airborne flux measurements with associated error estimates.

Future work should concentrate on developing a remote sensing LUE-based approach which combines a measure of greenness, such as NDVI, with a PRI based LUE estimate. Such an approach would facilitate spatial estimates of carbon exchange across the landscape in variable illumination conditions. Improved airborne eddy covariance measurements could be used to calibrate and validate an LUE-based model.

4.4.2 Conclusions

Aircraft observations of CO_2 fluxes were found to be sensitive to changes in incident solar radiation across the heterogenous Arctic landscape. PRI was also found to be sensitive to changes in incident solar radiation, which suggests that PRI has the potential to quantify the sensitivity of landscape scale carbon fluxes to incident radiation. No significant relationships were found between MODIS SVIs and airborne CO_2 flux measurements, most likely due to changing light conditions eliciting a photosynthetic response. PRI was found to be correlated with LUE. This correlation was probably due to the biological response of the PRI signal to changing illumination conditions, as a significant relationship was also found between PRI and PPFD.

Chapter 5

Modelling the dynamic changes in apparent reflectance due to chlorophyll fluorescence over short time-scales (seconds to minutes)

Abstract

Chlorophyll fluorescence is often referred to as the 'probe' of photosynthesis, and the promise is that new space-borne remote sensing observations of chlorophyll fluorescence will help to constrain global estimates of terrestrial photosynthesis. Numerical simulations of chlorophyll fluorescence are important as they provide a link between the complicated underlying physiology and the physically observable signal. A coupled physiological-radiative transfer model is presented that predicts changes in the apparent reflectance of a leaf, due to chlorophyll fluorescence, that occur on a timescale of seconds to minutes. The biochemical model is based on a relatively detailed model of the dynamics of the fate of absorbed light energy through photosystem II. The radiative transfer component is derived from empirically obtained fluorescence excitation-emission matrices and the PROSPECT leaf model. A Markov Chain Monte Carlo (MCMC) algorithm was used to optimise biochemical model parameters by fitting model simulations of transient chlorophyll fluorescence to measured reflectance spectra. The model successfully simulated the transient fluorescence decay curve and reproduced yield estimates for photochemical and non-photochemical quenching when validated against an independent data-set. The biochemical model is driven solely by incident radiation, to scale to the canopy and to use the model on trans-seasonal time scales the effects of temperature and photo-inhibition must be taken into account.

5.1 Introduction

Accurately measuring terrestrial photosynthesis from space is a key objective of present day Earth observation science. This is because the terrestrial biosphere is one of two natural sinks for anthropogenic CO_2 emissions (the other being the oceans). Chlorophyll fluorescence is often referred to as the *probe* of photosynthesis (Bolhar-Nordenkampf *et al.*, 1989; Baker, 2008) and as it is now possible to measure terrestrial chlorophyll fluorescence from space. The promise is that these new space observations will help to constrain global estimates of photosynthesis (Joiner *et al.*, 2011; Guanter *et al.*, 2007; Frankenberg *et al.*, 2011a). However, there is no single, ubiquitous relationship between chlorophyll fluorescence and the rate of photosynthesis which limits the applicability of simple empirical approaches.

The relationship between chlorophyll fluorescence and photosynthesis is affected by any number of factors including time of day, light intensity, temperature and water availability (Rosema *et al.*, 1998). Mechanistic models offer an alternative approach to purely empirical methods, and may go some way to explaining the variability of chlorophyll fluorescence under natural conditions. This is because mechanistic models aim to simulate fluorescence by modelling the physiological and physical processes that give rise to the emission. It follows that through the inversion of such a model it may be possible to use measurements of fluorescence to estimate the physiological state of the canopy, including processes such as the electron transfer rate (ETR) that directly affect the rate of photosynthesis. To simulate remote sensing observations of chlorophyll fluorescence it is necessary to include a representation of the dynamic biochemistry that causes the initial emission and a representation of the radiative transfer processes that transmit the signal from the site of the emission (the photosystems) to the observer (the spectrometer).

Chlorophyll fluorescence occurs when an electron in an electronically excited chlorophyll molecule falls to a lower energy state, thereby emitting a photon. Chlorophyll fluorescence competes with photochemistry (the photosynthetic reactions), constitutive heat dissipation, and regulatory heat dissipation (which is also referred to as non-photochemical quenching, NPQ) as an alternate pathway for absorbed light energy (see figure 5.1). Because the pathways are in direct competition, there is an intrinsic biochemical link between an observable quantity, chlorophyll fluorescence and photosynthesis. Each energy dissipation pathway can be thought of as a yield, with the sum of all the yields equal to unity. Yields are properly defined as the ratio of the rate constant of the process of interest (chlorophyll fluorescence, heat dissipation, photochemistry) to the sum of all the rate constants (Blankenship, 2002). More intuitively, yields can be thought of as the probability that absorbed light will follow a particular pathway.

A suite of active instrumentation can be used to measure relative changes in fluorescence kinetics. These instruments are used by plant physiologists to compute a range of photosynthetic parameters that relate to the rate constants of energy dissipation. Such measurements can also be used to validate and calibrate kinetic models of photosystem II (PSII). Porcar-Castell *et al.* (2006) developed a mechanistic model of PSII that is able to predict the photochemical, non-photochemical and fluorescence yields and ETR. ETR is generally assumed to be in equilibrium in canopy carbon assimilation models, however the reality is that changing light conditions can have a significant effect on net carbon uptake (Rascher and Nedbal, 2006). Therefore the inclusion of dynamic representations of light energy dissipation in land surface vegetation schemes may improve estimates of carbon exchange.

Passive remote sensing studies have focused mainly on retrieving the steady-state chlorophyll fluorescence signal, F_t (Meroni *et al.*, 2009). F_t can be calculated directly in absolute radiometric units, using the Fraunhofer Line Discriminator

(FLD) technique (Plascyk, 1975; Plascyk and Gabriel, 1975), which exploits 'dark' spectral lines in the Sun's and/or Earth's atmosphere. The effects of chlorophyll fluorescence on the apparent reflectance spectra (the ratio of reflected radiance to incident irradiance) of leaves can also be estimated using any number of reflectance indices (Meroni *et al.*, 2009). In separate studies Gamon *et al.* (1990), Zarco-Tejada *et al.* (2000a), Campbell *et al.* (2008) measured the dynamic changes in apparent reflectance due to chlorophyll fluorescence over a timescale of seconds to minutes, and showed that apparent reflectance measurements can be used to study the same phenomena as pulse amplitutde fluorometer (PAM) measurements.

Significant progress has been made in attempting to model the radiative transfer of the chlorophyll fluorescence signal, as observed by passive sensors. Rosema *et al.* (1991) developed a leaf and canopy level chlorophyll fluorescence model to simulate laser-induced fluorescence. The model was based on the Kubelka-Monk system of differential equations which model fluorescence as upward and downward fluxes and are solved numerically. The FluorMOD project (Miller *et al.*, 2005) was undertaken by the European Space Agency (ESA) to develop a full canopy model of chlorophyll fluorescence, as a precursor to a satellite mission. This work resulted in a leaf and canopy radiative transfer model based on PROSPECT (leaf) (Jacquemoud and Baret, 1990) and SAIL (canopy) (Verhoef, 1984) respectively. Middleton *et al.* (2008) found good agreement between canopy scale observations of chlorophyll fluorescence and an improved version of FluorMOD for a corn canopy. The Soil Canopy Observation, Photochemistry and Energy fluxes (SCOPE) model (van der Tol *et al.*, 2009b) consists of a physiological leaf model coupled to a modified version of the FluorMOD radiative transfer model and is designed to predict the steady state chlorophyll fluorescence signal, as well as a range of other canopy states such as net photosynthesis, at sub-hourly time-scales.

In this study a coupled biochemical radiative transfer model is presented that

predicts the leaf-level superposition of chlorophyll fluorescence on the apparent reflectance spectrum. The model works on time-scales of seconds to minutes and is based on two sub-models, a dynamic model of PSII (Porcar-Castell *et al.*, 2006) and a radiative transfer model based on PROSPECT (Jacquemoud and Baret, 1990). A Bayesian approach is used to calibrate the model, as this provides a rigorous framework for the incorporation of prior parameter knowledge and posterior estimates of parameter distributions and model error. The model is validated against an independent data-set and recommendations for scaling the model to the canopy are made.

5.2 Methods

5.2.1 Coupled biochemical radiative transfer model description

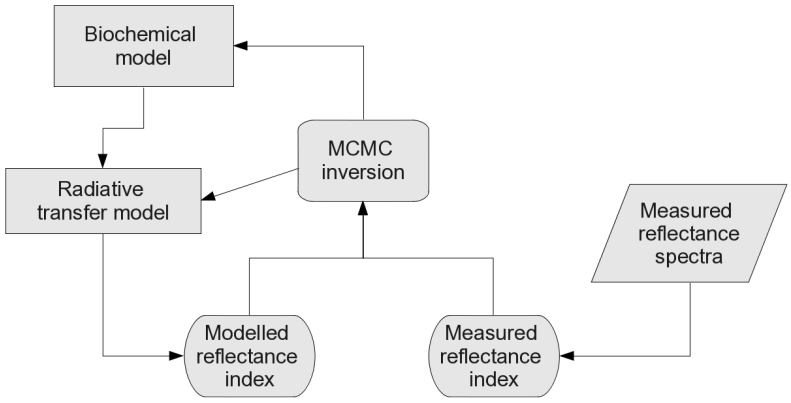

Figure 5.1: Flowchart for the combined predictive modelling and parameter estimation process.

The modelling scheme in this study consists of a biochemical model coupled

to a leaf radiative transfer model. The yield of chlorophyll fluorescence, ϕ_f, is predicted by the biochemical model, and is also an input for the leaf radiative transfer model, providing the direct interface between the two sub-models.

Model parameters are calibrated by fitting measured data to a time series of simulated apparent reflectance values, in the form of a fluorescence-based reflectance index. A Bayesian optimisation algorithm, adaptive Markov Chain Monte Carlo (MCMC), was used (Laine, 2008) to estimate parameter values as this allows for the incorporation of prior parameter knowledge and rigorous prediction of model error. The optimised model was then validated against an independent data set.

Biochemical model

The biochemical leaf model is designed to simulate the dynamics of energy flow through PSII at the timescale of seconds to minutes and is based on the Porcar-Castell *et al.* (2006) model. A graphical representation of the biochemical model is presented in figure 5.2. The model is driven by incident radiation alone (quantified as photosynthetic photon flux density, (PPFD)), and predicts a number of parameters related to chlorophyll fluorescence, including ϕ_f, ϕ_{NPQ} and ϕ_p. The model is based on the lake model assumption of PSII, which permits energy transfer between a set number, N, of PSII units. Each PSII is assumed to contain a set number of chlorophyll, xanthophyll, quinone and plastoquinone molecules (which are grouped together as plastoquinone-equivalent molecules).

To estimate ϕ_f, the ratio of the rate constant of fluorescence to the other rate constants is taken:

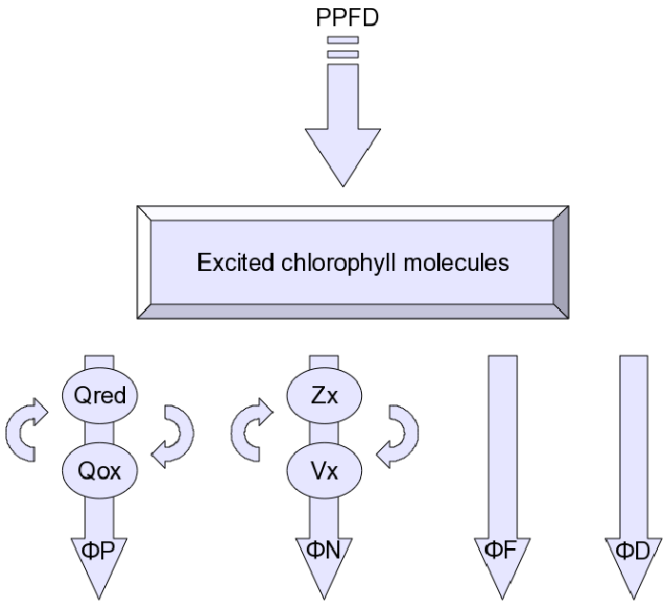

Figure 5.2: Diagram of the biochemical modelling scheme. Absorption of light energy causes excitation of chlorophyll molecules, the excited energy is then used in one of the four pathways (ϕ_p, ϕ_N, ϕ_F, ϕ_D). The photochemical, ϕ_p, and NPQ pathways, ϕ_N, are modulated by two dynamic processes, plastoquinone reduction and the xanthophyll cycle, that are represented in the biochemical model as differential equations.

$$\phi_f = \frac{k_F}{k_F + k_D + k_N E + k_P Q} \tag{5.1}$$

Where k_F, k_D, k_N, k_P are the rate constants of fluorescence, constitutive heat dissipation, non-photochemical quenching and photochemistry respectively. In equation 5.1, the rate constants, k_n and k_p, are adjusted from optimal values by E and Q. E and Q are referred to as *quenching coefficients* and are the dynamic core of the model. E is equal to the fraction of the xanthophyll molecules that have been converted to zeaxanthin and is therefore representative of the efficiency of

non photochemical quenching (NPQ). Q is equal to the fraction of plastoquinone-equivalent molecules that are in the oxidised state, and is representative of the efficiency of photochemical quenching. The number of chlorophyll molecules in an excited state, Chl_{on}, is solved for using a mass balance assumption:

$$\dot{Chl}_{on} = c - k_F \times Chl_{on} - k_D \times Chl_{on} - k_N \times Chl_{on} \times E - k_D \times Chl_{on} \times Q \quad (5.2)$$

The rate of light capture, c, is calculated as:

$$c = PPFD \times \alpha \times chl_{off} \quad (5.3)$$

where α is an empirical absorption parameter that represents the physical absorption properties of the leaf. $\dot{Chl}_{on}$ occurs at a much faster rate than other processes in the model and is therefore assumed to be in equilibrium ($\dot{Chl}_{on} = 0$):

$$Chl_{on} = \frac{c}{K_f \times Chl_{on} + K_d \times Chl_{on} + k_n \times Chl_{on} \times Z_x + k_p \times Chl_{on} \times PQ_{ox}} \quad (5.4)$$

If the total concentrations of xanthophyll molecules and quinone-equivalents are assumed to be in equilibrium and initial pool sizes of v_x, z_x, PQ_{ox} and PQ_{red} are estimated then it is possible to model the time-dependant behaviour of Q and E by coupled differential equations, using *building* and *relaxation* rate constants. Q is calculated as:

$$\dot{PQ}_{red.} = Chl_{on} \times k_p \times PQ_{ox} - k_{pq}^{relax} \times PQ_{red.} \quad (5.5)$$

$$Q = \frac{PQ_{ox}}{PQ_{ox} + PQ_{red}} \quad (5.6)$$

The second term of equation 5.5 is the rate of quinone-equivalent reduction and is determined by the rate constant of photochemistry, k_p, and the number of excited chlorophyll molecules. The third term is the rate of re-oxidation (relaxation) of this pool, and is controlled by a rate constant, k_{pq}^{relax}, and the size of the reduced quinone-equivalent pool. E is calculated as:

$$\dot{z}_x = k_{npq}^{build} \times v_x - k_{npq}^{relax} \times z_x \quad (5.7)$$

$$E = \frac{z_x}{v_x + z_x} \quad (5.8)$$

The second term of equation 5.7 represents the conversion of v_x to z_x (the rate of the building of NPQ) and is determined by the size of the v_x pool, a rate constant, k_{npq}^{build}. The third term of equation 5.7 represents the re-conversion of z_x to v_x and is controlled by the size of the z_x pool and a rate constant, k_{npq}^{relax}. The intermediary carotenoid pigment antheraxanthin is excluded from the system to reduce complexity. Equation 5.7 was solved analytically, whereas the solution to equation 5.5 was obtained using a forward difference approximation.

Leaf radiative transfer model

The model predicts apparent reflectance, ρ_a, as a function of wavelength, λ:

$$\rho_a(\lambda) = \rho(\lambda) + F_r(\lambda,\ \phi_f,\ N_\lambda) \tag{5.9}$$

where λ is wavelength in nm, $\rho(\lambda)$ is the intrinsic leaf reflectance as modelled by PROSPECT and F_r is the fluorescence contribution to apparent reflectance. F_r is dependant on the yield of fluorescence, ϕ_f, which is predicted by the biochemical model (equation 5.1). F_r is calculated by multiplying a reference *Excitation-Fluorescence matrix*, M_{ij}, by incident radiation, $N(\lambda)$[1] and summing across fluorescence absorbance wavelengths and finally normalising by incident radiation:

$$\pi F_r = \frac{\phi_f}{0.02} \times \frac{\sum_{i=400\ nm}^{750\ nm} N(\lambda) \times M_{ij}}{\sum_{i=400\ nm}^{750\ nm} N(\lambda)} \tag{5.10}$$

In this study the M_{ij} matrix supplied with the SCOPE model code was used as well as a modelled $N(\lambda)$ spectrum. As the EF matrix was empirically obtained for a plant with an $\phi_f = 0.02$, the corrective factor, $\frac{\phi_f}{0.02}$, is needed to predict F_r as a function of ϕ_f.

5.2.2 Experimental procedure and leaf measurements

Measurements were collected on lettuce (*Lactuca sativa* L.) seedlings during August and September 2010. Prior to measurements, the seedlings were dark adapted, using leaf hoods, for 2 hours. The seedlings were then moved into an

[1] Where $PPFD = \int_{450\ nm}^{750\ nm} N\ \mathrm{d}\lambda$.

full sunlight outdoor environment, placed in a non-reflective horizontal holder and the hoods were removed. Upon removal of the hoods contiguous measurements of reflectance spectra were immediately collected. An Ocean Optics (Ocean Optics, USA) USB 2000 spectrometer was used to collect spectra at a frequency of > 1 hz. The USB 2000 measures spectra at 1 nm full width half maximum resolution in the wavelength range 340 to 1021 nm. Reflectance spectra were calculated by normalising leaf spectra to measurements of a calibrated, near-lambertian reflective standard (Spectralon, Labsphere, North Sutton, NH, U.S.A). Spectra were sampled in the nadir position at a fixed distance from the adaxial side of the leaf, which resulted in a spot radius of less than 3 cm.

To reduce the dimensionality of the data, and to simplify the optimisation, a reflectance index, $R680$, that is known to be sensitive to changes in chlorophyll fluorescence (see figure 5.3 and Zarco-Tejada *et al.* (2000b)) was calculated using the following formula:

$$R680 = \frac{\rho_{680}}{\rho_{630}} \tag{5.11}$$

Where ρ_λ is reflectance at $_\lambda$ nm. The difference between a time-series of measured and simulated reflectance index values was used to optimise the model using an adaptive MCMC algorithm.

5.2.3 Calibration using the MCMC method

Bayesian methods, such as the Markov Chain Monte Carlo (MCMC) algorithm are attractive for two main reasons. Firstly they facilite the use of prior information, such as previously measured parameter values, in the calibration procedure and

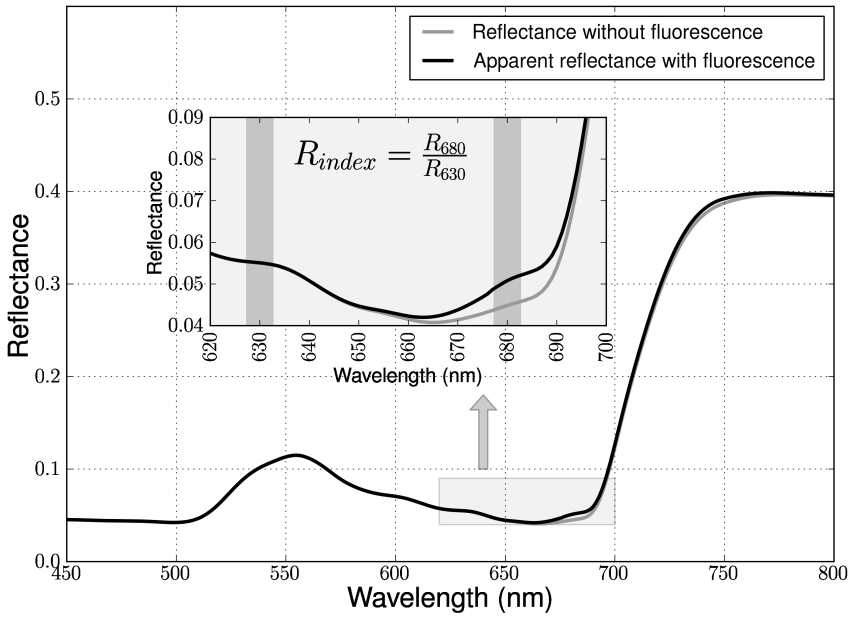

Figure 5.3: Modelled reflectance spectrum with and without fluorescence contribution. The spectral vegetation index, $R680/R630$, is shown in the insert.

secondly because they provide estimates of error for both optimised parameters and model predictions.

MCMC methods have received significant attention in recent years and a brief introduction is provided here (for more information on the foundations of the method and for some recent applications see Laine (2008)). The MCMC algorithm generates an iterative chain of guesses for each parameter based on prior information, referred to as *priors*, the algorithm converges when the chains becomes stationary. The stationary chains represent the posterior distributions of the parameters, by taking the mean (or other statistic) of the chain the 'best guess' for each parameter can be estimated. In addition, the posterior distributions also provide error estimates of the parameters and can be combined with knowledge of model error to calculate predictive error. In this study, Gaussian distributions were used for priors.

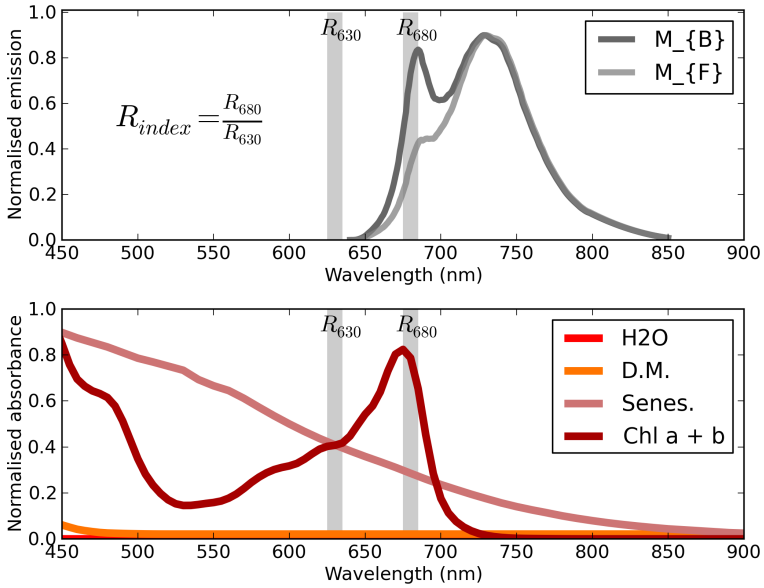

Figure 5.4: Spectra utilised in the radiative transfer model; the vertical grey lines show the wavelengths of the reflectance index used in the MCMC optimisation. Top: chlorophyll fluorescence emission spectra for adaxial and abaxial sides of a leaf. These spectra are scaled using the fluorescence yield parameter, ϕ_f, to predict leaf-level chlorophyll fluorescence. Bottom: PROSPECT specific absorbtion spectra. PROSPECT uses combinations of these spectra to predict leaf reflectance, apparent reflectance is then predicted by combining prediction of leaf level fluorescence with PROSPECT predictions of leaf level reflectance.

Validation data-set

Data from three Alder (*Alnus glutinosa* L.) trees were used to validate the model. This was supplied by Porcar-Castell (personal communication) and consisted of portable chlorophyll fluorometer (FMS-2, Hansatech Ltd) measurements of the photochemical, ϕ_p, and non-photochemical quenching, ϕ_n, yields, after dark adapted leaves were exposed to simulated sunlight. After 400 seconds of exposure

the light was switched off, therefore the ability of the model to simulate the recovery from high levels of NPQ could also be tested.

5.3 Results

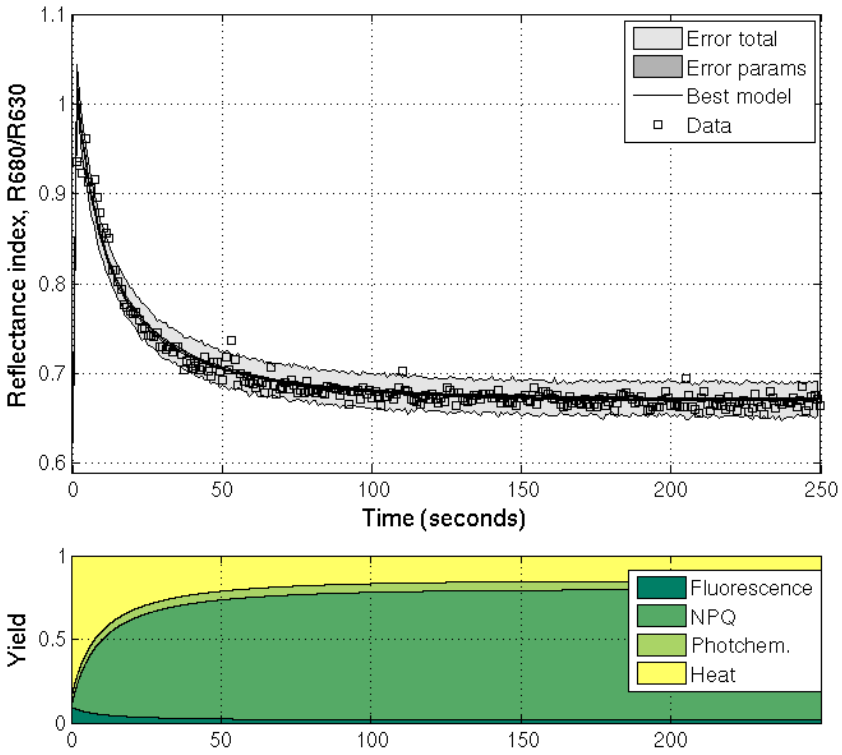

Figure 5.5: Top: Modelled and measured reflectance indices. Squares represent measured reflectance index values after a dark adapted leaf has been exposed to strong sunlight. The shaded regions represent two different predictions of error, the dark line is the *best guess* modelled prediction calculated using the posterior parameter distributions. Bottom: simulated biochemical yields for the optimised parameters.

5.3.1 Coupled biochemical radiative transfer model evaluation

The coupled model successfully reproduced the transient behaviour of the fluorescence-based reflectance index, $R680$, over a timescale of seconds to minutes, on exposure of a leaf to full sunlight, post dark-adaption. Figure 5.5 shows the measured and modelled behaviour of the reflectance index during the first few minutes of the transient period. The shaded region represents predictions of error, which is a combination of the posterior parameter error predictions and uncertainties related to the predictive model. The dark line that runs through the shaded error region is the best model prediction, it is calculated by taking the mean of the posterior parameter distributions (figure 5.6).

The model simulated the response of a dark-adapted leaf to high light conditions ($> 2000\ \mu\text{mol}\,\text{m}^{-2}\,\text{s}^{-1}$), whereby under such conditions NPQ is expected to dominate at steady state. As the leaves were dark adapted prior to the measurements, it was possible to derive estimates of initial conditions. After substantial dark adaption it is assumed that reversible NPQ, E, fully relaxes hence v_x = total number of xanthophylls and $z_x = 0$. It is also assumed that all reaction centres are open therefore Q is equal to unity, and PQ_{ox} = total number of quinone equivalents and $PQ_{red} = 0$. As well as the transient reflectance index behaviour, figure 5.5 also shows the modelled yields for the same model run. The NPQ yield slowly climbs from an initial value of 0 to a steady state yield of over 0.7. The photochemical yield rapidly falls from an initial value of greater than 0.8 to a steady state value of less than 0.05.

If a model is over-parametrised it may be possible to accurately reproduce a measurement, such as $R680$, with an unrealistic set of parameters. By validating the optimised model with independent measurements of different model states it is possible to reduce this risk. Figure 5.8 shows predictions of modelled yields,

ϕ_{fd}, ϕ_n, ϕ_p, based on the optimised parameters with yield measurements of Alder leaves. At 400 seconds the light was switched off, this enables the model to be tested for recovery behaviour. The model was able to reproduce the behaviour of the yields and produces good estimates of the steady state yields. However, there are some noticeable discrepancies between data and model predictions in the transient yields. The model overestimates the combined heat and fluorescence yields, ϕ_{fd}, and slightly underestimates the NPQ yield, ϕ_n.

5.3.2 Parameter estimation and validation

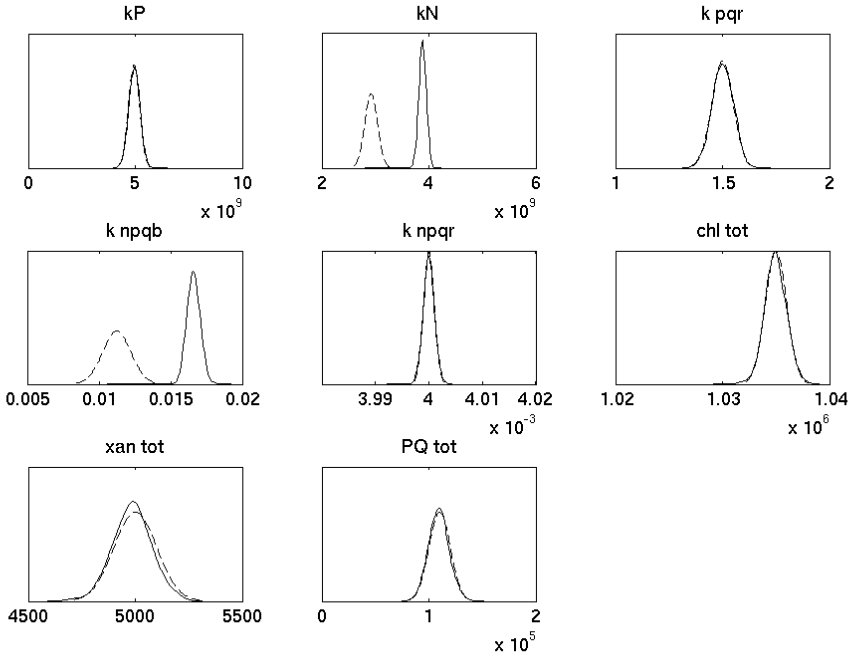

Figure 5.6: Prior (dotted lines) and posterior (solid lines) biochemical parameter distributions.

As the intrinsic leaf reflectance, ρ_l, was assumed to remain constant on the timescale of a model run, PROSPECT parameters were estimated prior to optimisation by adjusting model parameters to fit an example lettuce spectrum.

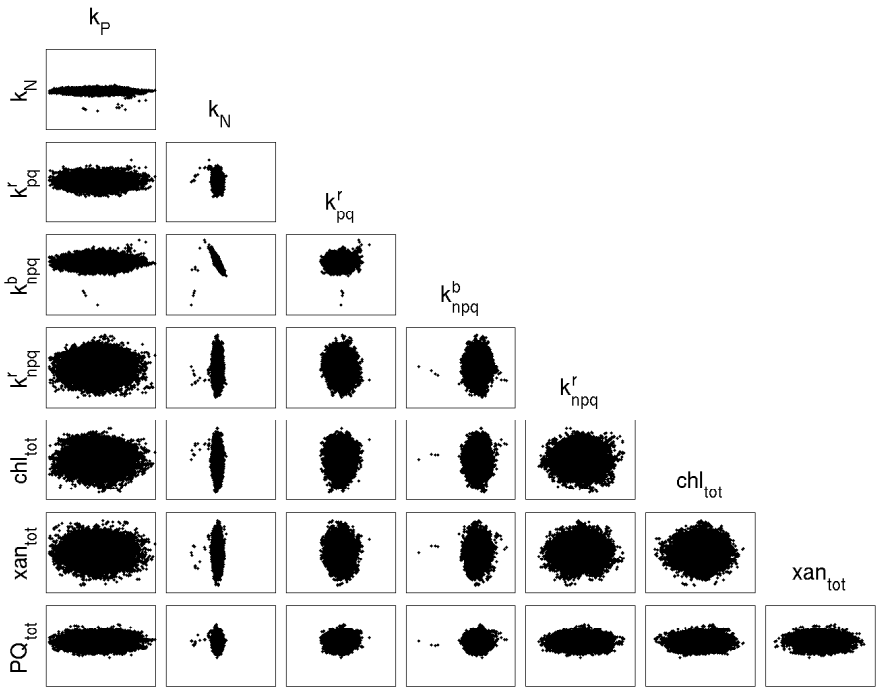

Figure 5.7: Posterior parameter correlations. Notice a relatively strong correlation between two NPQ parameters, k_N and k^b_{npq}.

The number of layers parameter was set at 3, chlorophyll content at 36.5 μg cm^{-2}, carotenoid content at 9 μg cm^{-2}, water content at 1e-3 cm, and dry matter at 0 μg cm^{-2}.

Posterior parameter statistics are shown in table 5.1 and distributions are plotted in figure 5.6. Prior information was available for the number of chlorophyll, xanthophyll and plastoquinone equivalent molecules as well as the rate constant of photochemistry, k_p, and the rate constant of NPQ, k_p (Porcar-Castell *et al.*, 2006). Gaussian priors were used to constrain these parameters. The rate constants of fluorescence and basal heat dissipation, k_f and k_d were not optimised, using values from Porcar-Castell *et al.* (2006). The validation data-set was used to guess first approximations for the relaxation and building rate constants, k^{relax}_{pq}, k^{build}_{npq},k^{relax}_{npq} and priors were assigned based on these initial guesses. The model converged to

narrow, posterior distributions for each of the parameters. The rate constant for the building of NPQ, k_{npq}^{build}, was estimated to be an order of magnitude greater than the rate constant for the relaxation of NPQ, k_{npq}^{relax}. The posterior mean value for k_N was almost twice that of the prior mean. There was little change between the prior and posterior distributions of the pigment pool parameters.

Correlations between biochemical parameters are shown as scatter plots in Figure 5.7. Correlated parameters can be an indication of deficiencies in the mathematical formulation of a model, as correlation implies a certain level of parameter redundancy. With the exception of the NPQ parameters K_N and k_{npq}^{build} there are no significant correlations between any of the parameters.

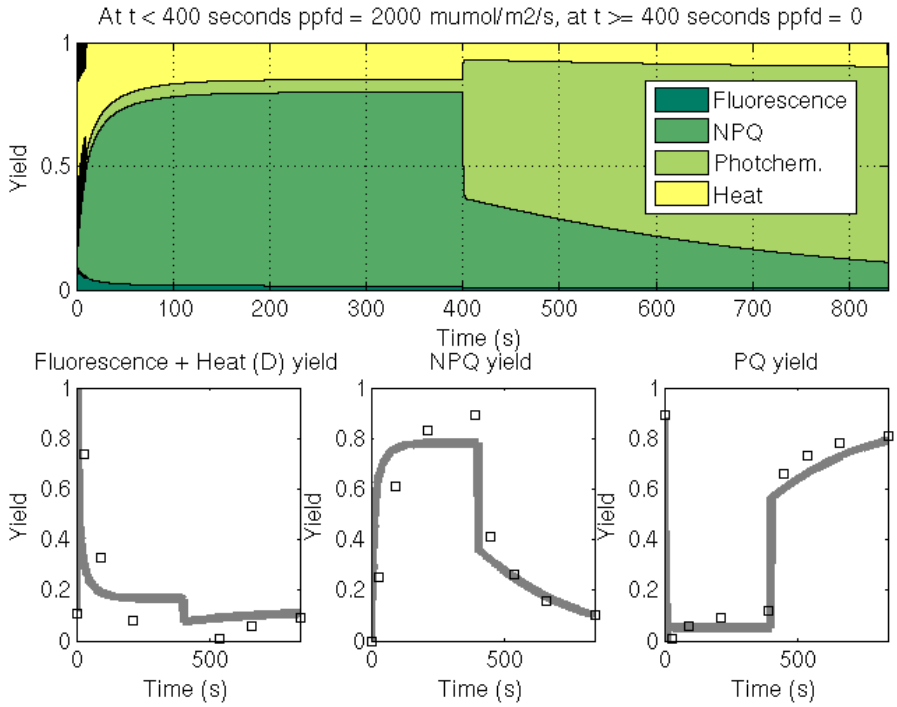

Figure 5.8: Time-series of biochemical model yields for the validation data set. Where black squares are measured data points and thick lines are the optimised modelled predictions.

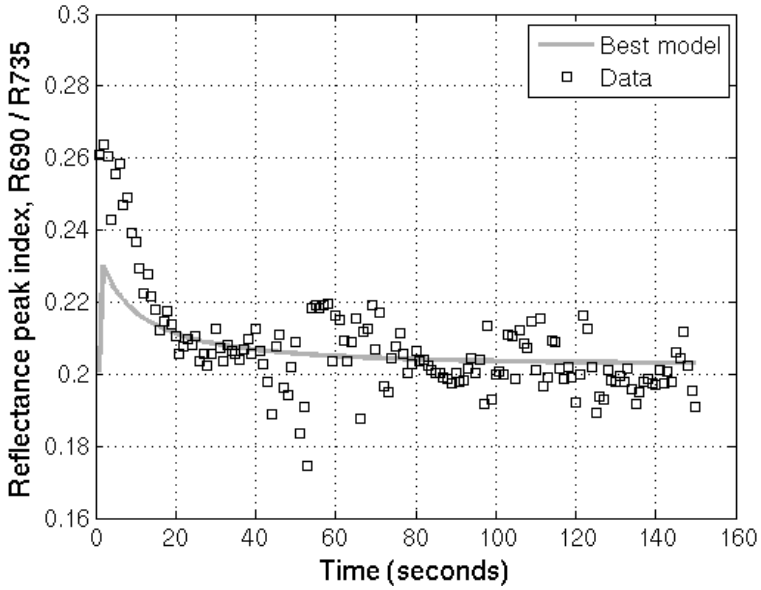

Figure 5.9: Time-series of the simulated and measured two peak reflectance index, $R690/R735$. This relfectance index is used to quantify the change of shape in the chlorophyll emission spectrum, the model is significantly different to the measured data during the first few seconds.

5.4 Discussion

The object of this study was to develop a leaf scale coupled biochemical radiative transfer model of chlorophyll fluorescence. The coupled model presented in this study was used to simulate the effects of dynamic changes in leaf reflectance due to chlorophyll fluorescence. By coupling a mechanistic representation of the energy flow through PSII to a radiative transfer model, changes to the reflectance index, $R680$, were simulated on exposure of a dark adapted leaf to full sunlight conditions.

The modelled reflectance index curve (figure 5.5) rises from a minimum initial condition to a maximum value and then decays over a period of minutes to the steady state. The decay curve is referred to as the 'Kautsky curve' in the plant

physiological literature. By optimising the model parameters the biochemical model that best simulated the decay was found. The effect of the slow decay of chlorophyll fluorescence on apparent reflectance has been measured previously using hyperspectral remote sensing at the leaf scale (Gamon *et al.*, 1990; Zarco-Tejada *et al.*, 2000a; Campbell *et al.*, 2008). The decay is controlled by a number of competing processes that act to *quench* the fluorescence signal over time. By mathematically modelling these processes, it is possible to simulate the fluorescence signal based on an understanding of leaf biochemistry. Our work builds on previous studies by linking a biochemical model to radiative transfer theory.

Although the model accurately captures the general behaviour of the fluorescence transient, including the steady state reflectance index level, there is some misfit during the first 20 seconds. During this period the model underestimates the magnitude of $R680$ (figure 5.5). This model misfit could either be caused by the biochemical model or the radiative transfer model. The biochemical model is based on the lake model assumption, which assumes perfect connectivity between PSII units. In reality PSII units are probably only partially connected, a decrease in connectivity would lead to an increase in fluorescence yield (Porcar-Castell, personal communication).

The excitation-emission matrix is used to convert incident radiation to emitted fluorescence. In this study a single, empirically excitation-emission matrix obtained under steady-state conditions was used to simulate transient chlorophyll fluorescence. This matrix is the source of potential errors. Firstly, a matrix obtained for one particular species, may not be viable for other species as different species have different emission spectra Campbell *et al.* (2008). Secondly, by using a single matrix to calculate fluorescence emission, it is assumed that the shape of the chlorophyll fluorescence emission remains constant. In reality the shape of the chlorophyll emission spectra is known to change during the transient phase

(Buschmann and Lichtenhaler, 1987). The shape of the emission spectra consists of two main Gaussian like peaks, one short wavelength peak (centred close to 690 nm) and one long wavelength peak (centred close to 730 nm) (see figure 5.4). The short peak[2] is due to emission from PSII whereas the longer wavelength peak is due mainly to PSII with some emission from PSI. During the transient phase the emission from PSI is known to be variable, in addition it has also been suggested that fluorescence due to re-absorption is higher during steady state conditions than at the maximum fluorescence level. Both of these factors may lead to a change in shape of the fluorescence emission spectra (Buschmann and Lichtenhaler, 1987). Because the shorter wavelength chlorophyll emission spectra and the chlorophyll absorption wavelengths overlap, some of the emitted fluorescence is re-absorbed and then re-emitted.

Chlorophyll re-absorption of emitted fluorescence is an important phenomena that affects not only the shape of the emission spectrum but also the positions of the peak values. It follows that changes in chlorophyll pool sizes will affect chlorophyll emission spectra through re-absorption. Using an empirical matrix neglects this effect and assumes a fixed chlorophyll concentration. The change in shape of the emission spectra during the transient phase can be quantified with the reflectance index $R690/R735$. When this index is plotted for modelled and measured reflectance spectra there is a clear difference between simulated and measured results during the first 20 seconds (figure 5.9). This suggests that a change in the shape of the chlorophyll emission spectra is at least partially responsible for the early model-simulation misfit.

MCMC optimisation was used to find a realistic set of parameters that best reproduced the measured reflectance index signal. For the sake of simplicity the optimisation was limited to one type of measurement, a fluorescence based

[2]The short wavelength actually consists of two smaller peaks, both due to PSII emission

reflectance index. However this approach has a serious limitation, the model is somewhat over-parametrised. This means that there are more parameters than can be feasibly estimated using the observed data, due to the complexity of the modelled system. The MCMC method offers a solution to this problem by allowing the incorporation of prior knowledge, and is therefore particularly suited to over parametrised models (Reichert and Omlin, 1997). It is often the case that models with numerous parameters can also contain correlated parameters, correlations between parameters can lead to unrealistic posterior parameter estimates. The rate parameters k_{npq}^{build} and k_{npq}^{relax} were found to be correlated which is due to the mathematical formulation of the model as both parameters occur in the same equation (equation 5.7).

The biochemical model used in this study contains a simplified, mechanistic representation of the xanthophyll cycle (equation 5.7). The xanthophyll cycle refers to the enzyme driven conversion of the carotenoid pigments violaxanthin, v_x, and zeaxanthin, z_x, via an intermediary pigment antheraxanthin. The model solves for the relative proportions of violaxanthin, v_x, and zeaxanthin, z_x but does not include antheraxanthin. This has the effect of reducing the size of the parameter space, but means that the model is not a true, mechanistic representation of the xanthophyll cycle. In this model the proportion of z_x is assumed to be equivalent to the efficiency of NPQ. Ebenhöh *et al.* (2011) used the same assumption as a basis for a slightly more detailed mechanistic model of NPQ. However results from Ebenhöh *et al.* (2011) suggested that this assumption is unrealistic, and that NPQ tends to saturate with relatively low proportions of z_x.

5.4.1 Future work

There are three main ways in which the model can be developed:

1. Extend the model to predict the Photochemical Reflectance Index (PRI) (Gamon *et al.*, 1992, 1993).

2. Scale the model from the leaf to the canopy.

3. Increase the number of shared parameters (model coupling) between the biochemical sub-model and the radiative transfer sub-model.

Because the xanthophyll cycle involves a change in concentrations of light absorbing pigment pools, it also triggers a change in leaf reflectance. PRI was developed by Gamon *et al.* (1992, 1993) as a way to measure changes in leaf reflectance, at 531 nm, due to the xanthophyll cycle. PRI has had widespread use in the remote sensing community at a range of scales (see Garbulsky *et al.* (2010) for a review of applications), although as far as the author is aware, there are no mechanistic models designed to predict PRI. Although a coupled model of NPQ and leaf radiative transfer was presented, the model cannot in its present state be used to simulate PRI. To predict PRI, a representation of the changes in leaf reflectance due to z_x must be made. Modelling the radiative transfer effects that produce the observed PRI signal is complicated by the fact that xanthophylls (or any pigment) have a different absorbance spectra *in vivo* in comparison to *in vitro*. The latest version of PROSPECT (v5) solves this problem by using an inversion technique to tease apart the relative contributions of leaf absorbers such as chlorophyll and bulk carotenoids (Feret *et al.*, 2008). Such a technique could potentially be adapted to estimate the affect of relative proportions of z_x and v_x on the leaf reflectance spectrum, providing adequate data exists (or can be measured) to perform the inversion, enabling the simulation of PRI.

The coupled model is designed to simulate changes in leaf reflectance but cannot be used to model effects of chlorophyll fluorescence on canopy reflectance. FluorMOD was developed as a canopy radiative transfer model capable of

predicting canopy chlorophyll and replacement with the full canopy model is a relatively simple task (although rigorous validation would be needed).

The current model cannot be used on timescales longer than a few minutes as it does not include the effects of temperature on slow NPQ. Slow NPQ occurs on the timescales of hours to days and is often referred to as photo-inhibition. Although an explicit formulation of slow NPQ/photo-inhibition was not included in the current model, Porcar-Castell (personal communication) is currently developing and testing such a model. SCOPE (van der Tol *et al.*, 2009a,b) is a full canopy model capable of simulating canopy chlorophyll fluorescence on seasonal timescales. SCOPE includes the effects of temperature by calculating a *photosystem deactivation* term which is used to scale chlorophyll fluorescence from an a-priori maximum value. Although our model uses a more explicit formulation of the xanthophyll cycle, the effects of temperature on NPQ could be simulated by using a similar mechanism to SCOPE. Canopy instrumentation such as the MONI-PAM (Heinz Walz GmbH, Effeltrich, Germany) (Porcar-Castell *et al.*, 2008) and above canopy hyperspectral radiometers will provide seasonal data-sets that are invaluable in validating both the leaf biochemistry and the fluorescence predictions.

Further improvements to the model could be achieved by increasing the level of coupling between the biochemical and radiative transfer models. The coupling between the biochemical and radiative transfer models was achieved by using a predicted state from the biochemical model, ϕ_f, as an input to the radiative transfer model. A future aim is to increase the level of coupling (number of shared parameters) between the two models. This could be achieved by linking the pigment size parameters in the biochemical model to the PROSPECT input parameter concentrations. Not only would this reduce the parameter space but it would also enable the prediction of the longer term (weeks to seasonal) effects of changes in pigment pool sizes on leaf reflectance.

5.4.2 Conclusions

The dynamic changes in leaf apparent reflectance on short time-scales due to the effects of chlorophyll fluorescence were successfully simulated. This study was designed as a precursor to a trans-seasonal full canopy scheme. To scale the biochemical model to the canopy, two main issues need to be addressed. Firstly the effects of temperature and photo-inhibition on leaf biochemistry need to be accounted for, and secondly the dynamic changes in leaf pigment pools need to be modelled on longer timescales and fully coupled to a full canopy radiative transfer model, such as FluorMOD.

Table 5.1: Prior and posterior parameter values for the biochemical sub-model. k_f and k_D were not optimised.

Name	Definition	Prior mean	Prior SD	Posterior mean	Posterior SD
k_P	rate constant for photochemistry	4.94e9	2.6e8	4.96e9	2.5e8
k_N	rate constant for NPQ	2.92e9	1.2e8	3.88e9	7.49e7
k_D	rate constant for non-basal heat	6.03e8	n/a	n/a	n/a
k_F	rate constant for fluorescence	6.7e7	n/a	n/a	n/a
k_{pq}^{relax}	rate constant for PQ relaxation (re-oxidation)	1.5	0.05	1.5	0.05
k_{npq}^{build}	rate constant for NPQ building	0.011	1e-3	0.016	4.8e-4
k_{npq}^{relax}	rate constant for NPQ relaxation	4e-3	1e-6	4e-3	1.08e-6
Chl_{tot}	number of chlorophyll a and b in population	1.035e6	1e3	1.035e6	1.03e3
xan_{tot}	number of V_x and Z_x in population	5000	100	4.98e3	90.23
PQ_{tot}	number of PQ_{equiv} in population	1.1e5	100	1.1e5	9.36e3

Chapter 6

General conclusions

The general aim of the thesis was to contribute to knowledge gaps in the interpretation and modelling of physiological remote sensing, working towards the goal of accurately inferring light use efficiency (LUE) from space. A detailed literature review and three original studies were conducted in order to address each question in turn. The leaf level experimental study (chapter 3) adds to the increasing evidence of the usefulness of physiological remote sensing signals in detecting a range of different stress effects. The airborne study highlights the potential for combining multi-scale and multi-instrument physiological remote sensing measurements in complex, heterogeneous landscapes to infer LUE. The final study presented a new paradigm for the modelling of optical signals, linking the leaf scale *physics* of radiative transfer to the sub-leaf scale *biology* of photosystem II.

The results presented in chapter 3 show how hyperspectral reflectance indices can be used to track the reduction and subsequent recovery of photosynthetic efficiency in saplings due to transplant shock. Post-transplantation, outplanted trees undergo a period of stress which results in increased mortality rates. Field

spectrometers are non-invasive and relatively cheap and therefore have practical potential for the detection of transplant shock effects, provided suitable algorithms are developed and validated. Hyperspectral reflectance, PAM fluorescence and gas exchange measurements were collected from a sample of transplanted trees over an 8 week period. The PRI was found to track the reduction and subsequent recovery in photosynthetic rate over the study period (Figure 3.3).

Although there was a clear trend in PRI over the duration of the study period, the coefficients of determination that were calculated between PRI and the other indicators of photosynthetic efficiency were not particularly strong ($R^2 = 0.22$ for PRI and LUE, and $R^2 = 0.34$ for PRI and $\Delta F/F'_m$). This was probably caused by measurement error introduced due to the prevailing meteorological conditions during the study period. There were few opportunities to collect spectra under clear sky conditions, therefore spectra were collected in cloudy and clear conditions. Cloud is known to reduce the accuracy of single beam spectrometer systems where leaf measurements are compared to a calibrated standard under the assumption of identical illumination conditions (Milton *et al.*, 2009). Measurements during clear sky conditions and/or using a dual beam system would probably increase the strength of the statistical correlations between the various photosynthetic parameters. In conclusion, physiological reflectance measurements can be used to track reductions in photosynthetic rates caused by transplant shock, however the accuracy of the measurements is impeded by using a single beam spectrometer in cloudy conditions.

The results presented in the second study (chapter 4) were from an airborne campaign conducted as part of the large scale ABACUS experiment. A mixture of satellite data and airborne hyperspectral and eddy covariance measurements were collected using the Edinburgh School of GeoSciences research aircraft. Airborne measurements of CO_2 fluxes were compared to MODIS vegetation indices and landscape LUE was estimated for birch forests by combining airborne flux

measurements with tower estimates of respiration and satellite-based estimates of fAPAR. In a recent study Zulueta *et al.* (2011) found moderate relationships between NDVI calculated from MODIS measurements and airborne eddy covariance measurements. This was not the case for this data-set, most likely due to changing light conditions during the measurement period driving changes in carbon exchange across the landscape. There were weak to moderate ($R^2 = 0.4$ in both cases) correlations found between PRI and LUE and between PRI and PPFD.

The GeoSciences research aircraft has recently been fitted with a hyperspectral imaging system, this has the potential to enable spatial estimates of LUE across the landscape from the actual footprint of the airborne eddy covariance estimates. In conclusion, we found that aircraft observations of CO2 fluxes are sensitive to incoming solar radiation across the heterogeneous Arctic landscape, and that hyperspectral reflectance indices such as the PRI have the potential to quantify this sensitivity.

A new coupled model was presented in chapter 5 that linked sub-leaf scale biological processes to a radiative transfer model in order to predict the effects of chlorophyll fluorescence emission on the apparent reflectance spectrum. The model was based on two preexisting models: a model of the dynamics of energy flow through photosystem II developed by Porcar-Castell *et al.* (2006) and the PROSPECT leaf model (Jacquemoud and Baret, 1990). A Bayesian calibration algorithm was used to optimise the model parameters and predict model error. The coupled model was able to predict the effects of photochemical and non-photochemical quenching on the fluorescence emission on the timescale of seconds to minutes and was validated against an independent data-set.

The model presented in chapter 5 was developed as a precursor to a full canopy scheme. At present there are perhaps only two other models that link radiative transfer estimates of chlorophyll fluorescence to physiology, the first being the

SCOPE model (van der Tol *et al.*, 2009b) and the second being an unpublished model developed by Magnani (2009) and described in Dayyoub (2011). There are two ways in which the model could be extended. The first is to develop a full canopy scheme and the second is to model the PRI signal. A full canopy radiative transfer model capable of predicting chlorophyll fluorescence has already been developed by the FluorMOD project (Miller *et al.*, 2005). The challenge here is extending the biochemical model to work on seasonal time-scales, although Porcar-Castell (personal communication) is already working on such a model. Any full canopy scheme would need rigorous validation. Excitingly, this data is already available, as above canopy hyperspectral radiometer measurements and PAM data have been collected at a Swedish research station for the past two seasons (2010, 2011) at a frequency of one measurement per five minutes.

Modelling the PRI signal is, in theory at least, a relatively simple extension to the model presented. The pool sizes of zeaxanthin, z_x, and violaxanthin, v_x, are state variables in the biochemical model, however they are not represented in PROSPECT. The radiative transfer is complicated by the fact that xanthophylls (or any pigment) have a different absorbance spectra *in vivo* in comparison to *in vitro*. An inversion process could possibly be used to tease apart the contribution to the reflectance spectrum of the relative sizes of the xanthophyll pools at different stages of the cycle. In the newest version of PROSPECT (v5) Feret *et al.* (2008) used such a technique to derive the specific absorbance coefficients for bulk chlorophyll (and the other absorbing materials represented in PROSPECT) from a calibration data-set. It is these coefficients that are re-used when PROSPECT is run in forward mode. In conclusion, a new modelling approach enabled the prediction of the leaf level effects of chlorophyll fluorescence on the apparent reflectance spectrum driven by the dynamics of PSII.

Appendices

.1 Publications

Decision Letter (TRES-PAP-2011-0731)

From: International Journal of Remote Sensing
s.paterson@ifac.cnr.it

To: Atherton, Jon
Reference(s) Documents to Author:
Date Sent:
26-Apr-2011
jon.atherton@sms.ed.ac.uk
CC:

Subject:

International Journal of Remote Sensing - Decision on Manuscript ID TRES-PAP-2011-0731

Body:

@@date to be populated upon sending@@

Dear Mr. Atherton

It is a pleasure to inform you that your manuscript entitled "The utility of optical remote sensing for characterising changes in the photosynthetic efficiency of Norway maple saplings following transplantation" has been recommended for acceptance, for publication in the International Journal of Remote Sensing.

The comments of the referee(s) who reviewed your manuscript are included at the bottom of this email.

A copy of your manuscript files will be transferred electronically to the publishers, Taylor & Francis, in due course. However, before that is done the manuscript will be checked by one of our editorial assistants Dr Craig Cassells or Mr Martin Andrews, for style, completeness of references and the quality of the figures. If there are any problems he will contact you to obtain clarification or replacement material. The 'final form' date will be the date we receive the final corrections, and/or upon which the appropriate editorial assistant finds the manuscript to be acceptable within our style standards. It is at this point that your manuscript will be considered finally accepted for publication; please be aware that if any problems with your article cannot be resolved in a timely manner it may be treated as being withdrawn from publication.

Please note that if your paper is for a Special Issue, it will not be sent to the publishers until all papers for that Special Issue are in final form.

Once the paper has been transferred to the publishers, you will receive an email explaining how to follow its progress on their Central Article Tracking System (CATS). You will also receive a copy transfer agreement, information about obtaining reprints, and information about accessing and correcting the proofs.

If you do not receive an email about your proofs 3 months after you have received the initial CATS email, please contact the journal Administrator at IJRS-Administrator@Dundee.ac.uk or submit an Article Status Form directly to the publishers.

Thank you for your contribution. On behalf of the Editors of the International Journal of Remote Sensing, we look forward to your continued contributions to our journal.

Yours sincerely

International Journal of Remote Sensing

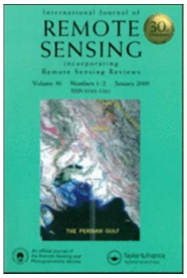

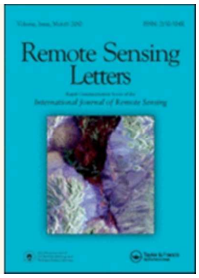

The utility of optical remote sensing for characterising changes in the photosynthetic efficiency of Norway maple saplings following transplantation

Journal:	*International Journal of Remote Sensing*
Manuscript ID:	TRES-PAP-2011-0731
Manuscript Type:	IJRS Research Paper
Date Submitted by the Author:	11-Nov-2011
Complete List of Authors:	Atherton, Jon; University of Edinburgh, School of GeoSciences Nichol, Caroline; Atmospheric and Environmental Sciences, School of GeoSciences Mencuccini, Maurizio; Atmospheric and Environmental Sciences, School of GeoSciences Simpson, Katie; Atmospheric and Environmental Sciences, School of GeoSciences
Keywords:	HYPERSPECTRAL DATA, FIELD RADIOMETRY
Keywords (user defined):	transplant shock, photosynthesis, xanthophyll

The utility of optical remote sensing for characterising changes in the photosynthetic efficiency of Norway maple saplings following transplantation

J. M. ATHERTON[§], C. NICHOL[§], M. MENCUCCINI[§] and K. SIMPSON[§]

[§]Institute of Atmospheric and Environmental Sciences, School of GeoSciences, University of Edinburgh, West Mains Road, Edinburgh, UK

Corresponding author:
J. M. Atherton
School of GeoSciences
Crew Building
Kings Buildings
University of Edinburgh
West Mains Road
Edinburgh EH9 3JN
Scotland, UK
Email: J.M.Atherton@sms.ed.ac.uk

Abstract

Following outplanting, trees undergo a period of stress referred to as transplant shock. Tree mortality rates are known to increase during this period, monitoring the effects of transplant shock is therefore key to improving the future survival rates of outplanted trees. Leaf reflectance spectra, measured by field spectrometry, can be used to derive reflectance indices that are related to a number of biophysical parameters including photosynthetic efficiency and leaf chlorophyll content. Field spectrometry has the advantage of being non-invasive and relatively cheap and is therefore a suitable candidate for monitoring the effects of transplant shock. The objective of this study was to assess the applicability of passive remote sensing as a tool to measure the reduction, and the subsequent recovery, of photosynthetic efficiency during the weeks following transplantation. Spectral reflectance, gas exchange and chlorophyll fluorescence measurements of Norway maple (*Acer platanoides* L.) saplings were collected over an 8 week period, following transplantation from a glasshouse to an outdoor environment. A marked depression in photosynthetic rate occurred in the weeks after outplanting followed by a gradual increase, with recovery occurring in the later stages of the experimental period. Spectral data were collected on newly planted saplings in both clear and cloudy conditions, and the relationships between spectral reflectance indices, photosynthetic light use efficiency (LUE), and the quantum yield of photosystem II, estimated using the fluorescence parameter $\Delta F/F'_m$, were explored. The Photochemical Reflectance Index, PRI, was weakly to moderately correlated with LUE ($R^2 = 0.22$, $p < 0.05$), $\Delta F/F'_m$ ($R^2 = 0.34$, $p < 0.05$) and PPFD ($R^2 = 0.30$, $p < 0.05$). Several chlorophyll-based spectral indices were moderately correlated with LUE, including ND705 ($R^2 = 0.45$, $p < 0.05$). As with LUE, there was a marked trend in PRI values over the study period but no trend was observed in ND705. The study demonstrates that hyperspectral remote sensing has the potential to be a useful tool in the detection and monitoring of the dynamic effects of transplant shock.

Keywords: Transplant shock, hyperspectral, photosynthesis, fluorescence

1. Introduction

Transplant shock describes the effects of a number of physiological stresses that occur following `outplanting' (replanting in a new environment). Transplant shock is characterised by reduced growth and increased mortality rates. The effects of transplant shock are most obvious in the days and months after planting, although reduced growth rates have been recorded several years after outplanting (Zaczek *et al.* 1997). During the acclimatisation period stored carbohydrates are used for new root growth, but if the stored carbohydrates are exhausted then the tree is at risk of death (Rietveld 1987). Any number of biotic and abiotic stress factors can contribute to the overall transplant shock effect, including: differences in the light environment or in the nutritional status between the nursery and field, drought stress, frost, mechanical damage or competition with surrounding vegetation (Close *et al.* 2004).

Measurements of the effects of transplant shock on outplanted trees fall into two broad categories: i. morphological and ii. physiological. Morphological measurements, such as the Tree Planting Index (Zaczek *et al.* 1997), Transplant Stress Index (South and Zwolinski 1997) and the Tree Health Index (Anastasiou and Brooks 2003), are based on repeated measures of tree height before, during and/or after the transplant shock period. Morphological measurements are simple and cheap, however it is only with physiological measurements that detailed information about the underlying biological state of the trees can be obtained. The drawback with physiological measurements is that they can be time-consuming and difficult to successfully apply and interpret. Examples of physiological measurements include leaf gas exchange (Close and Beadle 2003), chlorophyll fluorescence (Close and Beadle 2003) and leaf nitrogen levels (Anastasiou and Brooks 2003).

Optical remote sensing is a passive, non-destructive technique that has the potential to measure several aspects of the physiological effects of transplant shock. The physiological application of optical remote sensing is a rapidly advancing field and cheap, portable commercial systems are now available for operational use to end-users such as foresters. Leaf-level studies that employ optical remote sensing typically measure the leaf reflectance spectrum (in the visible to near-infrared wavelengths), which is the ratio of reflected radiance to incident irradiance (see figure 1). Changes in leaf-level physiology, such as pigment pool sizes, which may occur during the transplant shock period directly affect the measured reflectance spectrum. Spectral bands, defined by their respective wavelengths, that are sensitive to changes in physiology can then be selected to monitor changes in reflectance due to environmental stressors. The characteristic 'red-edge' feature of a leaf spectrum is visible as a sharp increase in reflectance between 675 – 750 nm. The red edge is caused by the contrast between strong chlorophyll absorption in the red region of the spectrum and a lack of absorption in the adjacent near-infrared region (Myneni *et*

al. 1995). Several reflectance indices, usually calculated as the ratio and/or differences between two or more spectral bands, that target the red-edge region of the spectrum have been developed to estimate leaf chlorophyll content across a range of species (Sims and Gamon 2002).

In addition to leaf chlorophyll content, reflectance spectra can also be used to detect changes in light use efficiency (LUE). LUE is defined as the ratio of photosynthetic rate to absorbed Photosynthetic Photon Flux Density (PPFD), and is an indicator of plant health. The Photochemical Reflectance Index (PRI) was developed by Gamon *et al.* (1992, 1993) as a way to measure reversible changes in carotenoid pigments, known as the xanthophyll cycle. The xanthophyll cycle is part of a complex system of reactions that acts to dissipate potentially harmful excess absorbed light energy as heat. PRI has been widely applied in a range of plant stress studies to gain insight into LUE (Thenot *et al.* 2002, Meroni *et al.* 2008, Sarlikioti *et al.* 2010, Garbulsky *et al.* 2011).

Reflectance spectra can also be used to detect changes in chlorophyll fluorescence, a process that is referred to as a 'direct probe' into the photosynthetic apparatus (Bolhàr-Nordenkampf *et al.* 1989, Baker 2008). Chlorophyll fluorescence is the re-emission of absorbed radiation at longer wavelengths and competes with photosynthesis and heat dissipation as an alternate pathway for absorbed light energy. As well as several reflectance indices that have been specifically developed to measure chlorophyll fluorescence, chlorophyll fluorescence can be measured in absolute radiometric units using a technique known as Fraunhofer infilling (see Meroni *et al.* (2009) for a list of fluorescence indices and a comprehensive review of the literature). Pulse Amplitude Modulated Fluorometers (PAMs) are active instruments that detect rapid changes in the chlorophyll fluorescence signal and can be used to estimate a range of photosynthetic efficiency parameters which reflect the underlying physiological status of the tree. Close and Beadle (2003) used PAM data to investigate the effects of photoinhibition on a sample of transplanted saplings, and found a marked depression in photosynthetic efficiency in the weeks following planting.

The objective of this study was therefore to investigate the applicability of passive remote sensing methods to detect changes in tree physiology during the transplant shock period. We present results from an experiment conducted under natural light conditions in which the photosynthetic recovery of transplanted Norway maple (*Acer platanoides* L.) saplings was investigated using a combination of gas exchange, PAM fluorescence and spectroradiometer measurements.

FIGURE 1 HERE

2. Methods

2.1 Bedding and experimental design

A population of 100 Norway maple saplings were planted between the 5th and the 9th June 2008. The saplings were planted on a purpose built plot in a 5 x 20 tree grid formation, at Kings Buildings, University of Edinburgh, UK. The saplings were 2.5 years old and 1.25 to 1.5 m tall at the time of purchase, and had previously been stored in a glasshouse for several weeks until the

leaves were fully developed. Measurements of leaf reflectance and gas exchange were collected on several days during an eight week period, from planting until the 5th August 2008. PAM fluorescence measurements were not carried out on 23rd June and 16th July but were carried out on all other measurement days. On the 23rd June measurements were collected from 14:00-16:00 local time, on the 5th August measurements were collected during early morning (09:00-09:30), midday (12:00-12:30) and late afternoon (15:30-16:00). On all other days measurements were collected between the hours of 10:00 and 13:00.

2.2 Spectral measurements

Repeated observations were carried out on leaves from a subset of 20 trees. The 20 trees were located at the southern end of the site, and were chosen for the homogeneity of the light conditions and for ease of access. An Analytical Spectral Devices FieldSpec Pro (ASD Inc., Boulder, CO, U.S.A.) was used to collect spectra in a single sensor biconical configuration. The spectrometer was used in conjunction with an 8 ° field of view fore-optic. Reflectance spectra were calculated by normalising leaf spectra to measurements of a calibrated, near-lambertian reflective standard (Spectralon, Labsphere, North Sutton, NH, U.S.A). Spectra were collected during both clear sky and cloudy conditions, with each leaf measurement followed by a measurement of the standard. Each spectrum was an average of 25 measurements and three spectra were collected per leaf sampled. Spectra were sampled in the nadir position at a fixed distance from the adaxial side of the leaf, which resulted in a spot radius of 2.81 cm.

2.3 Leaf gas exchange and PAM fluorescence

An LCPro+ portable photosynthesis system (ADC Bioscientific Ltd., U.K.) was used to collect measurements of photosynthetic rate at a fixed incident photosynthetic photon flux density (PPFD) of 870 μmol m^{-2} s^{-1}. Photosynthetic light use efficiency, LUE, was calculated as photosynthetic rate / PPFD. The quantum yield of photosystem II, $\Delta F/F'_m$, was estimated using a Walz Diving PAM (Heinz Walz GmbH, Effeltrich, Germany) as well as incident PPFD and leaf temperature. Photosynthesis and PAM fluorescence measurements were collected from the same leaves as the spectra, as close in time (under 5 minutes) as possible. A weather station positioned within 500 m of the plot recorded atmospheric pressure, rainfall, air temperature, wind speed, relative humidity, and short-wave radiation at 1 minute intervals.

TABLE 1 HERE

2.4 Reflectance processing and statistics

Statistical analysis and data processing were performed using the Python programming language. For the purposes of exploring the utility of spectral indices for monitoring photosynthetic efficiency during the transplant shock period, a number of spectral reflectance and first derivative indices were calculated (with the formulations and references listed in table 1). First derivative spectra were calculated using a Savitzky-Golay filter (Savitzky and Golay 1964). A per sample leaf average and standard error was calculated from the repeat spectra. A linear correlation analysis was conducted by calculating the coefficient of determination, R^2, between a

set of reflectance indices (table 1) and parameters of photosynthetic efficiency, PPFD and leaf temperature and linear models were developed between selected spectral indices and LUE, $\Delta F/F'_m$, PPFD and leaf temperature and using the SciPy (Python) statistics library.

FIGURE 2 HERE

3. Results

3.1 Meteorological conditions

Time series of half hourly average temperature and half hourly average solar flux during the experimental study period are shown in figure 2. The experimental period was predominately wet (data not shown) and cloudy. The maximum day time temperature during the study period was 24.7 ºC and the minimum night time temperature was 6.34 ºC.

FIGURE 3 HERE

3.2 Time course of photosynthetic parameters

Daily photosynthetic rate measurements are shown in figure 3a. The lowest value of photosynthetic rate, 0.79 μmol m^{-2} s^{-1}, was measured at the start of the sampling period on the 23rd June at 15:26. The maximum value of photosynthetic rate, 11.56 μmol m^{-2} s^{-1}, was measured at the end of the sampling period on the 5th August at 09:53. On the 5th August similar photosynthetic rates were measured during the early morning and noon periods with median values of 8.42 and 8.23 μmol m^{-2} s^{-1} respectively. Reduced photosynthetic rates were recorded during the late afternoon period (median value 5.69 μmol m^{-2} s^{-1}). All measurements of photosynthetic rate collected during the late afternoon period on the 5th August were greater in value than the maximum photosynthetic rate measured, 5.05 μmol m^{-2} s^{-1}, on the 23rd June.

The time course of measurements of $\Delta F/F'_m$ are shown in Figure 3b. The lowest daily median value, 0.34, was measured on the 23rd July. The maximum daily median value, 0.54, occurred on the final day of sampling, 5th August during the early morning and noon periods. A subsequent fall in $\Delta F/F'_m$ values was measured on the 5th August during the late afternoon period, with a median value of 0.50.

FIGURE 4 HERE

3.2 Remote sensing of photosynthetic efficiency

We explored relationships between leaf gas exchange, PAM fluorescence, reflectance indices and meteorological conditions to test the applicability of optical remote sensing for detecting the physiological effects of transplant shock. We explored a suite of spectral indices sensitive to physiological status by testing the linear correlation with other parameters of photosynthetic efficiency, PPFD and leaf temperature, these results are summarised in figure 4. We developed linear models between PRI (figure 5) and ND705 (figure 6) and parameters of photosynthetic efficiency, PPFD and leaf temperature. A moderate relationship, ($R^2 > 0.4$, $p < 0.05$), was found

between several chlorophyll-based spectral indices, namely SR705, ND705, mND705, and LUE. Weak to moderate relationships were found between PRI and LUE (R^2 = 0.22, $p < 0.05$), PRI and $\Delta F/F'_m$ (R^2 = 0.34, $p < 0.05$) and PRI and PPFD (R^2 = 0.3, $p < 0.05$). A moderate relationship was found between ND705 and LUE (R^2 = 0.45, $p < 0.05$). Weak relationships were found between ND705 and $\Delta F/F'_m$ (R^2 = 0.22, $p < 0.05$) and ND705 and PPFD (R^2 = 0.15, $p < 0.05$). No significant relationship (all $p >= 0.05$) was found between any of the spectral indices tested and leaf temperature (figure 4).

Figure 3c and figure 3d shows time courses for PRI and the chlorophyll-based index, ND705, respectively. The lowest median value of PRI, -0.062, occurred on the 23rd June and the maximum meidan value, 0.02, was recorded on the 5th August. PRI values on the 5th of August were higher in the early morning period when compared to the noon and late afternoon periods. There was little change in the median ND705 medians values over the full time-course of the experiment. However, on the 5th August the highest ND705 values are recorded during the early morning period with the lowest values occurring in the late afternoon.

Weak to moderate relationships ($0.2 > R^2 < 0.4$) were found between several fluorescence-based indices (zt 9, zt d1, zt d2, zt 11) and LUE and between fluorescence-based indices (zt 6 – zt 10, zt d1, zt d2, dob 1) and $\Delta F/F'_m$. Weak relationships were found between the first derivative indices, zt d1 and zt d2, and PPFD (R^2 = 0.24, $p < 0.05$ and R^2 = 0.24, $p < 0.05$ respectively).

FIGURE 5 HERE
FIGURE 6 HERE

4. Discussion

This study investigated the applicability of spectral reflectance indices for detecting the physiological effects of transplant shock on Norway maple saplings. The reduction and subsequent recovery of photosynthetic efficiency of a sample of saplings was tracked using gas exchange, chlorophyll fluorescence parameters and hyperspectral reflectance measurements. A correlation analysis was conducted for an extensive set of reflectance indices and parameters of photosynthetic efficiency and linear models were developed between selected reflectance indices and parameters of photosynthetic efficiency.

There was a clear reduction in the rate of photosynthesis at the beginning of the study followed by a transient recovery during the following weeks. Reduced photosynthetic rates are a typical symptom of transplant shock (Close *et al.* 2004), however reduced rates of photosynthesis can also be caused by sub-optimal environmental conditions. In particular it has been shown that Norway maple growth may be limited by extreme temperatures, low precipitation and high soil pH (Nowak and Rowntree 1990). Temperatures during the study were within the normal range for the time of year and rainfall was plentiful. This suggests that, assuming soil pH was constant during the study, temporal changes to meteorological conditions were not the limiting factor in relation to measured photosynthetic rates. Photosynthetic rate is also influenced by leaf growth, and as leaves mature both photosynthetic rate and leaf chlorophyll content undergo rapid changes (Dougherty *et al.* 1979). Although the sapling leaves used in this study were fully

expanded prior to planting and the chlorophyll index, ND705, did not show any clear trend over the experimental period, it is possible that some measurements may have been made on leaves that were close to the end of the developmental maturation process. It follows that the measured photosynthetic rates at the start of the study may have been reduced due to a combination of the effects of transplant shock and leaf growth.

As with LUE, there was a clear increase in PRI values over the study period (figure 3c) and we found that PRI was weakly to moderately correlated with LUE and $\Delta F/F'_m$. This is in agreement with Nakaji *et al.* (2007) who found similar correlations (R^2 = 0.38) with PRI and LUE under cloudy conditions. The PRI signal is a function of the changing state of the xanthophyll cycle, which is a biochemical response to excess light levels brought about by physiological stress. As transplant shock occurs, in part, due to the acclimatisation of plants to higher light environments (Close *et al.* 2004) the correlation we found between PRI and PPFD is to be expected (figure 5c). We found moderate correlations with spectral indices designed to measure leaf chlorophyll content, such as ND705, and LUE. However, unlike LUE and P RI, there was no clear trend in ND705 over the study period. Furthermore there were very weak or no significant relationships found between ND705 and $\Delta F/F'_m$ and PPFD. We propose that although chlorophyll-based indices can provide a general indication of photosynthetic rate, one must use indices that are sensitive to more rapid changes in plant biochemistry to capture the dynamic nature of the effects of transplant shock.

There was a slight positive trend in $\Delta F/F'_m$ over the study period, however data was missing in the early part of the study therefore no firm conclusions can be drawn. Close and Beadle (2003) found a similar trend in pre-dawn $\Delta F/F'_m$ for a sample of *Eucalyptus nitens* with the main difference being a longer recovery period (20 to 30 weeks), although the Close and Beadle (2003) study was conducted under low temperature conditions. In general, similar correlations were found between chlorophyll-based indices and chlorophyll fluorescence-based indices and parameters of photosynthetic activity (Figure 4). It is well known that fluorescence indices are sensitive to changes in total chlorophyll content and this could account for the similar relationships (Meroni *et al.* 2009). In any case, the relationship between absolute chlorophyll fluorescence and photosynthetic rate is not simple: under low light conditions fluorescence may be negatively correlated with photosynthetic rate and under high light conditions this relationship may reverse (Rosema *et al.* 1998), hence care must be taken when interpreting fluorescence-based indices as indicators of photosynthetic efficiency.

Due to the prevailing meteorological conditions during the study period (figure 2), there were few opportunities to collect spectra in clear sky conditions therefore spectra were collected under both clear and cloudy skies. Measurement error may be present in the spectra collected under cloudy conditions, which may have acted to reduce the correlations between spectral indices and LUE. Firstly, the limitation of the single-beam spectrometer method is that accurate measurements of reflectance rely on the assumption of identical illumination conditions between measurements of the leaf and reference panel (Milton *et al.* 2009). In practice, this error can be reduced by sampling in optimal low-cloud conditions and minimising the time lag between target and reference measurements. In this study, leaf and reference measurements were taken alternately to reduce the time difference to the order of seconds. A second possible source of error occurs due to bidirectional reflectance distribution function (BRDF) effects. The BRDF

describes, mathematically, how observed reflectance is dependant on the angle of the observer and the direction of the incoming radiation. Under diffuse light conditions, the BRDF of vegetation is different to the BRDF of vegetation under clear sky conditions. In particular, measured reflectance in the visible region of the spectrum increases linearly as the proportion of diffuse radiation increases (Gilabert and Melia 1993). As PRI, and several other spectral indices, make use of visible bands, the signal may be influenced by confounding effects under cloudy sky conditions unrelated to xanthophyll cycle activity.

Relatively few studies have been carried out that explore the use of passive (or active) remote sensing techniques for detecting the effects of transplant shock and as such we have several suggestions for further work. Firstly, by their nature, spectral measurements are indirect. Direct sampling of plant pigments during the recovery period would be useful in testing the hypothesis that PRI may be more useful than chlorophyll-based indices in detecting dynamic changes in photosynthetic efficiency during the transplant shock period. Secondly, a study under clear sky conditions or with a dual-beam spectrometer may increase the calculated correlation coefficients. Thirdly, this study concentrated on measuring the early onset effects of transplant shock. Transplant shock can also cause long term (seasonal and trans-seasonal) reductions in photosynthetic efficiency due to water stress (Barton and Walsh 2000), which may be measurable using physiological remote sensing. Nevertheless, we have demonstrated that hyperspectral remote sensing has the potential to be a useful tool in the detection and monitoring of the dynamic effects of transplant shock.

5. Acknowledgements

The work of J. Atherton was supported by a PhD studentship awarded as a Torrance bequest scholarship by The University of Edinburgh (UK) and Forest Research. We acknowledge the NERC Field Spectroscopy Facility for the loan of a PAM fluorometer. We would like to thank K. Anderson and P. J. Zarco-Tejada for their illuminating correspondence.

References

ANASTASIOU, C.J. AND BROOKS, J., 2003, Effects of soil PH, redox potential, and elevation on survival of *Spartina patens* planted at a west Central Florida salt marsh restoration site. *Wetlands*, 23, pp. 845-859.

BAKER, N.R., 2008, Chlorophyll Fluorescence: A Probe of Photosynthesis In Vivo. *Annual review of plant biology*, 59, pp. 89 - 113.

BARTON, A.J. AND WALSH, C.S., 2000, Effect of Transplanting on Water Relations and Canopy Development in *Acer*. *Journal of Environmental Horticulture,* 18, pp. 202,206.

BOLHÀR-NORDENKAMPF, H.R., LOŃG, S.P., BAKER, N.R., ÖQUIST, G., SCHREIBER, U. AND

LECHNER, E.G., 1989, Chlorophyll Fluorescence as a Probe of the Photosynthetic Competence of Leaves in the Field: A Review of Current Instrumentation. *Functional Ecology*, 3, pp. 497–514.

CLOSE, D. C., BEADLE, C. L. AND BROWN, P., 2004, The physiological basis of containerised tree seedling 'transplant shock': a review. *Australian Forestry*, 68, pp. 112–120.

CLOSE, D. C. AND BEADLE, C.L., 2003, Chilling-dependent photoinhibition, nutrition and growth analysis of *Eucalyptus nitens* seedlings during establishment. *Tree Physiology*, 23, pp. 217– 226.

DOBROWSKI, S., PUSHNIK, J., ZARCO-TEJADA, P. AND USTIN, S., 2005, Simple reflectance indices track heat and water stress-induced changes in steady-state chlorophyll fluorescence at the canopy scale. *Remote Sensing of Environment*, 97, pp. 403–414.

DOUGHERTY, P.M., TESKEY, R.O., PHELPS, J.E. AND HINCKLEY, T.M., 1979, Net Photosynthesis and Early Growth Trends of a Dominant White Oak (*Quercus alba* L.). *Plant Physiology*, 64, pp. 930–935.

GAMON, J., FILELLA, I. AND PEÑUELAS, J., 1993, The dynamic 531-nanometer Δ reflectance signal: a survey of twenty angiosperm species. In H.Y. Yamamoto and C.M. Smith (Eds.) *Photosynthetic responses to the environment*, pp. 172–177 (Rockville MD: American Society of Plant Physiologists).

GAMON, J., PEÑUELAS, J. AND FIELD, C., 1992, A narrow-waveband spectral index that tracks diurnal changes in photosynthetic efficiency. *Remote Sensing of Environment*, 41, pp. 35–44.

GARBULSKY, M., PEÑUELAS, J., GAMON, J., INOUE, Y. AND FILELLA, I., 2011, The photochemical reflectance index (PRI) and the remote sensing of leaf, canopy and ecosystem radiation use efficiencies: A review and meta-analysis. *Remote Sensing of Environment*, 115, pp. 281–297.

GILABERT, M. AND MELIÁ, J., 1993, Solar angle and sky light effects on ground reflectance measurements in a citrus canopy. *Remote Sensing of Environment*, 45, pp. 281–293.

GITELSON, A.A., GRITZ, Y. AND MERZLYAK, M.N., 2003, Relationships between leaf chlorophyll content and spectral reflectance and algorithms for non-destructive chlorophyll assessment in higher plant leaves. *Journal of Plant Physiology*, 160, pp. 271 – 282.

MERONI, M., PICCHI, V., ROSSINI, M., COGLIATI, S., PANIGADA, C., NALI, C., LORENZINI, G. AND COLOMBO, R., 2008, Leaf level early assessment of ozone injuries by passive fluorescence and photochemical reflectance index. *International Journal of Remote Sensing*, 29, pp. 5409–5422.

MERONI, M., ROSSINI, GUANTER, M.L., ALONSO, L., RASCHER, U., COLOMBO, R., AND MORENO, J., 2009, Remote sensing of solar induced chlorophyll fluorescence: review of methods and applications. *Remote Sensing of Environment*, 113, pp. 2037–2051.

MERZLYAK, M.N., GITELSON, A.A., CHIVKUNOVA, O.B. AND RAKITIN, V.Y., 1999, Non-destructive optical detection of pigment changes during leaf senescence and fruit ripening. *Physiologia Plantarum*, 106, pp. 135–141.

MILTON, E.J., SCHAEPMAN, M.E., ANDERSON, K., KNEÜBHLER, M. AND FOX, N., 2009, Progress in field spectroscopy. *Remote Sensing of Environment*, 113, pp. S92–S109, (Imaging

Spectroscopy Special Issue).

MYNENI, R., HALL, F., SELLERS, P. AND MARSHAK, A., 1995, The interpretation of spectral vegetation indexes. *Geoscience and Remote Sensing, IEEE Transactions on*, 33, pp. 481-486.

NAKAJI, T., IDE, R., OGUMA, H., SAIGUSA, N. AND FUJINUMA, Y., 2007, Utility of spectral vegetation index for estimation of gross CO2 flux under varied sky conditions. *Remote Sensing of Environment*, 109, pp. 274-284.

NOWAK, D.J. AND ROWNTREE, R.A., 1990, History and range of Norway Maple. *Journal of Arboriculture*, 16, pp. 291-296.

PEÑUELAS, J., FILELLA, I. AND GAMON, J., 1995, Assessment of photosynthetic radiation-use efficiency with spectral reflectance. *New Phytologist*, 131, pp. 291-296.

RIETVELD, R., 1987, Transplanting shock in bareroot conifer seedlings. *National Nursery Proceedings - 1987*, 6, pp. 49-71.

ROSEMA, A., SNEL, J., ZAHN, H., BUURMEIJER, W. AND HOVE, L.V., 1998, The Relation between Laser-Induced Chlorophyll Fluorescence and Photosynthesis. *Remote Sensing of Environment*, 65, pp. 143-154.

SARLIKIOTI, V., DRIEVER, S. AND MARCELIS, L., 2010, Photochemical reflectance index as a means of monitoring early water stress. *Annals of Applied Biology*, 157, pp. 81-89.

SAVITZKY, A. AND GOLAY, M.J.E., 1964, Smoothing and Differentiation of Data by Simplified Least Squares Procedures. *Analytical Chemistry*, 36, pp. 1627-1639.

SIMS, D. AND GAMON, J., August 2002, Relationships between leaf pigment content and spectral reflectance across a wide range of species, leaf structures and developmental stages. *Remote Sensing of Environment*, 81, pp. 337-354.

SOUTH, D.B. AND ZWOLINSKI, J.B., 1997, Transplant Stress Index: A proposed method of quantifying planting check. *New Forests*, 13, pp. 315-328.

THENOT, F., MÉTHY, M. AND WINKEL, T., 2002, The Photochemical Reflectance Index (PRI) as a water- stress index. *International Journal of Remote Sensing*, 23, pp. 5135-5139.

VOGELMANN, J.E., ROCK, B.N. AND MOSS, D., 1993, Red edge spectral measurements from sugar maple leaves. *International Journal of Remote Sensing*, 14, pp. 1563-1575.

ZACZEK, J.J., STEINER, K.C. AND BOWERSOX, T.W., 1997, Northern red oak planting stock: 6-year results. *New Forests*, 13, pp. 177-191.

ZARCO-TEJADA, P.J., PUSHNIK, J.C., DOBROWSKI, S. AND USTIN, S.L., 2003, Steady-state chlorophyll a fluorescence detection from canopy derivative reflectance and double-peak red-edge effects. *Remote Sensing of Environment*, 84, pp. 283 - 294.

ZARCO-TEJADA, P.J., MILLER, J.R., MOHAMMED, G.H. AND NOLAND, T.L., 2000a, Chlorophyll Fluorescence Effects on Vegetation Apparent Reflectance: I. Leaf-Level Measurements and Model Simulation. *Remote Sensing of Environment*, 74, pp. 582-595.

ZARCO-TEJADA, P.J., MILLER, J.R., MOHAMMED, G.H., NOLAND, T.L. AND SAMPSON, P.H., 2000b, Chlorophyll Fluorescence Effects on Vegetation Apparent Reflectance: II. Laboratory and Airborne Canopy-Level Measurements with Hyperspectral Data. *Remote Sensing of Environment*, 74, pp. 596- 608.

Table 1. Reflectance index reference table. Where ρ_x is apparent reflectance at x nm and D ρ_x is the first derivative spectra with respect to wavelength at x nm.

Shortened name	Formula	Pigment/process	Citation
broadband NDVI	$(\rho_{NIR} - \rho_{Vis.} / \rho_{NIR} + \rho_{Vis.})$	chlorophyll	Vogelmann *et al.* (1993)
SR 680	ρ_{800} / ρ_{680}	chlorophyll	Sims and Gamon (2002)
SR 705	ρ_{750} / ρ_{705}	chlorophyll	Sims and Gamon (2002)
mSR 750	$(\rho_{750} - \rho_{445}) / (\rho_{750} + \rho_{445})$	chlorophyll	Sims and Gamon (2002)
ND 680	$(\rho_{800} - \rho_{680}) / (\rho_{800} + \rho_{680})$	chlorophyll	Sims and Gamon (2002)
ND 705	$(\rho_{750} - \rho_{705}) / (\rho_{750} + \rho_{705})$	chlorophyll	Sims and Gamon (2002)
mND 705	$(\rho_{750} - \rho_{705}) / (\rho_{750} + \rho_{705} - 2 \times \rho_{445})$	chlorophyll	Sims and Gamon (2002)
inverse 1 to 5	$1 / (\rho_{500, 670, 530, 550, 700})$	chlorophyll	Gitelson *et al.* (2003)
r 750	$(\rho_{750} - \rho_{800}) / ((\rho_{750} - \rho_{695}) - 1)$	chlorophyll	Gitelson *et al.* (2003)
PRI	$(\rho_{531} - \rho_{570}) / (\rho_{531} + \rho_{570})$	carotenoids and chlorophyll	Gamon *et al.* (1992)
SIPI	$(\rho_{800} - \rho_{445}) / (\rho_{800} + \rho_{680})$	carotenoids and chlorophyll	Peñuelas *et al.* (1995)
PSRI	$(\rho_{678} - \rho_{500}) / \rho_{750}$	carotenoids and chlorophyll	Merzlyak *et al.* (1999)
zt 1	$(\rho^2_{683}) / (\rho_{675} \times \rho_{690})$	fluorescence	Zarco-Tejada *et al.* (2000a)
zt 2	ρ_{750} / ρ_{800}	fluorescence	Zarco-Tejada *et al.* (2000a)
zt 3	ρ_{685} / ρ_{655}	fluorescence	Zarco-Tejada *et al.* (2000a)
zt 4	ρ_{690} / ρ_{655}	fluorescence	Zarco-Tejada *et al.* (2000a)
zt 5	ρ_{680} / ρ_{630}	fluorescence	Zarco-Tejada *et al.* (2000b)
zt 6	ρ_{685} / ρ_{630}	fluorescence	Zarco-Tejada *et al.* (2000b)
zt 7	ρ_{687} / ρ_{800}	fluorescence	Zarco-Tejada *et al.* (2000b)
zt 8	ρ_{690} / ρ_{630}	fluorescence	Zarco-Tejada *et al.* (2000b)
zt 9	$\rho^2_{685} / (\rho_{675} \times \rho_{690})$	fluorescence	Zarco-Tejada *et al.* (2000a)
zt 10	ρ_{685} / ρ_{655}	fluorescence	Zarco-Tejada *et al.* (2000b)
zt 11	$\rho^2_{683} / (\rho_{675} \times \rho_{691})$	fluorescence	Zarco-Tejada *et al.* (2000a)
DPI	$(\rho_{688} \times \rho_{710}) / \rho^2_{697}$	fluorescence	Zarco-Tejada *et al.* (2003)
zt d1	$D\rho_{705} / D\rho_{722}$	fluorescence	Zarco-Tejada *et al.*

			(2000b)
zt d2	$D\rho_{730} / D\rho_{706}$	fluorescence	Zarco-Tejada *et al.* (2000b)
dob 1	ρ_{690} / ρ_{600}	fluorescence	Dobrowski *et al.* (2005)

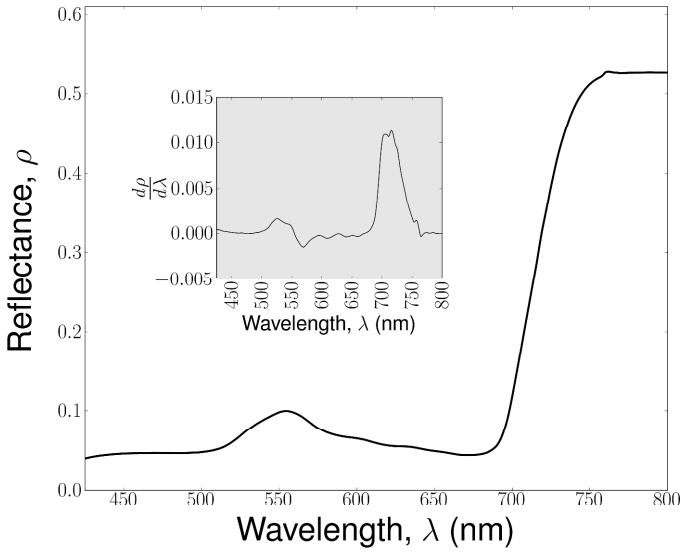

Figure 1: Example of a reflectance spectrum with the first derivative spectrum shown in the insert.

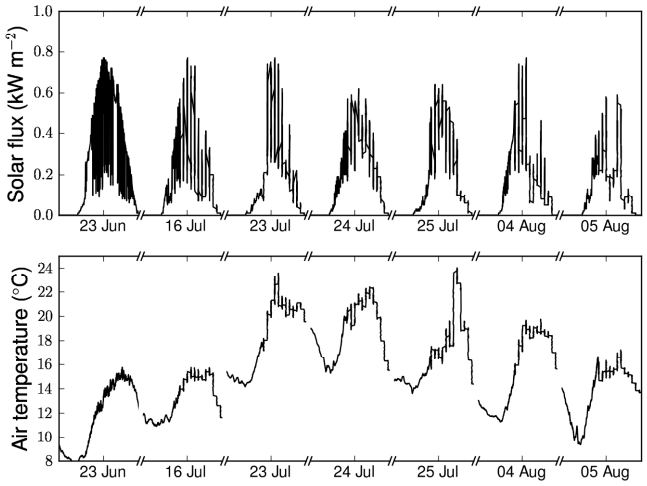

Figure 2: Meteorological conditions at the study site during the measurement days.

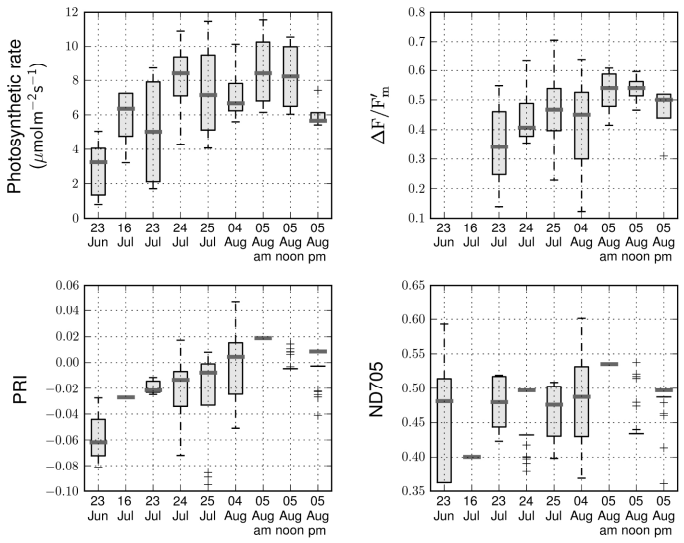

Figure 3: Daily distributions of parameters of photosynthetic efficiency and reflectance indices during post-transplant acclimatisation. The median, 25th and 75th percentiles are shown by the middle lines, lower limits and upper limits of the boxes. The whiskers represent the maximum and minimum value within 1.5 times the interquartile range, values outside this range are shown as outliers.

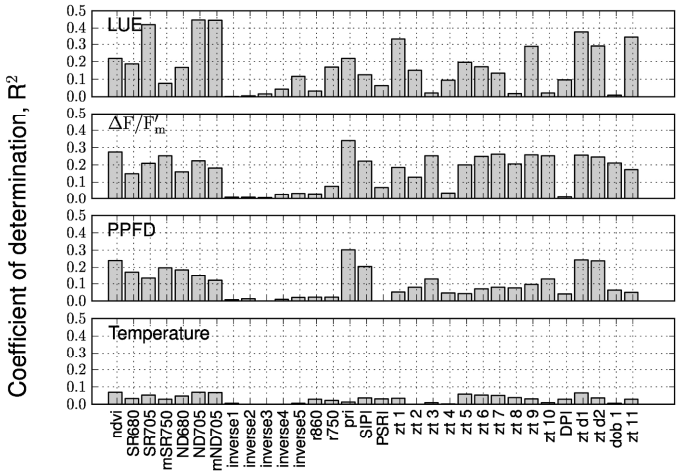

Figure 4: Coefficients of determination between a set of spectral reflectance indices and (a) LUE, (b) ΔF/F'm, (c) PPFD and (d) leaf temperature.

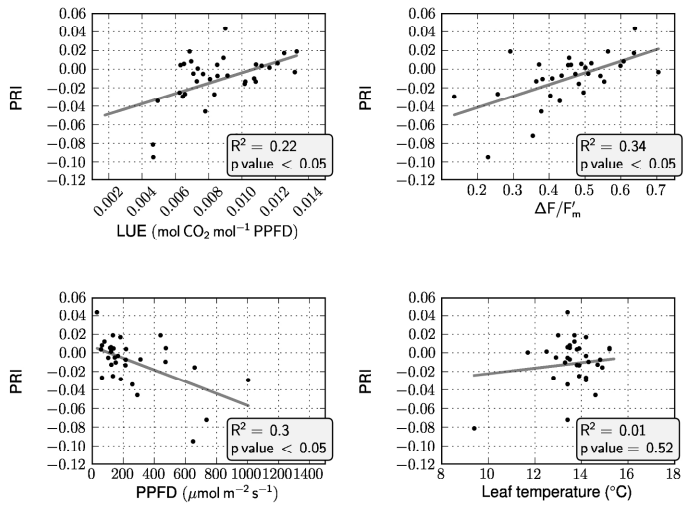

Figure 5: Linear regression models for (a) PRI Vs LUE, (b) PRI Vs ΔF/F′m, (c) PRI Vs PPFD and (d) PRI Vs leaf temperature.

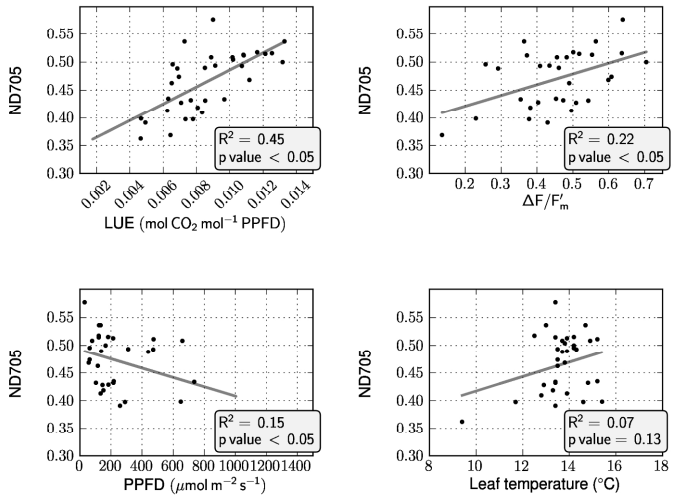

Figure 6: Linear regression models for (a) ND705 Vs LUE, (b) ND705 Vs ΔF/F'm, (c) ND705 Vs PPFD and (d) ND705 Vs leaf temperature.

.2 Model code

The following Matlab code was written for the simulations in chapter 5. The code calls the PROSPECT leaf model which can be downloaded from: `http://teledetection.ipgp.jussieu.fr/prosail/`

..1 Biochemical leaf model code

```
function out = fmod_biochem(ppfd,param_vec, ...
                                t_max,timestep)
% __Version __
% update of FMOD_EXPERIMENTAL
% largely based on
%  [Porcar-Castell,2005,FCB,Dyanamics of energy flow...]
%
%
debug = false;

if nargin < 4
  timestep = 0.02;
end
if nargin < 4
  t_max = 30;
end

ppfd_ts = ppfd * timestep;

% classic rate constants
kP_ts = param_vec(1) * timestep;
```

```
kF_ts = param_vec(2) * timestep;
kD_ts = param_vec(3) * timestep;
kN_ts = param_vec(4) * timestep;

% differential equation rate constants
k_pqr_ts = param_vec(5) * timestep;
k_npqb_ts = param_vec(6) * timestep;
k_npqr_ts = param_vec(7) * timestep;

% Model stoichometry
chl_tot = param_vec(8);
xan_tot = param_vec(9);
PQ_tot = param_vec(10);

% pH functional parameters => correlated with diff.
% eq. parameters PQ_reox_lim = 5000  % upper limit
% of pH scale factor, s^-1
PQ_reox_lim = param_vec(11) * timestep;

% 'fixed' parameters
chl_abs_e = 0.05;  % efficiency of energy capture
ac = 3.8e-20;      % effective absorp. area of chl.
conv_factor = 6.023e17;   % umoles to absolute units

%% initial conditions => include in parameters vector

% Dark adapted initial conditions
in_con = dark_con(PQ_tot, xan_tot);
PQ_on_ts = in_con(1);
```

```
PQ_off_ts = in_con(2);
PQ_ox_ts = in_con(3);
NPQ_on_ts = in_con(4);
vx_ts = in_con(5);
zx_ts = in_con(6);

% loop variables
ts_i = 1 * timestep;
ts = ts_i;
i = 1;

% analytical solution to xanthophyll cycle
vx_i = in_con(5);
zx_i = in_con(6);
k_npqb = param_vec(6);
k_npqr = param_vec(7);

% output, to do => state size for matlab interpreter
time_all = [0];
[chl_on, c] = calc_chl_ON(chl_tot,chl_abs_e, ppfd_ts, ...
                          ac,conv_factor,kF_ts,kD_ts, ...
                          kN_ts,kP_ts,PQ_ox_ts,NPQ_on_ts);
chl_on_ts = chl_on * timestep;

% 0 = fully oxidised, 1 = fully reduced
PQ_ox = [1 - PQ_on_ts / PQ_tot];

% 0 = no NPQ, 1 = full NPQ
NPQ_on = [zx_ts / xan_tot];
```

```
yF_all = [(kF_ts * chl_on_ts) / (c * timestep)];
yN_all = [(kN_ts* NPQ_on_ts * chl_on_ts) / (c * timestep)];
yP_all = [(kP_ts* PQ_ox_ts * chl_on_ts) / (c * timestep)];
yD_all = [(kD_ts * chl_on_ts) / (c * timestep)];


while ts <= t_max

  % steady state rate of excitation
  [chl_on, c] = calc_chl_ON(chl_tot,chl_abs_e, ppfd_ts, ...
                            ac,conv_factor,kF_ts,kD_ts, ...
                            kN_ts,kP_ts,PQ_ox_ts,NPQ_on_ts);
  chl_on_ts = chl_on * timestep;



  % pH related to the re-oxidation rate of the PQ pool
  PQ_reox = k_pqr_ts * PQ_on_ts;

  % violaxanthin to zeaxanthin conversion, NPQ formation
  zx_ts = zx_analytical(vx_i,zx_i,k_npqb,k_npqr,ts);

  % fraction of reduced PQ pool
  dot_PQ = (chl_on_ts * kP_ts/timestep *  PQ_ox_ts) ...
           - (k_pqr_ts * PQ_on_ts);
  PQ_on_ts = PQ_on_ts + dot_PQ;
  PQ_off_ts = PQ_tot - PQ_on_ts; % Q in porcar-castell
```

```
%==== DEBUG DEBUG DEBUG ====%
if debug;

  disp(['pH_scale_factor:' num2str(pH_scale_factor)])

  %if ts > .05
  %  return
  %end
end
%==== DEBUG DEBUG DEBUG ====%

% catch errors
if PQ_on_ts < 0
  PQ_on_ts = 0;
elseif PQ_on_ts > PQ_tot
  PQ_on_ts = PQ_tot;
end

if zx_ts < 0
  zx_ts = 0;
elseif zx_ts > xan_tot
  zx_ts = xan_tot;
end



vx_ts = xan_tot - zx_ts;

% number of oxidised (open) PQs
PQ_ox_ts = 1 - PQ_on_ts / PQ_tot; % or PQ_off_ts / PQ_tot
```

```
    % state of the NPQ pool (fraction if NPQ active)
    NPQ_on_ts = zx_ts / xan_tot;

    % calculate yields
    yF = (kF_ts * chl_on_ts) / (c * timestep);
    yN = (kN_ts* NPQ_on_ts * chl_on_ts) / (c * timestep);
    yP = (kP_ts* PQ_ox_ts * chl_on_ts) / (c * timestep);
    yD = (kD_ts * chl_on_ts) / (c * timestep);

    % output
    PQ_ox = [PQ_ox; PQ_ox_ts];
    NPQ_on = [NPQ_on ; NPQ_on_ts];
    time_all = [time_all ; ts];

    yF_all = [yF_all ; yF];
    yN_all = [yN_all ; yN];
    yP_all = [yP_all ; yP];
    yD_all = [yD_all ; yD];

    % indexing and timestep
    i = i + 1;
    ts = ts + ts_i;

end

out = [time_all,PQ_ox, NPQ_on, yF_all, yN_all,yP_all, ...
        yD_all];
```

```
%============== end of main ====================%
end

%%======== dark conditions ============%
function init_con = dark_con(PQ_tot, xan_tot)
%% initial conditions
% initial conditions => dark adapted
PQ_on_i = 0;
PQ_off_i = PQ_tot;
PQ_ox_i = 1 - PQ_on_i / PQ_tot;
NPQ_on_i = 0;
vx_i = xan_tot;
zx_i = 0;

init_con = [PQ_on_i, PQ_off_i,PQ_ox_i, NPQ_on_i,vx_i,zx_i];
end



%% ========== light absorption rate ==========%
function [chl_on,c] = calc_chl_ON(TOTchl,chl_abs_e,ppfd,...
                                  ac,conv_factor,kF,...
                                  kD,kN,kP,PQ_ox,NPQ_on)


% light absorbtion rate
c = light_abs_rate(TOTchl,chl_abs_e, ppfd, ac,conv_factor);

% number of chlorophyll in excited state
chl_on = c / (kF + kD + kN * NPQ_on + kP * PQ_ox);
end
```

```
function c = light_abs_rate(TOTchl,chl_abs_e , ppfd, ac, ...
                                conv_factor)
% Light absorbtion rate by chlorophyll a and b
c = TOTchl *chl_abs_e  * ppfd * ac * conv_factor;
end

%% ====== solution to the xanthophyll cycle ====== %%
function zx_ts = zx_analytical(vx_i,zx_i,k_npqb,k_npqr,t)
% Analytical solution to reversible reaction
%
%   V <-> Z
%
zx_ts = (zx_i * exp(-(k_npqb + k_npqr) * t) ) + ...
        ((k_npqb / (k_npqb + k_npqr )) * ...
         (vx_i + zx_i) * ...
         (1 -  exp(-(k_npqb + k_npqr) * t)) );
end
```

..2 Radiative transfer leaf model code

```
function [rindex_i, rindex,x,yF] = FmodProspect(params,...
                                                ts_max,...
                                                timestep,...
                                                init_rindex)
%
% coupled biochemical-physical model to predict
%   fluorescence index using empirical matrix from SCOPE.
%
% -- References ----
%
%  Miller et al, 2005, Development of a Vegetation
%    Canopy Model, report
%
%  Porcar-Castell, 2006, Dynamics of the energy
%    flow through photosystem II under changing light
%    conditions: a model approach, FPB(33)
%
%  van der Tol, 2009, An integrated model, Biogeosciences
%

phi_f_ref = 0.02; % CHECK THIS

% settings
addpath ../PROSPECT_5B_MATLAB/
verbose = false;

% calculate reflectance index for initial conditions?
if nargin < 4;
```

```
    init_rindex = false;
end

% params
wav_vnir = 350:1000;

%% 1.  LOAD DATA

% load irradiance, modelled (MODTRAN) or measured
rad = load('solar_rad_dummy.txt');
wav_E = rad(:,1);
E = rad(:,2);
N = E2N(E, wav_E); % convert units, FluorMOD report pp 72

% load empirical fluorescence matrix
[Mf_emp, Mb_emp] = load_empiricalMAC();

%% 2. CALL CASTELL LEAF MODEL

% Miller, 2005, eq [3.5.8]
ppfd = PAR_N(N, wav_E);

% Call biological model
out = fmod_biochem(ppfd,params,ts_max,timestep);
% out = [time_all,PQ_ox, NPQ_on, yF_all, yN_all, ...
%         yP_all,yD_all];

yF = out(:,4);
yN = out(:,5);
```

```
yP = out(:,6);
yD = out(:,7);


%% 3. CALL PROSPECT 5B

% prospect parameters and data
Nlayer =  params(12);
Cab = params(13);
Cw = params(14);
Cm = params(15);
Car = params(16);
Cbrown = params(17);

% Call PROSPECT
LRT = prospect_5B(Nlayer,Cab,Car,Cbrown,Cw,Cm);
refl = LRT(:,2);
tran = LRT(:,3);
wl = LRT(:,1);


%% 3. CALCULATE WHITE LIGHT FLUORESCENCE
wav_emiss = 640:850;
wav_absorb = 400:750;

% reflectance, where  wav_E == wav_N
Ij_b = white_fluor(N, Mb_emp, wav_absorb, wav_E);

% transmission
```

```
%Ij_f = white_fluor(N, Mf_emp, wav_absorb, wav_N);


%% 4. CALCULATE APPARENT REFLECTANCE
% (reflectance  + fluorescence)


% VECTORIZE, if more speed needed
refl_rescale = zeros(size(wav_vnir));
refl_rescale(:) = nan;
wl =  LRT(:,1);
refl_rescale(wav_vnir>=400 & wav_vnir<=851) = ...
    refl(wl>= 400 & wl<=851);
plot(wl)

rindex = [];

% loop over each timestep / f yield value.
for i = 1:length(yF)

  phi_f = yF(i);

  % scale fluorescence from max to realised
  F_refl = (phi_f / phi_f_ref * Ij_b) / pi;
  F_refl_rescale = zeros(size(wav_vnir));
  F_refl_rescale(wav_vnir>=640 & wav_vnir<=850) = F_refl;

  % calculate apparent reflectance and reflectance index
  app_refl = refl_rescale + F_refl_rescale;
```

```
  ridx = reflectance_index(app_refl, wav_vnir);

  % output
  rindex = [rindex; ridx];
end



%plot(app_refl)
%hold on
%plot(refl_rescale,'r')

%xlim([0,200])

%% STUFF FOR OPTIMISATION
% interp to 1 second for optimisation
x = out(:,1);
rindex_i = interp1(x, rindex, [1:ts_max]);
rindex_i = [rindex_i'];

% calculte reflectance index for initial conditions??
if init_rindex;
  rindex_i = [rindex(1); rindex_i];
end

% remove first three seconds worth of data because
%  we have prior knowledge of misfit
%rindex_i(1:3) = nan;
```

```
%%%%%%%%%%%%%%%% END OF MAIN %%%%%%%%%%%%%%%%%%%%%%%%%%%%
end

function ppfd = PAR_N(N, wav_N)
% integrate PAR over 400 - 750 nm
% Miller, 2005, eq [3.5.8]

wlow = find(wav_N==400);
whigh = find(wav_N==750);

ppfd = nansum(N(wlow:whigh)) * 10^6;
end

function rindex = reflectance_index(rho, wav_vnir)
% non vectorised
rindex = rho(wav_vnir == 680) ./ ...
         rho (wav_vnir == 630);
end



function N = E2N(E, wav_E)
% equation 3.5.7 from FlourMOD report, 2005
%  convert from W/m2/nm to mol_photons/m2/s/um
Na = 6.02214e23;
hc = 6.6208e-34 * 2.99797e8;
N = zeros(size(E));

% loop over wavelengths
for i = 1:length(wav_E)
```

```
  lambda = wav_E(i) * 10^-9;
  N(i) = E(i) / Na * lambda / hc;
end

end


function Ij = white_fluor(N, Mij, wav_absorb, wav_N)
% equation 3.5.6 from FlourMOD report, 2005
%  white light integration

f_wav_start_idx = find(wav_N==wav_absorb(1));
f_wav_end_idx = find(wav_N==wav_absorb(end));

N_f = N(f_wav_start_idx:f_wav_end_idx)';
N_f_ij = repmat(N_f,211,1);


Ij = nansum(N_f_ij .* Mij, 2) ./ nansum(N_f_ij, 2);

end


function [Mf, Mb] = load_empiricalMAC()
% load empirical f matrix data on Mac

Mfa_file = 'FdN_3.0.dat';          % Fluorescence file
Mba_file = 'FuN_3.0.dat';          % Fluorescence file
Mfa = load(Mfa_file);
```

```
Mba = load(Mba_file);
Mf = Mfa';                                % Fluorescence matrix Mf
Mb = Mba';
end



function [Mf, Mb] = load_empirical()
% load empirical f matrix data
path_input = '/home/s0793962/paper3/code/SCOPE/data/input/';
Mfa_file = 'FdN_3.0.dat';                 % Fluorescence file
Mba_file = 'FuN_3.0.dat';                 % Fluorescence file
Mfa = load([path_input,'fluormatrix/',Mfa_file]);
Mba = load([path_input,'fluormatrix/',Mba_file]);
Mf = Mfa';                                % Fluorescence matrix Mf
Mb = Mba';
end
```

Bibliography

Adams III, W., Demmig-Adams, B., Verhoeven, A.S. and Barker, D.H. (1995). 'photoinhibition' during winter stress: Involvement of sustained xanthophyll cycle-dependent energy dissipation. *Functional Plant Biology*, **22**, 261–276.

Allen, W., Gausman, H., Richardson, A. and Thomas, J. (1969). Interaction of isotropic light with a compact plant leaf. *J. Opt. Soc. Am.*, **59**, 1376–1379.

Allen, W., Gausman, H. and Richardson, A. (1970). Mean effective optical constants of cotton leaves. *J. Opt. Soc. Am.*, **60**, 542–547.

Anastasiou, C. and Brooks, J. (2003). Effects of soil ph, redox potential, and elevation on survival of spartina patens planted at a west central florida salt marsh restoration site. *Wetlands*, **23**, 845–859, 10.1672/0277-5212(2003)023[0845:EOSPRP]2.0.CO;2.

Baker, N. (2008). Chlorophyll fluorescence: A probe of photosynthesis in vivo. *Annual review of plant biology*, **59**, 89–113.

Barton, A.J. and Walsh, C.S. (2000). Effect of transplanting on water relations and canopy development in *Acer*. *Journal of Environmental Horticulture*, **18**, 202–206.

Barton, C. and North, P. (2001). Remote sensing of canopy light use efficiency

using the photochemical reflectance index: Model and sensitivity analysis. *Remote Sensing of Environment*, **78**, 264–273.

Blankenship, R. (2002). *Molecular Mechanisms of Photosynthesis*. Blackwell Science, Oxford, UK.

Bolhar-Nordenkampf, H.R., Long, S.P., Baker, N.R., Oquist, G., Schreiber, U. and Lechner, E.G. (1989). Chlorophyll fluorescence as a probe of the photosynthetic competence of leaves in the field: A review of current instrumentation. *Functional Ecology*, **3**, 497–514.

Buschmann, C. and Lichtenhaler, H. (1987). Reflectance and chlorophyll fluorescence signatures of leaves. In *Applications of chlorophyll fluorescence in photosynthesis research*.

Callaghan, T.V., Jonasson, S., Nichols, H., Heywood, R.B. and Wookey, P.A. (1995). Arctic terrestrial ecosystems and environmental change [and discussion]. *Philosophical Transactions of the Royal Society of London. Series A: Physical and Engineering Sciences*, **352**, 259–276.

Campbell, P.E., Middleton, E., Corp, L. and Kim, M. (2008). Contribution of chlorophyll fluorescence to the a pparent vegetation reflectance. *Science of The Total Environment*, **404**, 433–439.

Chen, J., LeBlanc, S., Cihlar, J., Desjardins, R. and J.I., M. (1999). Extending aircraft- and tower-based co2 flux measurements to a boreal region using a landsat thematic mapper land cover map. *Journal of Geophysical Research*, **104**, 16859–16877.

Close, D., Beadle, C. and Brown, P. (2004). The physiological basis of containerised tree seedling 'transplant shock': a review. *Australian Forestry*, **68**, 112–120.

Close, D.C. and Beadle, C.L. (2003). Chilling-dependent photoinhibition, nutrition and growth analysis of eucalyptus nitens seedlings during establishment. *Tree Physiology*, **23**, 217–226.

Coops, N.C., Hilker, T., Hall, F.G., Nichol, C.J. and Drolet, G.G. (2010). Estimation of light-use efficiency of terrestrial ecosystems from space: A status report. *BioScience*, **60**, 788–797.

Cramer, W., Kicklighter, D.W., Bondeau, A., Moore III, B., Churkina, G., Nemry, B., Ruimy, A., Schloss, A.L. and The Participants of The Potsdam NPP Model Intercomparison (1999). Comparing global models of terrestrial net primary productivity (npp): overview and key results. *Global Change Biology*, **5**, 1–15.

Damm, A., Elbers, J., Erler, A., Gioli, B., Hamdi, K., Hutjes, R., Kosvancova, M., Meroni, M., Miglietta, F., Moersch, A., Moreno, J., Schickling, A., Sonnenschein, R., Udelhoven, T., van der Linden, S., Hostert, P. and Rascher, U. (2010). Remote sensing of sun-induced fluorescence to improve modeling of diurnal courses of gross primary production (gpp). *Global Change Biology*, **16**, 171–186.

Dayyoub, A. (2011). *Novel techniques for the remote sensing of photosynthetic processes*. Ph.D. thesis, Universita di Bologna.

Demmig-Adams, B. and Adams III, W.W. (1996). The role of xanthophyll cycle carotenoids in the protection of photosynthesis. *Trends in Plant Science*, **1**, 21–26.

Demmig-Adams, B., Winter, K., Kruger, A. and Czygan, F.C. (1987). Photoinhibition and zeaxanthin formation in intact leaves: a possible role of the xanthophyll cycle in the dissipation of excess light energy. *Plant Physiology*, **84**, 218–224.

Desjardins, R., MacPherson, J., Schuepp, P. and Karanja, F. (1989). An evaluation of aircraft flux measurements of co_2, water vapor and sensible heat. *Boundary-Layer Meteorology*, **47**, 55–69.

Desjardins, R., MacPherson, J. and Schuepp, P. (2006). *Aircraft-Based Flux Sampling Strategies*. John Wiley and Sons, Ltd.

Dobrowski, S., Pushnik, J., Zarco Tejada, P. and Ustin, S. (2005). Simple reflectance indices track heat and water stress-induced changes in steady-state chlorophyll fluorescence at the canopy scale. *Remote Sensing of Environment*, **97**, 403–414.

Dougherty, P.M., Teskey, R.O., Phelps, J.E. and Hinckley, T.M. (1979). Net photosynthesis and early growth trends of a dominant white oak (*Quercus alba*) l. *Plant Physiology*, **64**, 930,935.

Drolet, G., Middleton, E., Huemmrich, K., Hall, F., Amiro, B., Barr, A., Black, T., McCaughey, J. and Margolis, H. (2008). Regional mapping of gross light-use efficiency using modis spectral indices. *Remote Sensing of Environment*, **112**, 3064–3078.

Drolet, G.G., Huemmrich, K.F., Hall, F.G., Middleton, E.M., Black, T.A., Barr, A.G. and Margolis, H.A. (2005). A modis-derived photochemical reflectance index to detect inter-annual variations in the photosynthetic light-use efficiency of a boreal deciduous forest. *Remote Sensing of Environment*, **98**, 212–224.

Ebenhöh, O., Houwaart, T., Lokstein, H., Schlede, S. and Tirok, K. (2011). A minimal mathematical model of nonphotochemical quenching of chlorophyll fluorescence. *Biosystems*, **103**, 196–204.

Farquhar, G.D., Caemmerer, S.V. and Berry, J.A. (1980). A biochemical model of photosynthesis co2 fixation in leaves of c3 species. *Planta*, **149**, 78–90.

Feret, J., François, C., Asner, G., Gitelson, A., Martin, R., Bidel, L., Ustin, S., Lemaire, G. and Jacquemoud, S. (2008). Prospect-4 and 5: Advances in the leaf optical properties model separating photosynthetic pigments. *Remote Sensing of Environment*, **112**, 3030–3043.

Filella, I., Porcar-Castell, A., Munné-Bosch, S., Bäck, J., Garbulsky, M.F. and Peñuelas, J. (2009). Pri assessment of long-term changes in carotenoids/chlorophyll ratio and short-term changes in de-epoxidation state of the xanthophyll cycle. *International Journal of Remote Sensing*, **30**, 4443–4455.

Flexas, J., Briantais, J. and Cerovic, Z. (2000). Steady-state and maximum chlorophyll fluorescence responses to water stress in grapevine leaves : A new remote sensing system. *Remote Sensing of Environment*, **297**, 283–297.

Foken, T., Wimmer, F., Mauder, M., Thomas, C. and Liebethal, C. (2006). Some aspects of the energy balance closure problem. *Atmospheric Chemistry and Physics*, **6**, 4395–4402.

Frank, D.C., Esper, J., Raible, C.C., Bontgen, U., Trouet, V., Stocker, B. and Joos, F. (2010). Ensemble reconstruction constraints on the global carbon cycle sensitivity to climate. *Nature*, **463**, 527–530.

Frankenberg, C., Butz, A. and Toon, G.C. (2011a). Disentangling chlorophyll fluorescence from atmospheric scattering effects in o2 a-band spectra of reflected sun-light. *Geophysical Research Letter*, **38**, L03801.

Frankenberg, C., Fisher, J.B., Worden, J., Badgley, G., Saatchi, S.S., Lee, J.E., Toon, G.C., Butz, A., Jung, M., Kuze, A. and Yokota, T. (2011b). New global observations of the terrestrial carbon cycle from gosat: Patterns of plant fluorescence with gross primary productivity. *Geophys. Res. Lett.*, **38**, L17706.

Gamon, J., Peñuelas, J. and Field, C. (1992). A narrow-waveband spectral index that tracks diurnal changes in photosynthetic efficiency. *Remote Sensing of Environment*, **41**, 35–44.

Gamon, J.A., Field, C.B., Bilger, W., Björkman, O., Fredeen, A.L. and Peñuelas, J. (1990). Remote sensing of the xanthophyll cycle and chlorophyll fluorescence in sunflower leaves and canopies. *Oecologia*, **85**, 1–7, 10.1007/BF00317336.

Gamon, J.A., Filella, I. and Peñuelas, J. (1993). *The dynamic 531-nanometer* Δ *reflectance signal: a survey of twenty angiosperm species*. Rockville, MD.

Gamon, J.A., Serrano, L. and Surfus, J.S. (1997). The photochemical reflectance index: An optical indicator of photosynthetic radiation use efficiency across species, functional types, and nutrient levels. *Oecologia*, **112**, 492–501.

Garbulsky, M., Peñuelas, J., Gamon, J., Inoue, Y. and Filella, I. (2010). The photochemical reflectance index (pri) and the remote sensing of leaf, canopy and ecosystem radiation use efficiencies: A review and meta-analysis. *Remote Sensing of Environment*, **115**, 281–297.

Garbulsky, M.F., Peñuelas, J., Papale, D. and Filella, I. (2008). Remote estimation of carbon dioxide uptake by a mediterranean forest. *Global Change Biology*, **14**, 2860–2867.

Garrity, S.R., Eitel, J.U. and Vierling, L.A. (2011). Disentangling the relationships between plant pigments and the photochemical reflectance index reveals a new approach for remote estimation of carotenoid content. *Remote Sensing of Environment*, **115**, 628–635.

Genty, B., Briantais, J.M. and Baker, N.R. (1989). The relationship between the quantum yield of photosynthetic electron transport and quenching of chlorophyll fluorescence. *Biochimica et Biophysica Acta (BBA) - General Subjects*, **990**, 87–92.

Gilabert, M. and Meliá, J. (1993). Solar angle and sky light effects on ground reflectance measurements in a citrus canopy. *Remote Sensing of Environment*, **45**, 281–293.

Gioli, B., Miglietta, F., Martino, B.D., Hutjes, R.W., Dolman, H.A., Lindroth, A., Schumacher, M., Sanz, M.J., Manca, G., Peressotti, A. and Dumas, E.J. (2004). Comparison between tower and aircraft-based eddy covariance fluxes in five european regions. *Agricultural and Forest Meteorology*, **127**, 1–16.

Gitelson, A., Buschmann, C. and Lichtenthaler, H. (1999). The chlorophyll fluorescence ratio f735/f700 as an accurate measure of the chlorophyll content in plants. *Remote Sensing of Environment*, **69**, 296–302.

Gitelson, A.A., Gritz, Y. and Merzlyak, M.N. (2003). Relationships between leaf chlorophyll content and spectral reflectance and algorithms for non-destructive chlorophyll assessment in higher plant leaves. *Journal of Plant Physiology*, **160**, 271–282.

Goerner, A., Reichstein, M. and Rambal, S. (2009). Tracking seasonal drought effects on ecosystem light use efficiency with satellite-based pri in a mediterranean forest. *Remote Sensing of Environment*, **113**, 1101–1111.

Grace, J., Nichol, C., Disney, M., Lewis, P., Quaife, T. and Bowyer, P. (2007). Can we measure terrestrial photosynthesis from space directly, using spectral reflectance and fluorescence? *Global Change Biology*, **13**, 1484–1497.

Guanter, L., Alonso, L., Gómez-Chova, L., Amorós-López, J., Vila, J. and Moreno, J. (2007). Estimation of solar-induced vegetation fluorescence from space measurements. *Geophys. Res. Lett.*, **34**, L08401.

Guo, J. and Trotter, C. (2004). Estimating photosynthetic light-use efficiency using the photochemical reflectance index: variations among species. *Functional Plant Biology*, **31**, 255–265.

Hall, F.G. (1999). Introduction to special section: Boreas in 1999: Experiment and science overview. *J. Geophys. Res.*, **104**, 27627–27639.

Hall, F.G., Hilker, T., Coops, N.C., Lyapustin, A., Huemmrich, K.F., Middleton, E., Margolis, H., Drolet, G. and Black, T.A. (2008). Multi-angle remote sensing of forest light use efficiency by observing pri variation with canopy shadow fraction. *Remote Sensing of Environment*, **112**, 3201–3211.

Hall, F.G., Hilker, T. and Coops, N.C. (2011). Photosynsat, photosynthesis from space: Theoretical foundations of a satellite concept and validation from tower and spaceborne data. *Remote Sensing of Environment*, **115**, 1918–1925.

Hartley, I.P., Hopkins, D.W., Garnett, M.H., Sommerkorn, M. and Wookey, P.A. (2008). Soil microbial respiration in arctic soil does not acclimate to temperature. *Ecology Letters*, **11**, 1092–1100.

Haxeltine, A. and Prentice, I.C. (1996). A general model for the light-use efficiency of primary production. *Functional Ecology*, **10**, 551–561.

Heikkinen, R.K., Birks, H.J.B. and Kalliola, R.J. (1998). A numerical analysis of the mesoscale distribution patterns of vascular plants in the subarctic kevo nature reserve, northern finland. *Journal of Biogeography*, **25**, pp. 123–146.

Heinsch, F., Zhao, M., Running, S., Kimball, J., Nemani, R., Davis, K., Bolstad, P., Cook, B., Desai, A., Ricciuto, D., Law, B., Oechel, W., Kwon, H., Luo, H., Wofsy, S., Dunn, A., Munger, J., Baldocchi, D., Xu, L., Hollinger, D., Richardson, A., Stoy, P., Siqueira, M., Monson, R., Burns, S. and Flanagan, L. (2006). Evaluation of remote sensing based terrestrial productivity from modis using regional tower eddy flux network observations. *Geoscience and Remote Sensing, IEEE Transactions on*, **44**, 1908–1925.

Hilker, T., Coops, N.C., Hall, F.G., Black, T.A., Wulder, M.A., Nesic, Z. and Krishnan, P. (2008). Separating physiologically and directionally induced changes in pri using brdf models. *Remote Sensing of Environment*, **112**, 2777–2788.

Hilker, T., Lyapustin, A., Hall, F.G., Wang, Y., Coops, N.C., Drolet, G. and Black, T.A. (2009). An assessment of photosynthetic light use efficiency from space: Modeling the atmospheric and directional impacts on pri reflectance. *Remote Sensing of Environment*, **113**, 2463–2475.

Hilker, T., Coops, N.C., Hall, F.G., Nichol, C.J., Lyapustin, A., Black, T.A., Wulder, M.A., Leuning, R., Barr, A., Hollinger, D.Y., Munger, B. and Tucker, C.J. (2011). Inferring terrestrial photosynthetic light use efficiency of temperate ecosystems from space. *J. Geophys. Res.*, **116**, G03014.

Hill, T.C., Quaife, T. and Williams, M. (2011a). A data assimilation method for using low-resolution earth observation data in heterogeneous ecosystems. *J. Geophys. Res.*, **116**, D08117.

Hill, T.C., Williams, M., Woodward, F.I. and Moncrieff, J.B. (2011b). Constraining ecosystem processes from tower fluxes and atmospheric profiles. *Ecological Applications*, **21**, 1474–1489.

Huemmrich, K., Gamon, J., Tweedie, C., Oberbauer, S., Kinoshita, G., Houston, S., Kuchy, A., Hollister, R., Kwon, H., Mano, M., Harazono, Y., Webber, P. and Oechel, W. (2010). Remote sensing of tundra gross ecosystem productivity and light use efficiency under varying temperature and moisture conditions. *Remote Sensing of Environment*, **114**, 481–489.

Huete, A., Justice, C. and Leeuwen, W. (1999). Modis vegetation index (mod 13) algorithm theoretical basis document.

Hutjes, R., Vellinga, O., Gioli, B. and Miglietta, F. (2010). Dis-aggregation of airborne flux measurements using footprint analysis. *Agricultural and Forest Meteorology*, **150**, 966–983.

IGBP Terrestrial Carbon Working Group (1998). The terrestrial carbon cycle: Implications for the kyoto protocol. *Science*, **280**, 1393–1394.

IPCC (2007a). *Climate Change 2007: Synthesis Report. Contribution of Working Groups I, II and III to the Fourth Assessment Report of the Intergovernmental Panel on Climate Change*.

IPCC (2007b). Polar regions (arctic and antarctic). climate change 2007: Impacts, adaptation and vulnerability. contribution of working group ii to the fourth assessment report of the intergovernmental panel on climate change. Tech. Rep. 4, Anisimov, O.A. and Vaughan, D.G. and Callaghan, T.V. and Furgal, C. and Marchant, H. and Prowse, T.D. and Vilhjalmsson, H. and Walsh, J.E.

Jacquemoud, S. and Baret, F. (1990). Prospect: A model of leaf optical properties spectra. *Remote Sensing of Environment*, **34**, 75 – 91.

Jacquemoud, S., Ustin, S., Verdebout, J., Schmuck, G., Andreoli, G. and Hosgood, B. (1996). Estimating leaf biochemistry using the prospect leaf optical properties model. *Remote Sensing of Environment*, **56**, 194–202.

Jacquemoud, S., Verhoef, W., Baret, F., Bacour, C., Zarco-Tejada, P.J., Asner, G.P., François, C. and Ustin, S.L. (2009). Prospect+sail models: A review of use for vegetation characterization. *Remote Sensing of Environment*, **113**, S56–S66.

Joiner, J., Yoshida, Y., Vasilkov, A.P., Yoshida, Y., Corp, L.A. and Middleton, E.M. (2011). First observations of global and seasonal terrestrial chlorophyll fluorescence from space. *Biogeosciences*, **8**, 637–651.

Kautsky, H. and Hirsch, A. (1931). Neue versuche zur kohlensöureassimilation. *Naturwissenschaften*, **19**, 964–964, 10.1007/BF01516164.

Kirby, S., Dobosy, R., Williamson, D. and Dumas, E. (2008). An aircraft-based data analysis method for discerning individual fluxes in a heterogeneous agricultural landscape. *Agricultural and Forest Meteorology*, **148**, 481–489.

Kljun, N., Calanca, P., Rotach, M.W. and Schmid, H.P. (2004). A simple parameterisation for flux footprint predictions. *BoundaryLayer Meteorology*, **112**, 503–523.

Krause, G.H. and Weis, E. (1991). Chlorophyll fluorescence and photosynthesis: The basics. *Annual Review of Plant Physiology and Plant Molecular Biology*, **42**, 313–349.

La Puma, I.P., Philippi, T.E. and Oberbauer, S.F. (2007). Relating ndvi to ecosystem co2 exchange patterns in response to season length and soil warming manipulations in arctic alaska. *Remote Sensing of Environment*, **109**, 225–236.

Laine, M. (2008). *Adaptive MCMC methods with applications in environmental and geophysical models*. Ph.D. thesis, Lappeenranta University of Technology.

Lichtenthaler, H. (1989). Possibilities for remote sensing of terrestrial vegetation by a combination of reflectance and laser-induced chlorophyll fluorescence. In *Geoscience and Remote Sensing Symposium, 1989. IGARSS'89. 12th Canadian Symposium on Remote Sensing., 1989 International*, vol. 3, 1349–1354.

Linderholm, H. (2006). Growing season changes in the last century. *Agricultural and Forest Meteorology*, **137**, 1–14.

Magnani, F. (2009). Assessment of vegetation photosynthesis through observation of solar induced fluorescence from space.

Maier, S., Guenther, K. and Stellmes, M. (2003). *Sun-induced fluorescence: a new tool for precision farming*, chap. 16, 209–222. American Society of Agronomy, Crop Science Society of America, Soil Science Society of America, Madison, Wisconsin, USA.

Malve, O., Laine, M., Haario, H., Kirkkala, T. and Sarvala, J. (2007). Bayesian modelling of algal mass occurrences- using adaptive mcmc methods with a lake water quality model. *Environmental Modelling and Software*, **22**, 966–977.

Maselli, F., Gioli, B., Chiesi, M., Vaccari, F., Zaldei, A., Fibbi, L., Bindi, M. and Miglietta, F. (2010). Validating an integrated strategy to model net land carbon exchange against aircraft flux measurements. *Remote Sensing of Environment*, **114**, 1108–1116.

Mauder, M., Desjardins, R.L., Oncley, S.P. and Macpherson, I. (2007). Atmospheric Response to a Partial Solar Eclipse over a Cotton Field in Central California. *Journal of Applied Meteorology & Climatology*, **46**, 1792–1803+.

Maxwell, K. and Johnson, G.N. (2000). Chlorophyll fluorescence - a practical guide. *Journal of Experimental Botany*, **51**, 659–668.

McBean, G., Alekseev, G., Chen, D., Forland, E., Fyfe, J., Groisman, P., King, R., Melling, H., Vose, R. and Whitfield, P. (2005). *Arctic climate: past and present*. Cambridge University Press, Cambridge.

Meroni, M., Picchi, V., Rossini, M., Cogliati, S., Panigada, C., Nali, C., Lorenzini, G. and Colombo, R. (2008). Leaf level early assessment of ozone injuries by passive fluorescence and photochemical reflectance index. *International Journal of Remote Sensing*, **29**, 5409–5422.

Meroni, M., Rossini, Guanter, M.L., Alonso, L., Rascher, R., U. andColombo and Moreno, J. (2009). Remote sensing of solar induced chlorophyll fluorescence: review of methods and applications. *Remote Sensing of Environment*, **113**, 2037–2051.

Merzlyak, M.N., Gitelson, A.A., Chivkunova, O.B. and Rakitin, V.Y. (1999). Non-destructive optical detection of pigment changes during leaf senescence and fruit ripening. *Physiologia Plantarum*, **106**, 135–141.

Metropolis, N., Rosenbluth, A.W., Rosenbluth, M.N., Teller, A.H. and Teller, E. (1953). Equation of state calculations by fast computing machines. *The Journal of Chemical Physics*, **21**, 1087–1092.

Middleton, E.M., Corp, L.A. and Campbell, P.K.E. (2008). Comparison of measurements and fluormod simulations for solarinduced chlorophyll fluorescence and reflectance of a corn crop under nitrogen treatments. *International Journal of Remote Sensing*, **29**, 5193–5213.

Miller, J., Berger, M., Goulas, Y., Jacquemoud, S., Louis, J., Mohammed, G., Moise, N., Moreno, J., Moya, I., Pedrós, R., Verhoef, W. and Zarco-Tejada, P. (2005). Development of a vegetation fluorescence canopy model.

Milton, E.J., Schaepman, M.E., Anderson, K., Kneübhler, M. and Fox, N. (2009). Progress in field spectroscopy. *Remote Sensing of Environment*, **113**, S92,S109, imaging Spectroscopy Special Issue.

Moorthy, I., Miller, J.R. and Noland, T.L. (2008). Estimating chlorophyll concentration in conifer needles with hyperspectral data: An assessment at the needle and canopy level. *Remote Sensing of Environment*, **112**, 2824–2838.

Moya, I. (2004). A new instrument for passive remote sensing 1. measurements of sunlight-induced chlorophyll fluorescence. *Remote Sensing of Environment*, **91**, 186–197.

Myneni, R. and Williams, D. (1994). On the relationship between fapar and ndvi. *Remote Sensing of Environment*, **49**, 200–211.

Myneni, R., Hall, F., Sellers, P. and Marshak, A. (1995). The interpretation of spectral vegetation indexes. *Geoscience and Remote Sensing, IEEE Transactions on*, **33**, 481 –486.

Myneni, R.B., Keeling, C.D., Tucker, C.J., Asrar, G. and Nemani, R.R. (1997). Increased plant growth in the northern high latitudes from 1981 to 1991. *Nature*, **386**, 698–702.

Nakaji, T., Ide, R., Oguma, H., Saigusa, N. and Fujinuma, Y. (2007). Utility

of spectral vegetation index for estimation of gross co2 flux under varied sky conditions. *Remote Sensing of Environment*, **109**, 274–284.

Nichol, C.J., Huemmrich, K.F., Black, T.A., Jarvis, P.G., Walthall, C.L., Grace, J. and Hall, F.G. (2000). Remote sensing of photosynthetic-light-use efficiency of boreal forest. *Agricultural and Forest Meteorology*, **101**, 131–142.

Nichol, C.J., Lloyd, J., Shibistova, O., Arneth, A., Röser, C., Knohl, A., Matsubara, S. and Grace, J. (2002). Remote sensing of photosynthetic-light-use efficiency of a siberian boreal forest. *Tellus B*, **54**, 677–687.

Nowak, D.J. and Rowntree, R.A. (1990). History and range of norway maple. *Journal of Arboriculture*, **16**, 291,296.

Oak Ridge National Laboratory Distributed Active Archive Center (ORNL DAAC) (2010). Modis subsetted land products, collection 5.

Ogunjemiyo, S.O., Kaharabata, S.K., Schuepp, P.H., MacPherson, I.J., Desjardins, R. and Roberts, D.A. (2003). Methods of estimating co2, latent heat and sensible heat fluxes from estimates of land cover fractions in the flux footprint. *Agricultural and Forest Meteorology*, **117**, 125–144.

Peñuelas, J., Filella, I. and Gamon, J.A. (1995). Assessment of photosynthetic radiation-use efficiency with spectral reflectance. *New Phytologist*, **131**, 291–296.

Pedrós, R., Goulas, Y., Jacquemoud, S., Louis, J. and Moya, I. (2010). Fluormodleaf: A new leaf fluorescence emission model based on the prospect model. *Remote Sensing of Environment*, **114**, 155–167.

Perez-Priego, O., Zarco-Tejada, P., Miller, J., Sepulcre-Canto, G. and Fereres, E. (2005). Detection of water stress in orchard trees with a high-resolution spectrometer through chlorophyll fluorescence in-filling of the o2-a band. *Geoscience and Remote Sensing, IEEE Transactions on*, **43**, 2860–2869.

Plascyk, J. (1975). The mkii fraunhofer line discriminator (fld ii) for airborne and orbital remote sensing of solar-stimulated luminescence. *Optical Engineering*, **14**, 339–346.

Plascyk, J. and Gabriel, F. (1975). The fraunhofer line discriminator mkii an airborne instrument for precise and standardized ecological luminescence measurements. *IEEE Transactions of Instrumentation and Measurement*, **24**, 306–313.

Porcar-Castell, A., Bäck, J., Juurola, E. and Hari, P. (2006). Dynamics of the energy flow through photosystem ii under changing light conditions: a model approach. *Functional Plant Biology*, **33**, 229–239.

Porcar-Castell, A., Pfündel, E., Korhonen, J.F.J. and Juurola, E. (2008). A new monitoring pam fluorometer (moni-pam) to study the short- and long-term acclimation of photosystem ii in field conditions. *Photosynthesis Research*, **96**, 173–179.

Quaife, T., Lewis, P., Kauwe, M.D., Williams, M., Law, B.E., Disney, M. and Bowyer, P. (2008). Assimilating canopy reflectance data into an ecosystem model with an ensemble kalman filter. *Remote Sensing of Environment*, **112**, 1347–1364, remote Sensing Data Assimilation Special Issue.

Rahman, A., Cordova, V., Gamon, J., Schmid, H. and Sims, D. (2004). Potential of modis ocean bands for estimating co2 flux from terrestrial vegetation: A novel approach. *Geophys. Res. Lett.*, **31**, L10503.

Rascher, U. and Nedbal, L. (2006). Dynamics of photosynthesis in fluctuating light. *Current Opinion in Plant Biology*, **9**, 671–678.

Rascher, U., Gioli, B. and Miglietta, F. (2008). Flex fluorescence explorer: A remote sensing approach to quantify spatio-temporal variations of photosynthetic efficiency from space. In J. Allen, E. Gantt, J. Golbeck and B. Osmond, eds., *Photosynthesis. Energy from the Sun*, 1388–1390, Springer Netherlands.

Reichert, P. and Omlin, M. (1997). On the usefulness of overparameterized ecological models. *Ecological Modelling*, **95**, 289–299.

Riedel, S.M., Epstein, H.E. and Walker, D.A. (2005). Biotic controls over spectral reflectance of arctic tundra vegetation. *International Journal of Remote Sensing*, **26**, 2391–2405.

Rietveld, R. (1987). Transplanting shock in bareroot conifer seedlings. *National Nursery Proceedings - 1987*, **6**, 49–71.

Rosema, A., Verhoef, W., Schroote, J. and Snel, J. (1991). Simulating fluorescence light-canopy interaction in support of laser-induced fluorescence measurements. *Remote Sensing of Environment*, **37**, 117–130.

Rosema, A., Snel, J., Zahn, H., Buurmeijer, W. and Hove, L.V. (1998). The relation between laser-induced chlorophyll fluorescence and photosynthesis. *Remote Sensing of Environment*, **65**, 143–154.

Rouse, J.W., Haas, R.H., Schell, J.A. and Deering, D.W. (1973). Monitoring vegetation systems in the Great Plains with ERTS. In *Proceedings of the Third ERTS Symposium*, vol. 1, 309–317, NASA.

Running, S. and Hunt Jr., E. (1993). *Generalization of a forest ecosystem process model for other biomes, BIOME-BGC, and an application for global-scale models*. Academic Press, Inc. New York.

Running, S., Nemani, R., Glassy, J. and Thornton, P. (1999). Modis daily photosynthesis (psn) and annual net primary production (npp) product (mod17) algorithm theoretical basis document. Tech. Rep. 3.

Sarlikioti, V., Driever, S. and Marcelis, L. (2010). Photochemical reflectance index as a mean of monitoring early water stress. *Annals of Applied Biology*, **157**, 81–89.

Saucier, A., Duncan, M. and Austin, G. (1991). Mean flux estimation and cospectra of airborne carbon dioxide and water vapour eddy flux measurements in the planetary surface layer. *Boundary-Layer Meteorology*, **55**, 227–254.

Savitzky, A. and Golay, M.J.E. (1964). Smoothing and differentiation of data by simplified least squares procedures. *Analytical Chemistry*, **36**, 1627–1639.

Sellers, P., Randall, D., Collatz, G., Berry, J., Field, C., Dazlich, D., Zhang, C., Collelo, G. and Bounoua, L. (1996). A revised land surface parameterization (sib2) for atmospheric gcms. part i: Model formulation. *Journal of Climate*, **9**, 676–705.

Sielewiesiuk, J. and Gruszecki, W.I. (1991). A simple model describing the kinetics of the xanthophyll cycle. *Biophysical Chemistry*, **41**, 125–129.

Sims, D. and Gamon, J. (2002). Relationships between leaf pigment content and spectral reflectance across a wide range of species, leaf structures and developmental stages. *Remote Sensing of Environment*, **81**, 337–354.

South, D.B. and Zwolinski, J.B. (1997). Transplant stress index: A proposed method of quantifying planting check. *New Forests*, **13**, 315–328, 10.1023/A:1006546627342.

Stow, D. (2004). Remote sensing of vegetation and land-cover change in arctic tundra ecosystems. *Remote Sensing of Environment*, **89**, 281–308.

Stoy, P., Williams, M., Spadavecchia, L., Bell, R., Prieto-Blanco, A., Evans, J. and van Wijk, M. (2009). Using information theory to determine optimum pixel size and shape for ecological studies: Aggregating land surface characteristics in arctic ecosystems. *Ecosystems*, **12**, 574–589, 10.1007/s10021-009-9243-7.

Suárez, L., Zarco-Tejada, P.J., Berni, J.A.J., González-Dugo, V. and Fereres, E. (2009). Modelling pri for water stress detection using radiative transfer models. *Remote Sensing of Environment*, **113**, 730–744.

Thenot, F., Méthy, M. and Winkel, T. (2002). The photochemical reflectance index (pri) as a water-stress index. *International Journal of Remote Sensing*, **23**, 5135,5139.

Triantaphylidès, C., Krischke, M., Hoeberichts, F.A., Ksas, B., Gresser, G., Havaux, M., Van Breusegem, F. and Mueller, M.J. (2008). Singlet oxygen is the major reactive oxygen species involved in photooxidative damage to plants1[w]. *Plant Physiology*, **148**, 960–968.

Tucker, C. (1979). Red and photographic infrared linear combinations for monitoring vegetation. *Remote Sensing of Environment*, **8**, 127–150.

van der Tol, C., Verhoef, W. and Rosema, A. (2009a). A model for chlorophyll fluorescence and photosynthesis at leaf scale. *Agricultural and Forest Meteorology*, **149**, 96–105.

van der Tol, C., Verhoef, W., Timmermans, J., Verhoef, A. and Su, Z. (2009b). An integrated model of soil-canopy spectral radiances, photosynthesis, fluorescence, temperature and energy balance. *Biogeosciences*, **6**, 3109–3129.

van Gorsel, E., Delpierre, N., Leuning, R., Black, A., Munger, J.W., Wofsy, S., Aubinet, M., Feigenwinter, C., Beringer, J., Bonal, D., Chen, B., Chen, J., Clement, R., Davis, K.J., Desai, A.R., Dragoni, D., Etzold, S., Grnwald, T., Gu, L., Heinesch, B., Hutyra, L.R., Jans, W.W., Kutsch, W., Law, B., Leclerc, M.Y., Mammarella, I., Montagnani, L., Noormets, A., Rebmann, C. and Wharton, S. (2009). Estimating nocturnal ecosystem respiration from the vertical turbulent flux and change in storage of co2. *Agricultural and Forest Meteorology*, **149**, 1919–1930.

Verhoef, W. (1984). Light scattering by leaf layers with application to canopy reflectance modeling: The scattering by arbitrarily inclined leaves (sail) model. *Remote Sensing of Environment*, **16**, 125–178.

Veroustraete, F., Sabbe, H. and Eerens, H. (2002). Estimation of carbon mass fluxes over europe using the c-fix model and euroflux data. *Remote Sensing of Environment*, **83**, 376–399.

Vogelmann, J.E., Rock, B.N. and Moss, D. (1993). Red edge spectral measurements from sugar maple leaves. *International Journal of Remote Sensing*, **14**, 1563–1575.

Williams, M., Schwarz, P.A., Law, B.E., Irvine, J. and Kurpius, M.R. (2005). An improved analysis of forest carbon dynamics using data assimilation. *Global Change Biology*, **11**, 89–105.

Williams, M., Bell, R., Spadavecchia, L., Street, L.E. and Van Wijk, M.T. (2008). Upscaling leaf area index in an arctic landscape through multiscale observations. *Global Change Biology*, **14**, 1517–1530.

Zaczek, J.J., Steiner, K.C. and Bowersox, T.W. (1997). Northern red oak planting stock: 6-year results. *New Forests*, **13**, 177–191, 10.1023/A:1006578007777.

Zarco-Tejada, P., González-Dugo, V. and Berni, J. (2012). Fluorescence, temperature and narrow-band indices acquired from a uav platform for water stress detection using a micro-hyperspectral imager and a thermal camera. *Remote Sensing of Environment*, **117**, 322–337, remote Sensing of Urban Environments.

Zarco-Tejada, P.J., Miller, J.R., Mohammed, G.H. and Noland, T.L. (2000a). Chlorophyll fluorescence effects on vegetation apparent reflectance: I. leaf-level measurements and model simulation. *Remote Sensing of Environment*, **74**, 582–595.

Zarco-Tejada, P.J., Miller, J.R., Mohammed, G.H., Noland, T.L. and Sampson, P.H. (2000b). Chlorophyll fluorescence effects on vegetation apparent reflectance: Ii. laboratory and airborne canopy-level measurements with hyperspectral data. *Remote Sensing of Environment*, **74**, 596–608.

Zarco-Tejada, P.J., Pushnik, J.C., Dobrowski, S. and Ustin, S.L. (2003). Steady-state chlorophyll a fluorescence detection from canopy derivative reflectance and double-peak red-edge effects. *Remote Sensing of Environment*, **84**, 283–294.

Zarco-Tejada, P.J., Miller, J.R., Harron, J., Hu, B., Noland, T.L., Goel, N., Mohammed, G.H. and Sampson, P. (2004). Needle chlorophyll content estimation through model inversion using hyperspectral data from boreal conifer forest canopies. *Remote Sensing of Environment*, **89**, 189–199.

Zulueta, R.C., Oechel, W.C., Loescher, H.W., Lawrence, W.T. and Paw U, K.T. (2011). Aircraft-derived regional scale co2 fluxes from vegetated drained thaw-lake basins and interstitial tundra on the arctic coastal plain of alaska. *Global Change Biology*, **17**, 2781–2802.